

IMPROVEMENT OF ALUMINA MECHANICAL AND ELECTRICAL PROPERTIES USING MULTI- WALLED CARBON NANOTUBES AND TITANIUM CARBIDE AS A SECONDARY PHASE.



SANELE GOODENOUGH NYEMBE

A dissertation submitted to the Faculty of Engineering and the Built Environment, University of Witwatersrand, Johannesburg, in fulfillment of the requirements for the degree of Master of Science in Engineering.

Johannesburg, 2011.

Declaration

I declare that this dissertation is my own unaided work. It is being submitted for the degree of Master of Science in Engineering to the University of the Witwatersrand, Johannesburg. It has not been submitted before for any degree or examination to any other University.

Sanele Goodenough Nyembe

Signature.....

..... Day of Year

Abstract

The objective of this research was to improve alumina (Al_2O_3) mechanical and electrical properties by reinforcement using multi-walled carbon nanotubes (MWCNTs) and titanium carbide (TiC). The objective of the study was achieved with interesting and challenging difficulties along the way. The MWCNTs were initially coated with boron nitride (hBN) in order to improve the Alumina-CNTs interface which was previously discovered to be weak and also to protect them from reacting with Al_2O_3 during sintering. The coating of CNTs with hBN was done using nitridation method. This method was unsuccessful since it was not possible to coat each CNT individually. Dispersing hBN coated CNTs proved to be impossible without peeling the off the hBN coating. The “flaking off “of the hBN coating from the CNTs revealed that the CNT-hBN interface was weak; therefore uncoated CNTs were used for this study.

The starting powders (Al_2O_3 , TiC and CNTs) were individually dispersed before they were mixed together. TiC and Al_2O_3 were dispersed using an ultrasonic probe which was done successfully. The CNTs were dispersed by an ultrasonic probe and then attritor milled with the use of polyvinylpyrrolidone (PVP) as a dispersant. The dispersed Al_2O_3 and TiC (30 wt%) powders were mixed in a planetary ball mill. The composite powder was sieved and sintered using SPS with temperature and pressure programmed to be $1700^\circ C$, 35MPa respectively. In making the Al_2O_3 +CNT composite powder, the already dispersed Al_2O_3 and CNTs (1 wt%) were mixed in a planetary ball mill, after sieving the powder it was sintered using SPS at $1600^\circ C$, 35MPa (programmed conditions). Lastly in making the Al_2O_3 +CNT+TiC composite, the already dispersed TiC, CNTs and Al_2O_3 were all mixed in a planetary ball mill, after sieving it was sintered using SPS at $1650^\circ C$, 35MPa (programmed conditions). For comparison of properties, dispersed monolithic Al_2O_3 was also sintered using SPS at $1600^\circ C$, 35 MPa. The density results showed that the monolithic Al_2O_3 was 99.8% dense, , Al_2O_3 +CNTs was 99.4%, Al_2O_3 +TiC+CNTs was 99.2% and Al_2O_3 +TiC sample was 99.0%. The mechanical properties of the samples were measured using the indentation method. The hardness and fracture toughness of the samples were; Al_2O_3 = $3.3MPa\sqrt{m}$ (17 GPa), Al_2O_3 +CNTs = $4.2MPa\sqrt{m}$ (18 GPa), Al_2O_3 +TiC = $4.8 MPa\sqrt{m}$ (23 GPa) and Al_2O_3 +TiC+CNT= $5.0 MPa\sqrt{m}$ (23 GPa). The electrical properties showed that incorporating CNTs and TiC into Al_2O_3 improved Al_2O_3 electrical conductivity. The measured electrical conductivity of the ceramic samples were; Al_2O_3

$\approx 0 \text{ S.m}^{-1}$, $\text{Al}_2\text{O}_3+\text{CNTs}= 30 \text{ S.m}^{-1}$, $\text{Al}_2\text{O}_3 +\text{TiC} + \text{CNTs} = 6855 \text{ S.m}^{-1}$ and $\text{Al}_2\text{O}_3+\text{TiC} = 9664 \text{ S.m}^{-1}$. The CNTs improved Al_2O_3 mechanical properties slightly inhibiting grain growth by pinning the grain boundary movement and also by crack bridging. The Al_2O_3 electrical conductivity was increased by the CNTs network that was located along the alumina grain boundaries. The TiC improved Al_2O_3 mechanical properties slightly inhibiting grain growth and through crack deflection mechanism. The addition of TiC into Al_2O_3 increased the electrical conductivity by serving as a conducting continuous secondary phase.

The results show that the CNT-hBN interface is weak. The addition of CNTs and TiC into monolithic Al_2O_3 slightly improved its mechanical and electrical properties but its density was slightly compromised. CNTs and TiC slightly improved monolithic alumina hardness by inhibiting Al_2O_3 grain growth and the fracture toughness through crack deflection and crack bridging mechanisms. The CNTs network located at the Al_2O_3 grain boundaries not only aided in improving Al_2O_3 hardness but also served as transport medium for electrons hence increasing the Al_2O_3 electrical conductivity. Addition of TiC into Al_2O_3 increased its electrical conductivity by conducting electrons from one TiC grain to the adjacent grain. The large increase in electrical conductivity upon addition of TiC is due to the presence of a continuous TiC phase within Al_2O_3 .

Dedication

All glory goes to God for guiding me throughout my life. I would like to dedicate this work to my family that has been there for me from the beginning. Firstly to my parents that made sure that I go to school from the first grade up until the post graduate level, Mrs. Thandi Mavis Nyembe and Mr Petros Riet Nyembe, since no man can choose a womb in which they come to this earth, If I could be given a change to make that choice I will chose the same in which I came through.

Secondly I would like to dedicate this to my sister Winnie Nyembe who took the role of being a parent to my siblings for many years and for believing in me from the beginning of my academic career. Thirdly I would love to dedicate this to all my siblings that have been there for me and giving me motivation, Thamie Nyembe, Syabonga Nyembe, Mthokozisi Gumede and Zama Nyembe, and also to my late brother Sphesihle Nyembe, who I am sure is looking down at me and smiling, I love you all.

Acknowledgements

I would like to express my gratitude and appreciation to the following people for their invaluable aid and their contribution to the successful completion of this study;

Professor I. Sigalas: For being the best and easy to work with Supervisor, for his fatherly love, valuable comments and with his financial assistance. Thank you for words of encouragement and mentorship. I wish God continues to bless you.

Dr. M. Herrmann: For his useful comments and co-operation during the laboratory work throughout this work. Thank you for your useful and effective writing skills you taught me and lastly for your useful explanations regarding my work.

Oluwagbenga Temidayo Johnson and Wallace Matizamhuka: For their invaluable help in the laboratory as they were my senior colleagues. Johnson for his sleepless nights when he was conducting SEM analysis on my samples, I appreciated that a lot, I hope God continues to bless you.

Dr. Daniel Wamwangi: I would like to thank him for his aid and useful suggestions in measuring electrical conductivity of my samples, from Physics Department at the University of Witwatersrand

Professor Alexander Ziegler: For his help in the SEM analysis and also teaching me how to use it on my own, from Biology Department, University of Witwatersrand

Ceramic group: I would like to thank all my colleagues for their useful suggestion and help in the laboratory especially Amanda Mckie, Jethro Garreth and Peter Bush, you help was much appreciated.

Family: I would like to thank all my family members that gave me motivation through out this the period I was doing my Masters. I do not believe I would have managed to finish my Masters in record time if it wasn't for you all.

Friends: I would also like to give special thank to all my friends at the University of Witwatersrand that believed in me and gave me useful advice. To all of my friends that are not at Witwatersrand that kept me motivated and made sure that I see my Masters project through. I love you all

Financial Sponsors: The continuous financial support from Element Six (Pty) Ltd – Diamond Research Laboratory and DST/NRF Centre of Excellence in Strong Materials (CoE-SM), Financial Aid Office of the University of the Witwatersrand are both acknowledged since without their financial support this research would not have succeeded.

Table of Contents

Declaration.....	i
Abstract.....	ii
Dedication.....	iv
Acknowledgements.....	v
Table of Contents.....	vii
List of Figures.....	x
List of Tables.....	xv
1.0 Introduction.....	1
1.1 Justification of the study.....	2
1.2 Objective of the study.....	3
1.3 Scope of the research.....	3
1.4 Contribution to knowledge.....	4
1.5 Structure of the dissertation.....	5
2.0 Literature review.....	6
2.1 Alumina ceramic.....	7
2.1.1 Sintering conditions of alumina.....	8
2.1.2 Dispersion of alumina powder.....	8
2.2 Carbon Nanotubes (CNTs).....	9
2.2.1 Structure and properties.....	9
2.2.2 Synthesis.....	11
2.2.3 Purification.....	13
2.2.4 Dispersion of carbon nanotubes.....	13
2.3 Titanium Carbide.....	14
2.4 Reinforcement of Alumina.....	15
2.4.1 Zirconia reinforcement.....	15
2.4.2 Niobium carbide reinforcement.....	16
2.4.3 Titanium Carbide Reinforcement.....	18
2.4.4 Carbon nanotubes reinforcement.....	22
2.5 Boron nitride.....	29
2.6 Coating CNTs with hexagonal Boron Nitride (hBN).....	31

2.6.1	Urea route.....	31
2.6.2	Nitridation route.....	33
3.0	Experimental Procedure.....	36
3.1	Materials and Characterization	36
3.1.1	Materials used	36
3.1.2	Equipment used.....	37
3.2	Preparation of multi walled carbon nanotubes (MWCNT).....	46
3.3	Dispersion of pure alumina powder	48
3.4	Dispersion of pure Titanium Carbide powder.....	48
3.5	Coating carbon nanotubes with hexagonal boron nitride.....	50
3.6	Suspension formation and mixing of the suspensions	51
3.6.1	Al ₂ O ₃ + CNTs suspension formation	51
3.6.2	Al ₂ O ₃ + TiC suspension formation	52
3.6.3	Al ₂ O ₃ + TiC + CNTs suspension formation.....	52
3.7	Compaction of Al ₂ O ₃ + CNT sample.....	53
3.8	Sintering of the composites powders	53
3.9	Thermal Etching of pure Al ₂ O ₃ and [Al ₂ O ₃ +CNTs) samples	54
3.10	Density Measurements.....	54
3.11	Cutting, mounting and polishing the sintered samples	55
3.12	Fracture surface of Al ₂ O ₃ + CNTs	56
3.13	Analysis of materials.....	56
4.0	Experimental findings	59
4.1	Preparation of the Carbon nanotubes	60
4.2	Coating and dispersion of Carbon nanotubes with hBN	61
4.3	Compaction of Al ₂ O ₃ + CNT sample.....	63
4.4	Sintering curves of the samples	63
4.4.1	Al ₂ O ₃ sample.....	63
4.4.2	[Al ₂ O ₃ +CNTs] sample	65
4.4.3	[Al ₂ O ₃ +TiC] sample.....	66
4.4.4	[Al ₂ O ₃ +CNTs +TiC] sample	67
4.1	Density measurements of the sintered ceramics	68
4.2	Microstructural analysis of the sintered samples	69

4.2.1	Alumina sample	69
4.2.2	[Al ₂ O ₃ + CNTs (3 vol. %)] sample	71
4.2.3	[Al ₂ O ₃ + TiC (30 wt. %)] sample	76
4.2.4	Al ₂ O ₃ + CNT + TiC	79
4.3	Mechanical Properties.....	80
4.4	Electrical Properties	80
4.4.1	Pure Alumina	80
4.4.2	Al ₂ O ₃ +CNTs	81
4.4.3	Al ₂ O ₃ + TiC.....	81
4.4.4	Al ₂ O ₃ + CNTs +TiC.....	82
5.0	Discussion.....	84
5.1	Preparation of carbon nanotubes.....	84
5.2	Coating of CNTs.....	85
5.3	Relationship between microstructure and densification	88
5.3.1	Addition of CNTs into Alumina	88
5.3.2	Addition of TiC into Alumina.....	93
5.3.3	Addition of CNTs and TiC into Al ₂ O ₃	95
5.4	Relationship between microstructure and hardness	96
5.4.1	Addition of CNTs into Alumina	96
5.4.2	Addition of TiC into Alumina.....	97
5.5	Relationship between microstructure and fracture toughness.....	98
5.1.1	Addition of CNTs into Alumina	98
5.1.2	Addition of TiC into Alumina.....	100
5.1.3	Addition of CNTs and TiC into Al ₂ O ₃	102
5.6	Electrical properties measurements	103
6.0	Conclusions and Future Work.....	107
7.0	References.....	111
8.0	Appendix.....	116

List of Figures

Figure 1: Illustration of different types of CNTs, (a) SWCNT (b) DWCNT and (c) MWCNT.....	9
Figure 2: Models of three atomically perfect SWNT structures.....	10
Figure 3: Schematic representation of carbon arc discharge method	11
Figure 4: Growth mechanism of carbon nanotubes through CVD	12
Figure 5: Polished section of $\text{Al}_2\text{O}_3 - \text{ZrO}_2$ after sintering.....	15
Figure 6: SEM image showing microstructure of NbC/ Al_2O_3 composite (polished surface) white NbC grains within grey Alumina.....	16
Figure 7: Comparison of hardness and relative density of Al_2O_3 and Al_2O_3 -NbC materials investigated in this work with other Al_2O_3 composite systems	17
Figure 8: Comparison of fracture toughness and flexural strength of Al_2O_3 and Al_2O_3 -NbC materials investigated in this work with other Al_2O_3 composite systems	17
Figure 9: Optical microscope images of $\text{Al}_2\text{O}_3 + \text{TiC}$ (26.3 wt. %) + TiH_2 (3.7 wt. %) sintered at 1840 °C in N_2 (a) as sintered (b) sintered and then hot isostatically pressed at 1300 °C and 100 MPa in Argon.....	19
Figure 10: Optical microscope images of $\text{Al}_2\text{O}_3 + \text{TiC}$ (30 wt. %) composites; (a) (b) milled and hot pressed (c) (d) pressureless sintered (e) (f) pressureless sintered and hot isostatically pressed	21
Figure 11: Shrinkage, relative density and electrical resistance vs. volume% of CNT in CNT/Alumina powder	23
Figure 12: Flexural strength (a) and fracture toughness (b) vs. volume % of CNT in CNT/Alumina powder	24
Figure 13: SEM micrograms of Alumina reinforced with 3 vol. % of CNTs, showing (a) grain interface bridging (b) CNT bridging (c) both grain interface and CNT bridging (d) fracture surface showing CNT pull outs.....	25
Figure 14: The SEM images of the fracture surface of the composite sintered at 1450°C.....	27
Figure 15: The SEM images of the fracture surface of the composite sintered at 1500°C.....	27
Figure 16: FESEM micrograms of the indentation crack of a SPS-consolidated 3.5 vol. % CNT in Al_2O_3 ceramic composite.....	28

Figure 17: hexagonal crystal structure exhibited by hBN	29
Figure 18: Schematic representation of functionalizing CNTs with nitric acid	31
Figure 19: FESEM images of h-BN coated MWCNT's (a) heavily coated MWCNT's and (b) less coated MWCNT's.....	32
Figure 20: TEM images of hBN coated MWCNTs	32
Figure 21: SEM images of heat treated-MWCNT after coating.....	34
Figure 22: TEM images of BN coated MWCNT's ((a) and (b)), the solid lines indicate the line-scan EELS analysis (b) and (d) are HRTEM images of the framed region in (a) and (c) respectively	34
Figure 23: The ultrasonic probe, HD 2200	38
Figure 24: The particle size analyzer, Mastersizer 2000	39
Figure 25: The attritor ball mill szegvari attritor system type B.....	39
Figure 26: Planetary ball mill, Fritsch Pulverisette 6	40
Figure 27: The spark plasma sintering (SPS) machine, HP D 5/2.....	41
Figure 28: The tube furnace, Elite TSH17/75/150.....	42
Figure 29: Vickers hardness tester, V-100-A2	43
Figure 30: The DC 41-40 SMU	44
Figure 31: Optical microscope, Axiotech 25 HD	45
Figure 32: A Philips scanning electron microscope, XL30 series	46
Figure 33: Transmission electron microscope, model 3000	46
Figure 34: The TEM images of CNTs showing that the CNTs had no amorphous carbon (a) and they had smooth surface (b).....	48
Figure 35: Particle size distribution of pure alumina, it shows unimodal particle size distribution with $d(0.1)=0.14 \mu\text{m}$, $d(0.5) = 0.22 \mu\text{m}$ and $d(0.9)=0.33 \mu\text{m}$	48
Figure 36: A graph showing the variation of viscosity in suspensions as a function of the Lubrizol content at a constant shear rate (200s^{-1}).	49

Figure 37: Particle size distribution of TiC with 6.5 wt. % lubrizol, it shows unimodal particle size distribution with $d(0.1)=0.14 \mu\text{m}$, $d(0.5) = 0.18 \mu\text{m}$ and $d(0.9) = 0.23 \mu\text{m}$	50
Figure 38: Particle size distribution of TiC with 8.5 wt. % lubrizol, it shows unimodal particle size distribution with $d(0.1) 0.51 \mu\text{m}$, $d(0.5)= 0.57 \mu\text{m}$ and $d(0.9)=0.64 \mu\text{m}$	50
Figure 39: Indication of how the diagonals of the Vickers indentations and the crack lengths were measured	57
Figure 40: Images of the (Al_2O_3 , [$\text{Al}_2\text{O}_3 + \text{CNTs}$ (3 vol. %)] and [$\text{Al}_2\text{O}_3+\text{TiC}$ (30 wt. %)] samples, the black samples being the conducting samples.....	59
Figure 41: TEM images of multi walled carbon nanotubes in a mixture with amorphous carbon as pointed by the red arrows.	60
Figure 42: TEM image of carbon nanotube showing that it had a diameter of 42 nm	61
Figure 43: TEM images of hBN coated CNTs ((a), (c)) and uncoated CNTs ((b), (d)) the hBN coating is shown by the interface pointed by the arrows which is only present on the coated CNTs but not the uncoated CNTs.....	62
Figure 44: TEM images of CNTs coated with hBN, the uneven surface of the CNTs shows that the coating was flaking off due to the ultrasonication.	62
Figure 45: Optical microscope images of [$\text{Al}_2\text{O}_3 + \text{CNT}$ (3 vol. %)] green compact	63
Figure 46: Relationship between temperature and piston travel (a) and temperature and piston speed (b) during sintering of Al_2O_3 sample	64
Figure 47: Relationship between temperature and piston travel (a) and temperature and piston speed (b) during sintering of [$\text{Al}_2\text{O}_3 + \text{CNTs}$ (3 vol.%)] sample.....	65
Figure 48: Relationship between temperature and piston travel (a) and temperature and piston speed (b) during sintering of [$\text{Al}_2\text{O}_3 +\text{TiC}$ (30 wt%)] sample	66
Figure 49: Relationship between temperature and piston travel (a) and temperature and piston speed (b) during sintering of [$\text{Al}_2\text{O}_3 +\text{CNTs} +\text{TiC}$] sample	67
Figure 50: Optical microscope images of pure alumina showing that the sintering was successful since there are no pores showing on the polished cross section.	69
Figure 51: SEM images of alumina thermally etched at 1200°C for 60 min., showing alumina grain size between $2 - 4 \mu\text{m}$	70

Figure 52: SEM images of alumina thermally etched at 1300°C for 60 min., showing alumina grain size between 2 – 4 μm	70
Figure 53: Optical microscope image of [Al ₂ O ₃ + CNT (30 wt. %)] dispersed aggressively, sintered at 1600°C, 35 MPa	71
Figure 54: Optical microscope image of [Al ₂ O ₃ + CNT (30 wt. %)] dispersed less aggressively, sintered at 1600°C, 35 MPa	71
Figure 55: SEM images of [Al ₂ O ₃ + CNTs (3 vol. %)] sample that was aggressively milled, showing a distribution of carbon nanotubes (as black spots) within alumina.	72
Figure 56: SEM images of [Al ₂ O ₃ + CNTs (3 vol. %)] sample that was milled less aggressively, showing a distribution of carbon nanotubes (as black spots) within alumina.	72
Figure 57: SEM images [Al ₂ O ₃ + CNTs (3 vol. %)] sample, thermally etched at 1300°C under argon atmosphere, showing grain size between 0.3 – 0.5 μm. the EDS shows that carbon atoms are mostly found along the cracks and grain boundaries (as pointed by the arrows).	74
Figure 58: SEM images of [Al ₂ O ₃ + CNTs (3 vol. %)] fractured surface showing CNTs sticking out of the alumina matrix as shown by the arrows.	75
Figure 59: Optical microscope image of [Al ₂ O ₃ + TiC (30 wt. %)] sintered at 1600°C, 35 MPa	76
Figure 60: Optical microscope image of [Al ₂ O ₃ + TiC (30 wt. %)] sintered at 1700°C, 35 MPa	76
Figure 61: SEM images of [Al ₂ O ₃ + TiC (30 wt. %)] sintered at 1600°C, 35 MPa.....	77
Figure 62: SEM images of [Al ₂ O ₃ + TiC (30 wt. %)] sintered at 1700°C, 35 MPa.....	77
Figure 63: SEM images of [Al ₂ O ₃ + TiC (30 wt. %)] sample, showing the path of a crack propagated through the surface of the polished sample. The TiC grains deflect the crack therefore changing the crack path.	78
Figure 64: SEM images of [Al ₂ O ₃ + TiC (30 wt. %)] sample fractured surface, the curved spaces could be where the TiC were attached to the alumina matrix.....	78
Figure 65: Optical microscope images of [Al ₂ O ₃ + CNT (3vol. %) + TiC (30 wt. %)] sintered at 1650°C, 35 MPa.....	79
Figure 66: SEM images of [Al ₂ O ₃ + CNT (3vol. %) + TiC (30 wt. %)] sintered at 1650°C, 35 MPa, showing that the TiC and CNTs (shown by the arrows) were well distributed within the alumina matrix.	79
Figure 67: Relationship between voltage and current on the Al ₂ O ₃ + CNTs sample	81

Figure 68: Relationship between voltage and current on the Al ₂ O ₃ + TiC sample	81
Figure 69: Relationship between voltage and current on the Al ₂ O ₃ + CNTs + TiC sample.....	82
Figure 70:Variation of Al ₂ O ₃ density when it is reinforced with CNTs and TiC and the mixture of TiC and CNTs.....	95
Figure 71: Variation of Al ₂ O ₃ fracture toughness after reinforce with CNTs and TiC and the mixture of TiC and CNTs	102
Figure 72: Variation of Al ₂ O ₃ hardness when it is reinforced with CNTs and TiC and the mixture of TiC and	103
Figure 73: Shrinkage, relative density and electrical resistance vs. volume % of CNT in CNT/Alumina powder ^[39]	Error! Bookmark not defined.

List of Tables

Table 1: Properties of Alumina ceramic	7
Table 2: Properties that are displayed by different types of CNT	10
Table 3: Titanium Carbide ceramic properties	14
Table 4: Effects of pressing pressure on densification of $\text{Al}_2\text{O}_3 + \text{TiC}$ (30 wt. %)	18
Table 5: Comparison of properties of $\text{Al}_2\text{O}_3 + \text{TiC}$ (26.3 wt. %) + TiH_2 (3.7 wt. %) sintered in N_2 at 1840 °C. Subsequently hot isostatically pressed in Argon	18
Table 6: Properties of pressureless-sintered $\text{Al}_2\text{O}_3+\text{TiC}$ (30 wt. %) composites made by the reaction machined above and sintered in Argon.....	20
Table 7: The MWCNTs dimensions and density.....	22
Table 8: Fracture toughness of CNT reinforced Al_2O_3 and pure Al_2O_3 , measured at room temperature	26
Table 9: The hBN properties.....	30
Table 10: The list of materials used and their manufacturer’s specifications.....	36
Table 11: Sintering conditions used for sintering different composite powders using SPS	53
Table 12: The grinding and polishing steps that were used to polish all the samples	55
Table 13: The dimensions of the samples and the calculated area	58
Table 14: The density results for all the samples, with their theoretical densities and the sintering temperatures.....	68
Table 15: Mechanical properties of alumina with different reinforcements.....	80
Table 16: Electrical properties of the different samples	83
Table 17: The comparison of MWCNTs properties obtained in this study and in the literature..	84
Table 18: Comparison of the results obtained after coating MWCNTs using Nitridation and Urea route	86
Table 19: Comparison of the results obtained after coating MWCNTs with the results from the literature	87

Table 20: Comparison of the results obtained after sintering monolithic Al_2O_3 and the results from the literature	90
Table 21: Comparison of the results obtained after sintering Al_2O_3 + CNTs and the results from the literature	91
Table 22: Comparison of the results obtained after sintering Al_2O_3 + TiC and the results from the literature	94
Table 23: Comparison of the mechanical properties obtained after sintering Al_2O_3 + CNTs and the results from the literature	96
Table 24: Comparison of hardness property obtained after sintering Al_2O_3 + TiC and the results from the literature	98
Table 25: Comparison of the fracture toughness and density obtained after sintering Al_2O_3 + CNTs and the results from the literature	99
Table 26: Comparison of fracture toughness obtained after sintering Al_2O_3 + TiCs and the results from the literature	101

Chapter One

1.0 Introduction

Alumina ceramics belong to the group of oxide ceramics which are the most commonly used commercially today because of their thermal stability at high temperatures and their relative low production cost. These ceramics are also chemically stable at high temperatures in an oxidizing atmosphere (oxygen atmosphere). In this group of ceramics the oxygen ion (O^{2-}) has a filled shell electron configuration ($1s^2s^2p^6$), which makes electron transfer complete therefore making the bonding in these ceramics mostly ionic rather than covalent ^[1]. The group of ceramic oxides is further divided into Traditional and Advanced ceramics. The traditional ceramics are those based on natural raw materials such as clays. Alumina falls under the advanced ceramics group, which requires careful attention of processing and higher purity and quality of the starting materials.

There are two main properties of alumina that limit its use commercially. It has a low fracture toughness compared to other ceramics (between 3 – 5 MPa√m). The fracture toughness of alumina depends on the densification obtained during sintering and the purity of the starting powder ^[2]. The other property that limits the use of alumina is its non conducting behavior [ref]. The high electrical resistivity of this material makes it impossible to cut alumina ceramic into smaller pieces by electron discharge machining (EDM); but instead diamond blades are used. This increases production cost and hence the final market cost. Several efforts have been made to increase alumina fracture toughness by incorporating a second phase within this material's powder before sintering [ref].

Materials like zirconia, niobium carbide and titanium carbide have been incorporated into alumina to try and increase its fracture toughness; this will be discussed in detail in Chapter 2. Cutler *et al.* ^[3] reported that reinforcement of alumina with TiC and hot pressing the powder increased the alumina fracture toughness but compromised the other properties like density and hardness. CNTs were also used to increase alumina's fracture toughness and electrical conductivity. Sun *et al.* ^[4] reported that the problems encountered after reinforcing alumina with CNTs was that after hot pressing (temperature; 1300-1600°C, 30MPa) and pressure-less sintering

(1600°C) the CNTs were destroyed by the sintering conditions and therefore could not serve as reinforcement. Sun *et al.* ^[4] also reported that even if the CNTs survived the sintering conditions they had poor adhesion to the alumina matrix; this was confirmed by a large number of CNT pull-outs as seen on the alumina fractured surface. These problems made it difficult to reinforce alumina with CNTs. Estilli *et al.* ^[5] reported that the addition of CNTs (1wt. %) to the alumina sintered using SPS at 1600°C increased alumina fracture toughness by 67% and the samples were 99% dense.

1.1 Justification of the study

It has been reported by other researchers that the reinforcement of alumina with CNTs presents challenges that are yet to be solved. The CNTs have a high potential of improving alumina electrical properties so that it can be cut using electron discharge machine (EDM) as opposed to diamond blades which are currently used to cut this material. EDM cutting is cheaper than using diamond blades hence the cost of this material will be reduced if it can be cut using EDM.

The main focus of this study is to improve Al₂O₃ fracture toughness and its electrical conductivity by reinforcement with CNTs and TiC. In this study the following approach will be used to achieve this goal.

It will be attempted to solve the problem of poor adhesion of CNTs to the alumina matrix by coating them with hexagonal boron nitride (hBN), which is chemically similar to graphite but has superior properties comparatively. It is proposed to use hBN as an interface between CNTs and the alumina matrix. Previously it has been proved that CNTs cannot withstand the high temperature sintering conditions when a hot press is used ^[4]. This type of furnace heats up to the sintering temperature at a very low heating rate this increases the chances of destroying CNTs during sintering. It is proposed to use Spark Plasma Sintering (SPS) for this work. SPS heats up to the sintering temperature at a high heating rate. This method will reduce dwelling time at high temperatures thus reducing the risk of CNT destruction during sintering.

TiC will be used to mainly improve alumina hardness and fracture toughness properties since it is harder phase than Al₂O₃ and have higher thermal expansion coefficient to alumina (TiC = 8.31

E-4 and 7.5×10^{-4})^[6]. The challenges that were previously experienced while reinforcing Al_2O_3 with TiC would be eliminated by using sub-micron TiC powder with a similar particle size to that of the Al_2O_3 and sintering the composite powder using SPS. This would minimize the thermal expansion mismatch effects of TiC and Al_2O_3 , which are believed to reduce density. Alumina with a high fracture toughness and high electrical conductivity, will allow it to be used in most industries.

1.2 Objective of the study

The main objective of the research is to improve the Al_2O_3 fracture toughness and electrical conductivity that inhibit its wide use commercially and industrially. These properties will be improved by reinforcing alumina with TiC and CNTs through the following objectives:

- ✓ Coating CNTs with hBN and dispersing them.
- ✓ Dispersing Alumina, TiC and CNT's individually with the aid of necessary dispersants and mixing them through milling.
- ✓ Densifying the mixture of Alumina, TiC and CNT's using SPS.
- ✓ Microscopy analysis and mechanical properties measurements of the sintered ceramics.
- ✓ Measurements of electrical properties of the sintered ceramics

1.3 Scope of the research

This study was divided into three groups. The first group involved alumina and CNT's, the second group involved alumina and TiC and lastly the third group involved alumina + CNTs + TiC. Alumina was dispersed by ultrasonication and CNT's were dispersed by both ultrasonication and milling. After mixing the alumina and CNTs mixture it was dried and sieved and then sintered using SPS. Pure alumina was also sintered at the same sintering conditions as the mixture of alumina and CNTs for comparison. The sintered pieces were analyzed by microscope (Optical and SEM); then mechanical and electrical properties were measured. The second part of the work was to study the Alumina and TiC system. TiC was dispersed using a dispersant through milling and it was then mixed with already dispersed alumina. The mixture

was mixed, dried and sieved then sintered using SPS. The sintered pieces were analyzed by microscope (Optical and SEM), and then mechanical and electrical properties were measured. After the first two systems were understood subsequently the third group was mixed and then sintered. The mechanical and electrical properties were then measured.

1.4 Contribution to knowledge

The objective of this work is to improve fracture toughness and electrical properties of Al_2O_3 by reinforcing it with TiC and CNT. By using the methodology proposed above the following contribution to knowledge is expected:

- ✓ Provide suitable sintering conditions for $\text{Al}_2\text{O}_3 + \text{CNT}$ system
- ✓ Provide suitable sintering conditions for $\text{Al}_2\text{O}_3 + \text{TiC}$ system
- ✓ Provide suitable sintering conditions for $\text{Al}_2\text{O}_3 + \text{CNT} + \text{TiC}$ system from the sintering conditions of the above mentioned systems.
- ✓ Study hardening mechanisms provided by TiC and CNTs in alumina through micro-structural analysis.
- ✓ Study toughening mechanism provided by TiC and CNTs in alumina through micro-structural analysis

1.5 Structure of the dissertation

The dissertation is sectioned into 6 chapters, starting with **Chapter 2**, which gives the background information about the main materials that were used. Literature review (Chapter 2) starts by discussing the background information about alumina (Al_2O_3), carbon nanotubes (CNTs), titanium carbide (TiC) and boron nitride (BN). Chapter 2 further describes how Al_2O_3 has been reinforced before by ZrO_2 , NiC, TiC and CNTs mainly trying to increase Al_2O_3 fracture toughness.

Chapter 3 (Experimental details) starts by giving the list of materials to be used with their supplier specifications. The equipment used with their suppliers and types/models are also listed. This chapter gives details of all the experiments that were carried out. The findings that were obtained from the experiments are given in Results sections (**Chapter 4**) with all the analysis and detail of how the results were obtained. **Chapter 5** (Discussion) describes in detail the results that were obtained linking them to the findings that were obtained by other researchers as reported in the literature review section (chapter 2). The dissertation ends with the **Chapter 5** (Conclusion). This chapter gives conclusions that were drawn from the results; this chapter also gives the recommendations for future work for this study.

Chapter Two

2.0 Literature review

For most of the “advanced” ceramics like alumina (Al_2O_3), Zirconium Oxide ZrO_2 , Titanium oxide (TiO_2), research was initially done for structural applications. However problems due to the high production cost and reliability of these materials have made most researchers to pursue applications utilizing different properties of these materials, such as optical, electrical and high chemical inertness^[1]. Therefore different methods have been employed in trying to improve the mechanical, electrical and optical properties of these materials. In this work alumina was the main focus.

This research was motivated by the potential that the multi-walled carbon nanotubes (MWCNTs) can improve the mechanical and electrical properties of ceramics due to their superior properties. Alumina is a ceramic material that is widely used commercially but its use is limited due to its low fracture toughness and non electrical conducting behavior^[7]. Incorporation of MWCNTs and titanium carbide (TiC) into alumina has the potential of improving both mechanical and the electrical conductivity of alumina.

This chapter begins by giving background information of each material that is used during the course of the study, namely Al_2O_3 , TiC and CNTs. It further describes how Al_2O_3 has been reinforced with different materials previously to improve its mechanical properties. It also covers the difficulties experienced and results obtained. This chapter is completed by describing the methods for coating the CNTs with hexagonal Boron Nitride (hBN).

2.1 Alumina ceramic

Alumina is categorized as an advanced ceramic. This material is produced with controlled quality and purity of the raw materials, and for which the processing conditions are carefully controlled. Other advanced ceramic oxides include ZrO_2 and TiO_2 [1].

Alumina enjoys wide industrial use because of its combination of mechanical properties, high corrosion resistance and low price [8]. Representative properties of this material are given in Table 1.

Table 1: Properties of Alumina ceramic [1] [9] [10] [11]

Fracture toughness MPa \sqrt{m}	Hardness (GPa)	Thermal conductivity (W/ m. K) at 25 °C	Flexural strength (MPa)	Modulus of elasticity (GPa)	Density (g/cm⁻³)	Poisson ratio
3 - 5	15 - 20	18	275 – 700	393	3.99	0.27 – 0.30

Alumina exists in different transitional oxide forms with the alpha (α) phase also known as Corundum being the most stable at low temperatures. It has a mixture of covalent and ionic bonding which gives rise to its properties [2]. The properties exhibited by alpha phase are dependent on the starting particle size and processing conditions [2]. The different transitional alumina phases are denoted as γ , δ , χ , l, k and η . These alumina meta-stable phases are transformable to other phases by variation of temperature [2]. The most commercially used and the most stable form of alumina is corundum (α). It is widely used for its properties; hardness, high thermal conductivity, wear resistance, high strength and stiffness etc. One of the major problems inhibiting use of this material is its low fracture toughness compared to other ceramics [7]. Furthermore, alumina is electrically non conductive, and therefore finishing of parts made with this material needs to be done by cutting as opposed to electron discharge machining [7].

Alumina is commercially used in wear pads, high temperature insulators, gas laser tubes, seal rings etc ^[10]. Improving mechanical properties of alumina has been continuously researched during the past several decades. In terms of improving alumina properties, fracture toughness, hardness and electrical conductivity are the most important in order to widen alumina uses commercially and industrially. There are various methods of toughening alumina ceramics that have been studied and utilised in the last decade without greatly compromising the other properties like hardness and density. These will be discussed later in the chapter.

2.1.1 Sintering conditions of alumina

The particle size of the alumina powder directly affects the sintering temperature and the densification rate ^[10]. Different researchers have reported different sintering conditions to sinter alumina and they are all affected by the particle size of the starting alumina powder. It was reported that high density (99.9 % of theoretical) was reached after sintering at ambient pressure at a temperature of 1577 °C and 1277 °C for 1 and 2 hours respectively for powder with particle sizes 0.5 µm and 0.1 µm respectively ^[10]. S.W Kim and W.S Chung sintered alumina at ambient pressure and at a temperature of 1550°C for powder with 0.5 µm particle size. They obtained a 99.9 % density (Theoretical density 3.98 g cm⁻³). It was concluded that the smaller the alumina particle size the lower the sintering temperature to produce highly dense ceramic ^[12]. Hot pressing and SPS were also investigated and the results showed that 98 - 99.9 % relative density was achieved with applied pressure ranging from 10 – 30 MPa and sintering temperature of 1500°C ^[2].

2.1.2 Dispersion of alumina powder

Dispersing fine powders is generally difficult since the amount of dispersant used needs to be proportional to the surface area of the powder ^[2]. The most effective way of dispersing fine particle sized alumina in deionised water is by pH adjustment to 4.4 with an acid ^[5]. If an acid cannot be used due to compatibility with the solvent being used or if it has negative effects on the system being studied, other more aggressive methods like ultrasonication and milling have been used ^[4].

2.2 Carbon Nanotubes (CNTs)

2.2.1 Structure and properties

CNTs are an interesting new molecular form of carbon that belongs to the fullerene family [13]; they were first discovered in 1991 [14]. CNTs have played a significant role in both science and engineering due to their combination of good properties. They are the first material to have a combination of good thermal, electrical/electronic and mechanical properties [14]. CNTs are carbon allotropes that have sp^2 intra atomic bonds which are stronger than those displayed by diamond, which are sp^3 [15]. The structure of carbon nanotubes can be described as a nanoscale graphene cylinder with a very high aspect ratio. There are 3 different types of CNTs available commercially; they are described according to the number of graphene sheets rolled to form a cylinder with varying diameters. They are namely, single walled carbon nanotubes (SWCNTs), double walled carbon nanotubes (DWCNTs) and multi walled carbon nanotubes (MWCNTs) [16], with the SWCNT and MWCNT being the most common ones. The difference between SWCNT, DWCNT and MWCNT (Fig. 1) is mainly the number of graphene sheets within the tube which give rise to the different properties.

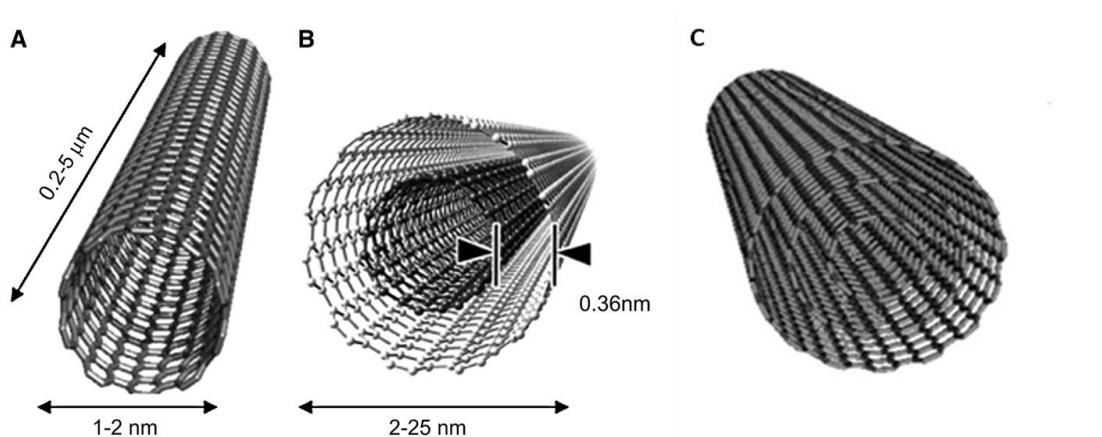


Figure 1: Illustration of different types of CNTs, (a) SWCNT (b) DWCNT and (c) MWCNT [17]

CNTs can also have different conformation namely zigzag, armchair and chiral (Fig. 2).

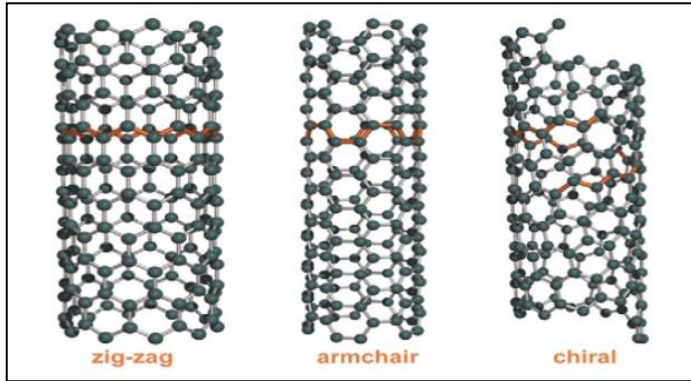


Figure 2: Models of three atomically perfect SWNT structures ^[18]

These properties that CNTs display make them ideal for a wide range of applications ^[14]. Their properties are listed in Table 2.

Table 2: Properties that are displayed by different types of CNTs ^{[12] [14] [18] [19]}

Properties	Magnitudes
Young's modulus (TPa)	≈ 1
Tensile strength (GPa)	63
Thermal conductivity (W/m. K)	
<ul style="list-style-type: none"> • SWCNTs 	5800
<ul style="list-style-type: none"> • MWCNT 	3000
Density (g/cm^{-3})	1.3

CNTs have Young's modulus that is up to 5 times higher than that of steel and tensile strength that is up to 50 times higher than that of steel ^[14]. Their thermal conductivities are significantly higher than that of diamond and copper which are 2000 ^[14] and 400 W/ m. K ^[14] respectively. The resistivity of SWNTs was found to be $\approx 10^{-4} \Omega.\text{cm}$ at 300 K ^[20] and MWNTs are able to

carry a current density of $10^7 - 10^9 \text{ Acm}^{-2}$ [21] thus making CNTs the most conductive tubes than any other known tubes/wires.

2.2.2 Synthesis

2.2.2.1 Carbon arc discharge

Carbon arc discharge is the earliest method used for production of CNTs [22]. The reaction furnace was equipped with two graphite electrodes (one being the cathode and the other the anode). An inert gas was introduced into the furnace while there was a large current applied to the two graphite electrodes. The applied current consequently creates a spark between the two electrodes which instantaneously vaporised the tip of the anode and this carbon gas formed the carbon nanotubes along the walls of the reaction chamber/furnace. The nanotubes produced through this method are free of defects. However other forms of carbonaceous species are also formed which are difficult to separate and the production efficiently is also considered as low. The schematic presentation of carbon arc discharge is shown in Figure 3.

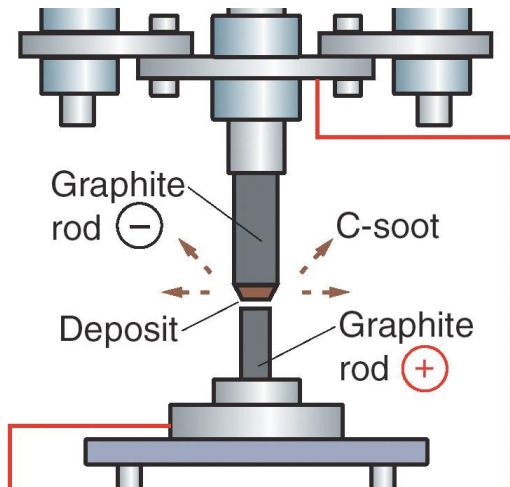


Figure 3: Schematic representation of carbon arc discharge method [23]

2.2.2.2 Chemical Vapour Deposition

CNTs can be produced by a process called chemical vapour deposition (CVD) [24]. This process uses a hydrocarbon gas as a carbon source (e.g. Acetylene) which is catalyzed by a transition metal catalyst (e.g. Fe, Ni, Co) at high temperature between 400 – 1000 °C depending on the type of CNTs needed, for example when MWCNTs are needed the furnace temperature will be adjusted to 800°C and when a mixture of MWCNT and SWCNTs is needed the temperature will be set at 850 °C as published by Iyuke *et al.* [25]. The flow rate at which the carbon source enters the furnace is important in determining which type of CNTs will be formed. The schematic demonstration of the catalysis is shown in Figure 4.

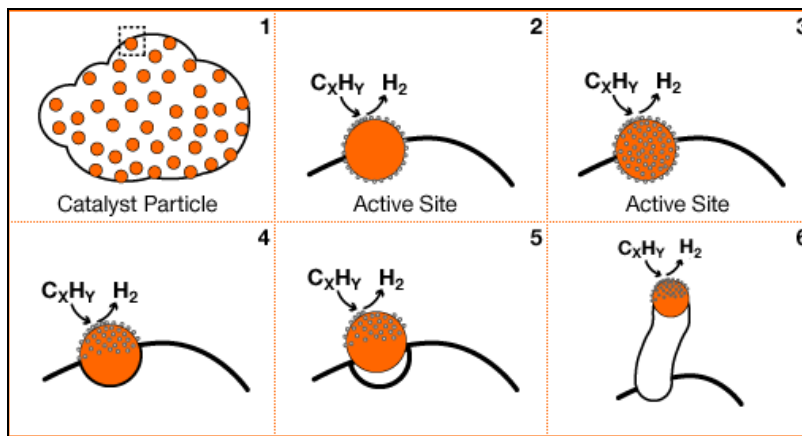


Figure 4: Growth mechanism of carbon nanotubes through CVD [26]

This method of producing CNTs consists of a vertical heat reactor which can have a sensitive microbalance at the centre of the heat reactor to monitor any mass changes. A mass between 5-10 mg of iron based catalyst (e.g. ferrocene or Fe₂O₃) is placed at the centre of the heat reactor on a platinum container. The production first step is to decompose the iron compound at a temperature $\approx 700^{\circ}\text{C}$ to form Fe²⁺ ions which serve as the active sites during the production of the CNTs. The heating reactor is connected to the gas pipe which contains a mixture of the hydrocarbon and hydrogen. After the iron compound has been decomposed at a high temperature the hydro carbon gas line is opened at a specific flow rate and the hydrocarbon will react with the active sites of the catalysts to form CNTs [27] (Fig. 4).

2.2.3 Purification

CNTs can be purified according to three different methods namely; chemical, physical and multi steps technique ^[18]. Chemical purification is the most commonly used technique where the CNTs are purified using an acid which automatically induces some functional groups (-OH and -COOH) on to the tubes (functionalization). During chemical purification the metallic impurities are dissolved in an acid and the carbonaceous impurities get oxidized, reducing the amorphous carbon content ^[18]. Physical purification is a method used if the final CNT needed should have less structural defects since with this method no oxidation takes place. Oxidation can create structural defects as the walls of the CNTs. This method works on the basis of the physical size, standard gravity and magnetic properties of the sample and does not involve oxidation ^[18]. Multi – step purification is basically the use of both chemical and physical purification methods ^[18].

2.2.4 Dispersion of carbon nanotubes

CNTs are non polar, therefore they mix with non polar solvents (like dissolve like). After functionalization the tubes contains alcohol (-OH) and carboxyl (-COOH) groups which makes them CNTs slightly polar. Therefore functionalized CNTs were dispersed in continuously ultrasonicated deionised water with small addition of polyvinylpyrrolidone (PVP) ^[28]. MWCNTs were also dispersed in deionised water with the use of the dispersant polyethylene amine (concentration of 300 ppm) then ultrasonicated ^[4].

2.3 Titanium Carbide

Titanium carbide (TiC) is one of the transition metal carbides that is widely used commercially for its unique combination of properties. It has a black appearance and a face centered cubic (FCC) structure [29]. Titanium carbide wide commercial use is due to its high melting point of 3065°C (3338 K) [30], high hardness, high strength even at high temperatures [29], high thermal conductivity, high wear and corrosion resistance and chemical stability [31] [32] [33]. It is mostly used in tools bits, structural components that operate at high temperatures, in wear resistant parts [29] and also for tribological applications [34]. Properties of TiC are listed in Table 3.

Table 3: Titanium Carbide ceramic properties [35] [36]

Properties	Density (g.cm ⁻³)	Hardness (GPa)	Fracture toughness (MPa √m)	Electrical Resistivity (Ω*m)	Yield Strength (GPa) for single crystal
	4.92	24	4 – 6	0.003...0.008	20

Titanium Carbide ceramic can be produced through different methods. Traditionally it was synthesized by TiO₂ powder reduction using carbon black [30] [31] but this method is unfavourable since it requires high temperature (1700 - 2100°C) and high reaction time (10 - 24 hours) [31] [32] [33]. It has also been produced by sol-gel processes, self-heated sintering and carbothermal reaction [37] [38], but these methods have shown some drawbacks by producing non-stoichiometric composition, formation of TiC_xO_y and also formation of coarse sintered structure [30]. A new method called Magnesium Thermal Reduction (MTR) of producing TiC which eliminates all the drawbacks of the other methods has been recently introduced [31]. In MTR titanium and carbon atoms are initially in the form of chlorides (TiCl₄ and CCl₄) and are reacted in the presence of liquid magnesium to produce TiC. Some of the properties of TiC ceramics are affected by the starting powder purity and particle size. The higher the purity and finer the particles, the higher would be the mechanical strength [30].

2.4 Reinforcement of Alumina

2.4.1 Zirconia reinforcement

D.S Patil *et al.* [39] worked on transformation toughening method as a way of improving alumina fracture toughness. The alumina starting powder had a particle size of 0.52 μm and that of zirconia was 0.2 μm . The ZrO_2 content in alumina was 15 vol. %. The composite powder was pressed at a pressure of 276 MPa to form a green compact which was sintered in air at 1450°C for 90 minutes. The sintered piece was further hot pressed at 1450°C under 10.35 MPa pressure for 2 hours in argon atmosphere. The density of the sintered piece was 98% of the theoretical (TD; 4.235 g cm^{-3}). Zirconia was evenly distributed within the alumina structure (Fig.5) after sintering.

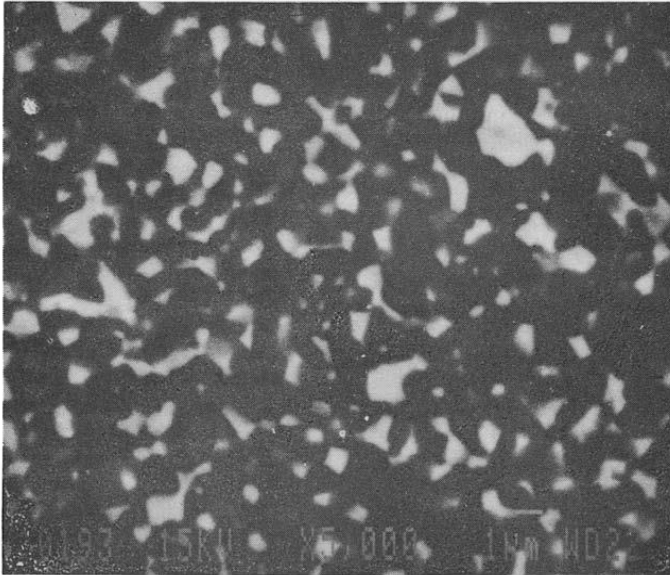


Figure 5: Polished section of $\text{Al}_2\text{O}_3 - \text{ZrO}_2$ after sintering. Showing the distribution of ZrO_2 within the Al_2O_3 matrix [39]

The hardness and fracture toughness of the sintered ceramic were measured using the indentation method. Hardness and fracture toughness was determined to be 17.8 GPa and 4.8 $\text{MPa}\sqrt{\text{m}}$ respectively. Fracture toughness of zirconia reinforced alumina was above that of pure alumina (3.35 $\text{MPa}\sqrt{\text{m}}$). This property was increased by the fine Zirconia particles (Fig. 5) present in the alumina matrix after sintering. The presence of the fine zirconia particles in alumina gives rise to transformation toughening during crack propagation [39].

2.4.2 Niobium carbide reinforcement

Acchar *et al.* [36] used niobium carbide (NbC) to increase alumina fracture toughness. The starting alumina powder had an average particle size of 2.3 μm and a specific surface area of 1.5 $\text{m}^2\cdot\text{g}^{-1}$. It was anticipated that reinforcing alumina with niobium carbide would improve the mechanical properties and suppress grain growth by pinning grain boundaries during the sintering process [36]. NbC was mixed with alumina powder and the mixture was milled for 5 hours in a planetary ball mill to achieve a 30 wt% of NbC in alumina. The NbC/ Al_2O_3 powder was hot pressed at 1650°C with 30 MPa applied pressure in flowing Argon gas. The NbC was evenly distributed within the alumina powder (Fig. 6) during mixing.

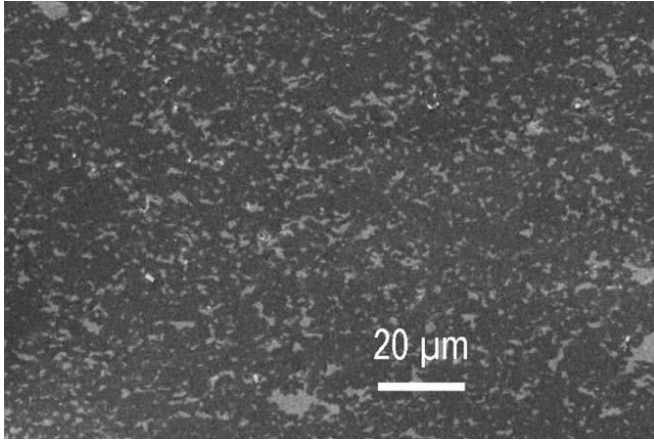


Figure 6: SEM image showing microstructure of NbC/ Al_2O_3 composite (polished surface) white NbC grains within grey Alumina [36].

The ceramic density was 99 % of the theoretical (Theoretical density = 3.99 g cm^{-3}), the hardness was measured to be 19.7GPa and the fracture toughness was found to be 4.5 $\text{MPa}\sqrt{\text{m}}$. A comparison of mechanical properties between this reinforcement (NbC/ Al_2O_3) and other reinforcement was made (Fig. 7 and 8).

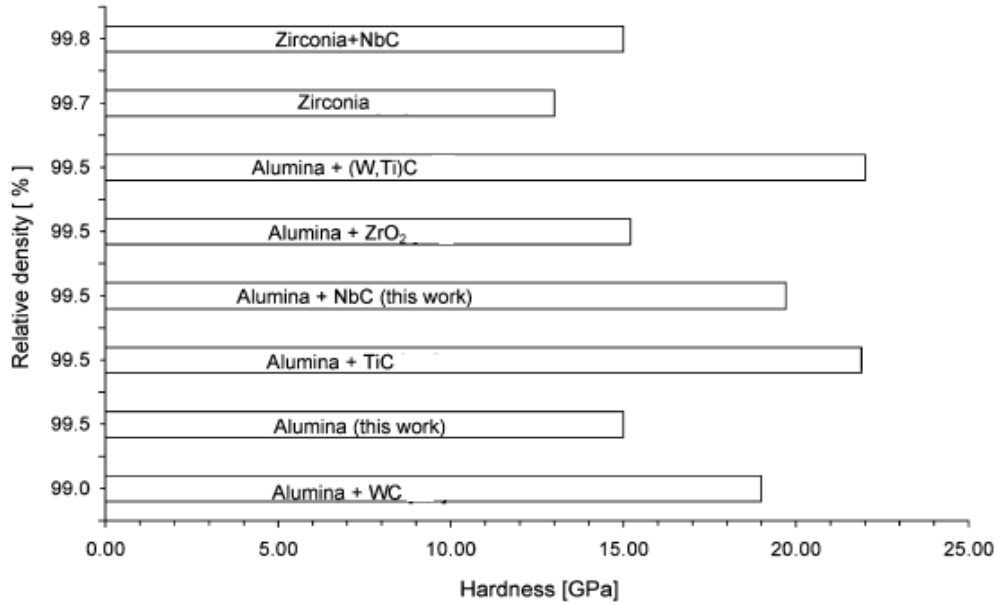


Figure 7: Comparison of hardness and relative density of Al₂O₃ and Al₂O₃-NbC materials investigated in this work with other Al₂O₃ composite systems [36]

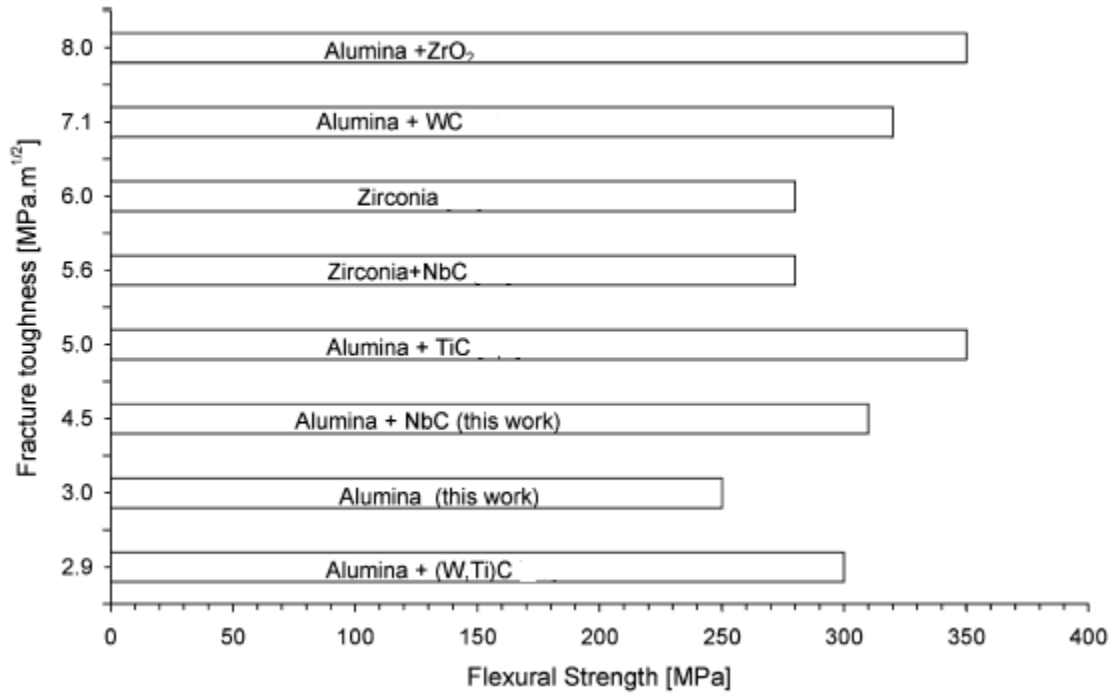


Figure 8: Comparison of fracture toughness and flexural strength of Al₂O₃ and Al₂O₃-NbC materials investigated in this work with other Al₂O₃ composite systems [36]

2.4.3 Titanium Carbide Reinforcement

Cutler *et al.* [3] studied the reinforcement of alumina ceramics with TiC. Reinforcing alumina with TiC has the potential of increasing fracture toughness by inhibiting grain growth during sintering [3]. The amount of TiC that is currently used to reinforce alumina commercially is 30 wt. %. They used the same composition for their alumina reinforcement. In this study Al₂O₃ and TiC were processed with two different methods; the first method utilised titanium (Ti) as the sintering aid; the second method used an exothermic reaction to synthesize TiC [3].

In the first method, alumina and TiC were milled with titanium hydride (TiH₂) in hexane for 24 hours for dispersion and homogenous mixing. The composite powder was wet sieved through a 325 µm sieve and then dry sieved through 80 µm sieve. TiH₂ was added into the composite powder to form as Ti liquid phase during sintering to further densify the ceramic [3]. The composite powder was sintered at temperatures between 1860 and 1875°C, and a pressure of 35 MPa for 10 min. Parallel to this some composite powder was hot isostatically pressed at different temperatures between 1300°C – 1600°C. Pressure was varied from 100-200 MPa. The results obtained are shown in Tables 4 and 5.

Table 4: Effects of pressing pressure on densification of Al₂O₃ + TiC (30 wt. %) [3].

Pressure (MPa) For green compaction	Green Density (% of the theoretical density	Shrinkage (%)	Density (% of the theoretical density)	
			Sintered ^a	Hot isostatic pressed ^b
135	58.5	15.7	96.5	99.8
205	59.5	15.3	97.3	99.8
275	60.2	14.9	97.0	99.8
345	60.3	14.5	97.0	99.8

^a Pressurelessly sintered at 1875°C for 10 min. in Argon

^b Hot isostatically pressed at 1600°C and 200 MPa in Argon

Table 5: Comparison of properties of Al₂O₃ + TiC (26.3 wt. %) + TiH₂ (3.7 wt. %) sintered in N₂ at 1840 °C. Subsequently hot isostatically pressed in Argon [3].

HIP conditions	Density(g cm ³)	Density (% of the theoretical density)	Strength (MPa)	Hardness (GPa)	Toughness (MPa√m)
As sintered	4.22	97.5	415 ± 5.5	17.3 ± 0.2	4.3 ± 0.4
1300°C, 100 MPa	4.24	97.9	555 ± 58	17.8 ± 0.4	4.2 ± 0.4
1600°C, 100MPa	4.33	100.0	681 ± 28	19.4 ± 0.5	4.1 ± 0.2
1700°C, 200 MPa	4.31	99.5	717 ± 10	19.7 ± 0.2	4.2 ± 0.3

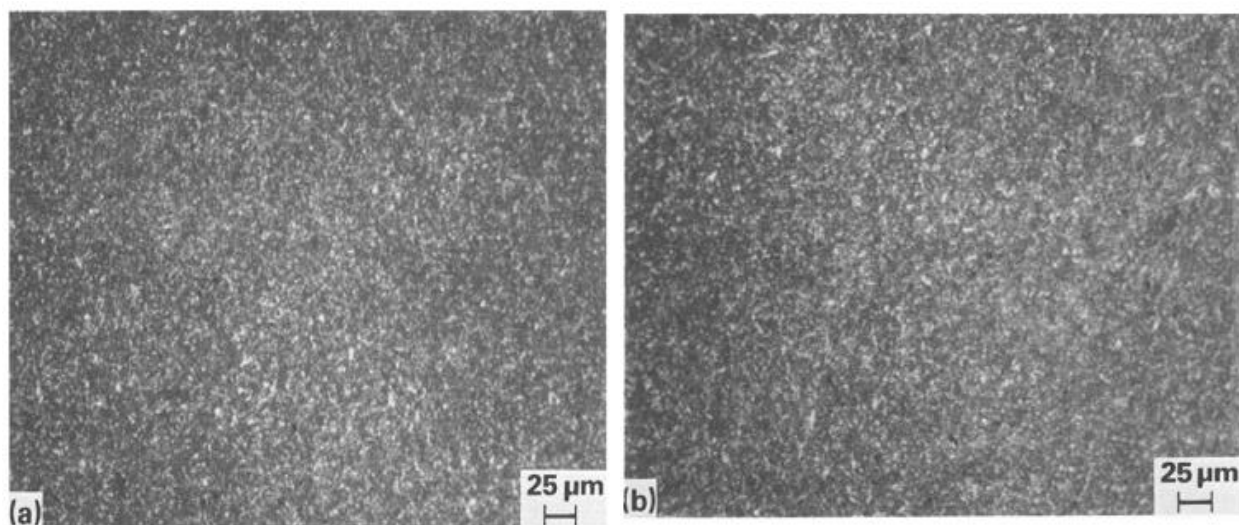


Figure 9: Optical microscope images of Al₂O₃ + TiC (26.3 wt. %) + TiH₂ (3.7 wt. %) sintered at 1840 °C in N₂ (a) as sintered (b) sintered and then hot isostatically pressed at 1300 °C and 100 MPa in Argon ^[3]

The second method involved the use of TiC synthesized via an exothermic reaction. In this route alumina and TiO₂ were dispersed by milling in hexane. The composite powder was wet sieved through a 325 sieve and dry sieved through an 80 sieve. It was then placed in a graphite foil and reacted in the quartz tube at a temperature of 660°C; the powders spontaneously reacted to form Al₂O₃ and TiC. The composite powder was ball milled again and hot pressed at 1650°C, 35MPa

for 10 minutes in argon. The powder was alternatively sintered pressureless at a temperature between 1875 and 1950°C for 10 min. as shown in Table 6.

Table 6: Properties of pressureless sintered Al₂O₃+TiC (30 wt. %) composites made by reaction mentioned above and sintered in Argon ^[3].

Sintering conditions	Density g (cm⁻³)	Strength (MPa)	Hardness (GPa)	Toughness (MPa√m)
Sintered at 1875°C	4.23	387 ± 80	22.0 ± 1.3	4.4 ± 0.3
Hot pressed	4.25	548 ± 113	22.8 ± 0.9	4.9 ± 0.8

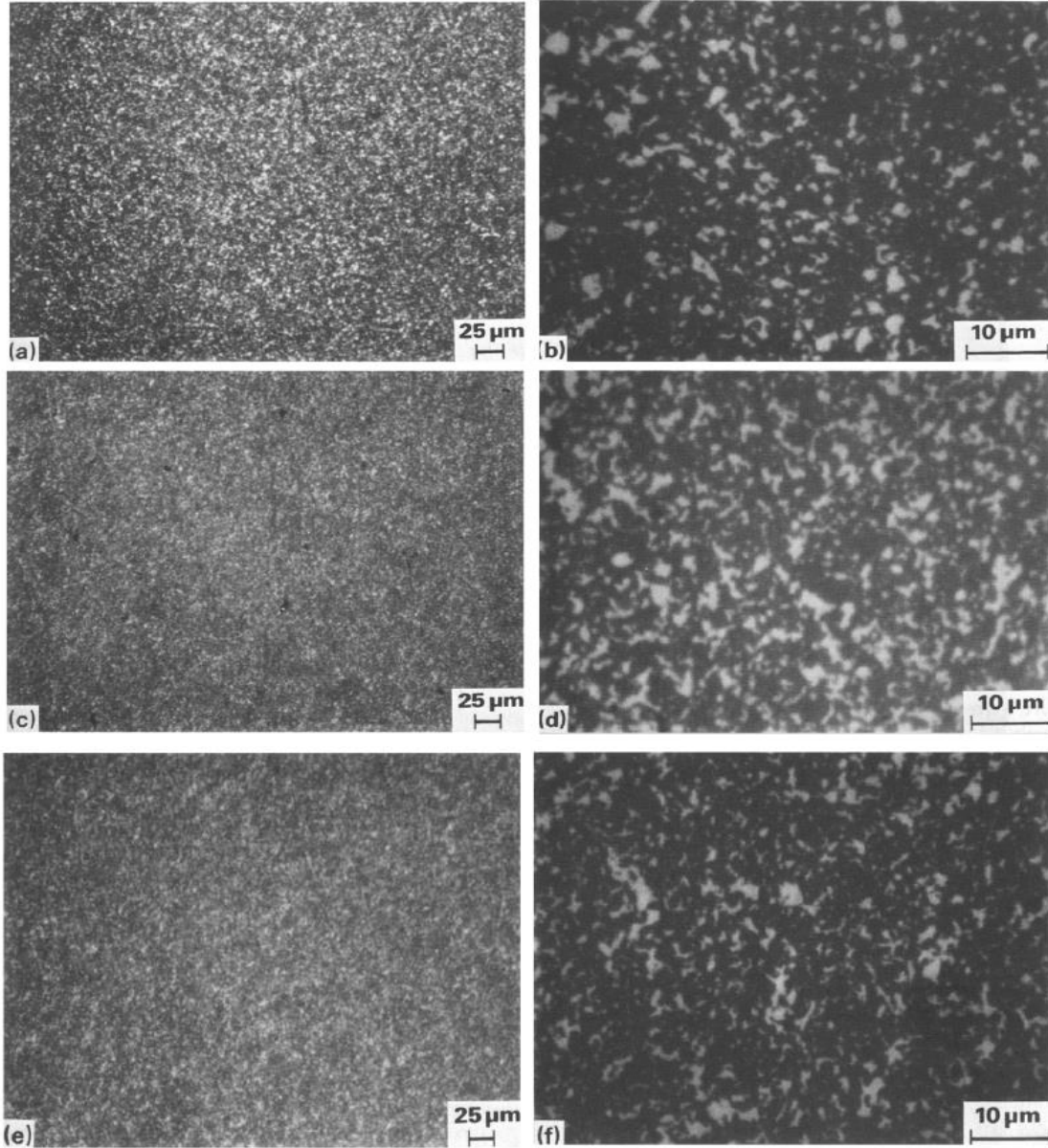


Figure 10: Optical microscope images of $\text{Al}_2\text{O}_3 + \text{TiC}$ (30 wt. %) composites; (a) (b) milled and hot pressed (c) (d) pressure less sintered (e) (f) pressure less sintered and hot isostatically pressed [3]

2.4.4 Carbon nanotubes reinforcement

Kim *et al.* [40] reinforced alumina with MWCNTs to increase the material's fracture toughness hence increasing its industrial applications. It was also intended to use the same reinforcement to increase the thermal and electrical conductivity of this material. The MWCNT used for their experiments were purified up to 98 % purity and with dimensions shown in table 7.

Table 7: The MWCNTs dimensions and density. [40]

Properties	Values
Diameter (nm)	2 – 20
Length (μm)	2 - 5
Density (g cm^{-3})	1.3

The alumina powder used had 0.5 μm grain size (Sumitomo chemical) containing 0.1 wt% MgO. The MgO was used to prevent aggregation between the CNTs and also to improve their distribution through the matrix [40]. CNTs were ultrasonicated and dispersed in ethanol, and were then poured into alumina powder which was also in ethanol. The volume fractions of CNTs added were within the range of 0 – 3 vol. %. Homogeneous distribution of the CNTs through alumina was achieved by further ball milling the CNT/ Al_2O_3 mixture with ZrO_2 balls for 5 hours. After drying the slurry in an oven the powder was compacted in a mold under pressure of 20 MPa and was further pressed in a cold isostatic press at 200 MPa pressure. The green compacts were pressureless sintered at 1550°C in argon.

The results obtained from these experiments showed that the relative density, shrinkage and electrical resistance of the sintered pieces varied with the volume % of the CNTs as shown in Fig.11.

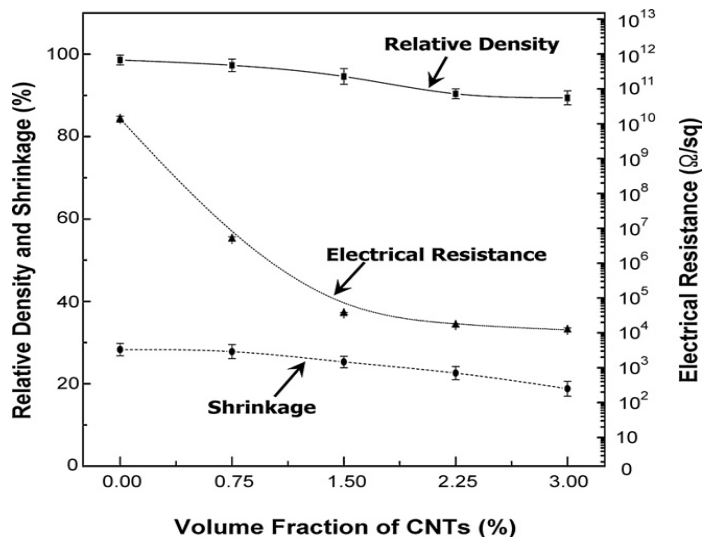


Figure 11: Shrinkage, relative density and electrical resistance as a function of vol% of CNT in CNT/Alumina powder ^[40]

Relative density decreased as the vol. % of CNTs increased and when 3 vol. % of CNTs was used the density decreased by 8%. The reduction of density with increasing CNTs vol% is possibly due to the poor packing of CNTs within the alumina powder during sintering; this constantly increases the pore volume fraction with increasing CNT content. The decrease in density could also be due to different densities of alumina (3.99 g.cm^{-3}) and CNTs (1.3 g.cm^{-3}). The graph in Figure 11 shows that the electrical resistance of the ceramic decreases rapidly up to 1.5 vol. % of CNTs and then slightly decreases as amount of CNTs increased from 1.5 to 3vol.%. When more than 1.5 vol. % of CNT was added, the pore volume fraction increased (shown by reduction of density) which decreased electrical conductivity. The electrical resistance slightly decreased which means that the ceramic reached its electrical conductivity threshold with the amount of CNTs added.

The flexure strength and fracture toughness of the sintered piece also varied with vol. % of the CNT in alumina powder (Fig. 12).

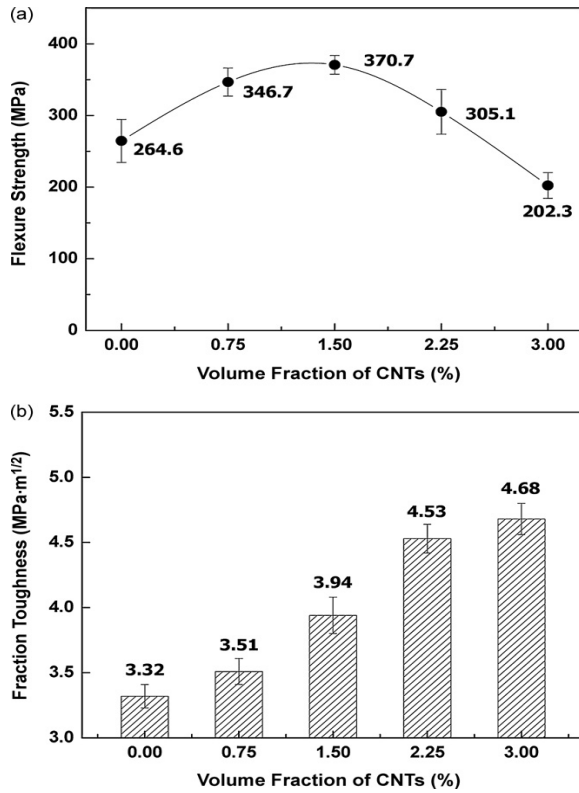


Figure 12: Flexural strength (a) and fracture toughness (b) vs. volume % of CNT in CNT/Alumina powder ^[40]

Flexural toughness increased with addition of CNTs up to ~ 1.5 vol. %, this can be attributed to the strengthening mechanism of CNTs. The alumina reinforced with 1.5 vol. % CNTs had flexural strength approximately about 40 % higher than that of pure alumina. The decrease in flexure strength when the amount of CNTs is above 1.5 vol.% was due to the increase in porosity within the material. The fracture toughness increased with vol. % of the CNTs. The maximum value reached was 4.68 MPa \sqrt{m} at 3 vol. % of CNTs as shown in Fig.12. The fracture toughness improved upon addition of CNTs while hardness, flexure strength and stiffness decreased with more CNTs added. The ambiguity was due to indentation method used for measuring hardness and fracture toughness ^{[41] [42]}. The increase in fracture toughness was both due to crack bridging and grain interface bridging, as they are both well-known toughening mechanisms.

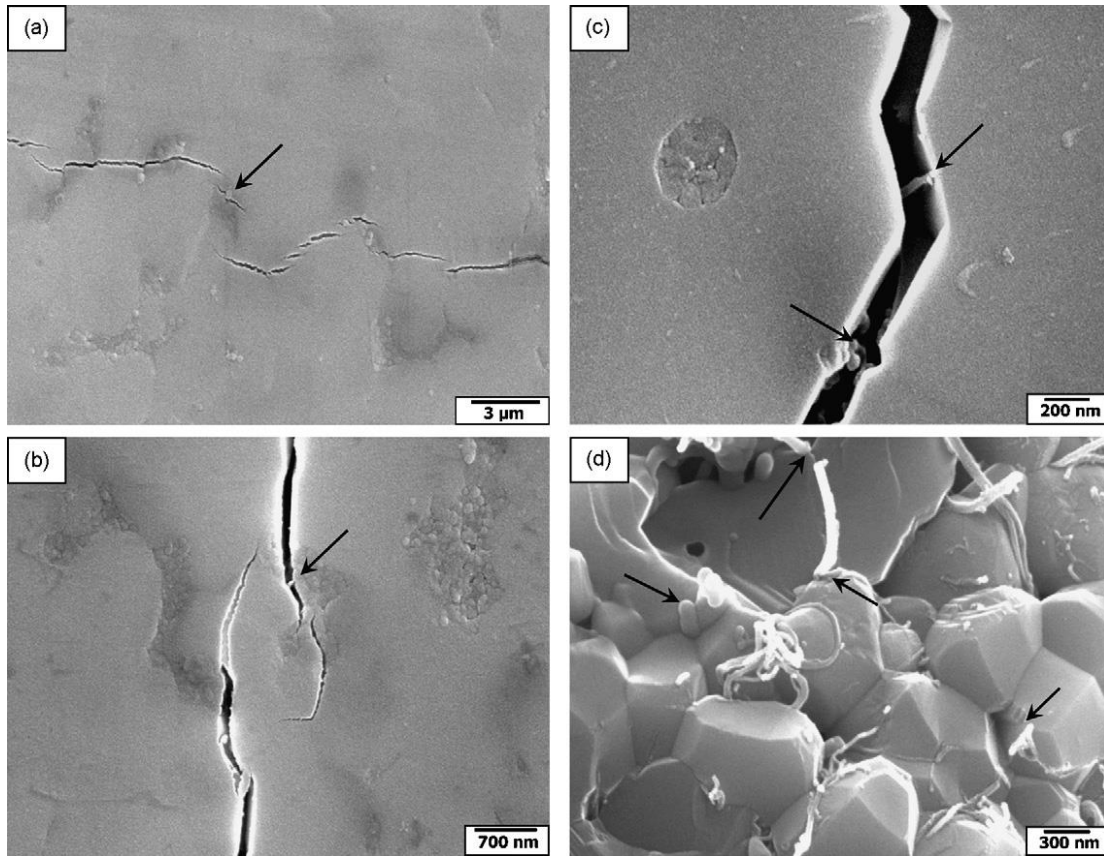


Figure 13: SEM micrograms of Alumina reinforced with 3 vol. % of CNTs, showing (a) grain interface bridging (b) CNT bridging (c) both grain interface and CNT bridging (d) fracture surface showing CNT pull outs ^[40]

The results obtained showed that an increase in CNTs volume fraction within the alumina matrix beyond 1.5 vol. % increases the pore volume fraction (porosity) which negatively affects the flexure strength, electrical conductivity and density of the ceramic. Therefore in order to achieve both toughening and strengthening of alumina, the CNT volume fraction range that must be used is 1.5 – 2.25 ^[40].

Sun *et al.* ^[4] worked on the similar system of reinforcing alumina with MWCNTs but the ceramic piece was formed by hot pressing. The CNTs used had an average length of 100 nm and a diameter ~10 nm and the alumina powder had particle sizes ranging between 200 – 300 nm (Taimei chemical). The CNTs and alumina powder were mixed using a colloidal route. CNTs were dispersed in deionised water with the use of polyethylene amine (concentration of 300ppm) as a dispersant, and alumina was dispersed in deionised water with polyacrylic acid as the

dispersant ^[4]. The suspensions were mixed together in a beaker with vigorous stirring using a stirrer bar; the coated CNTs from the mixing were then transferred to another alumina suspension with 50 wt% ethanol, and the final CNT composition was ~ 1wt% of the amount of alumina. The final suspension was then dried and sieved to homogeneously distribute the CNTs within the powder. The composite powder was then hot pressed to 30 MPa pressure under Argon atmosphere at different temperatures for an hour (temperatures used were 1350, 1400, 1450 and 1500°C). Pure alumina was also hot pressed under similar conditions for comparison. The measured densities of the sintered parts were 98.9 % for CNT reinforced alumina and 99.9 % (of the theoretical density) for pure alumina.

The results obtained showed that the fracture toughness varied with temperature (Table 8).

Table 8: Fracture toughness of CNT reinforced Al₂O₃ and pure Al₂O₃, measured at room temperature ^[4]

Sintering temperature (°C)	Al ₂ O ₃	Al ₂ O ₃ + 1 wt% MWCNT's
1350	3.0 ± 0.28	4.0 ± 0.50
1400	3.7 ± 0.45	3.7 ± 0.41
1450	3.9 ± 0.50	3.9 ± 0.59
1500	3.7 ± 0.34	2.2 ± 0.15

The results showed that the fracture toughness increased for the reinforced alumina compared to pure alumina at low temperatures. At high temperatures the fracture toughness of the reinforced alumina decreased below that of pure alumina. This phenomenon can be explained by CNTs instability at high temperatures ^[4] and poor adhesion of CNTs to the alumina matrix as it is shown by the large number of pull out in figure 14 (b). A comparison between a piece sintered at 1450 and 1500°C was done to examine any changes in the alumina structure. It was observed that at 1500°C the alumina grains became more rounded and porous as shown by the arrows (Fig. 14).

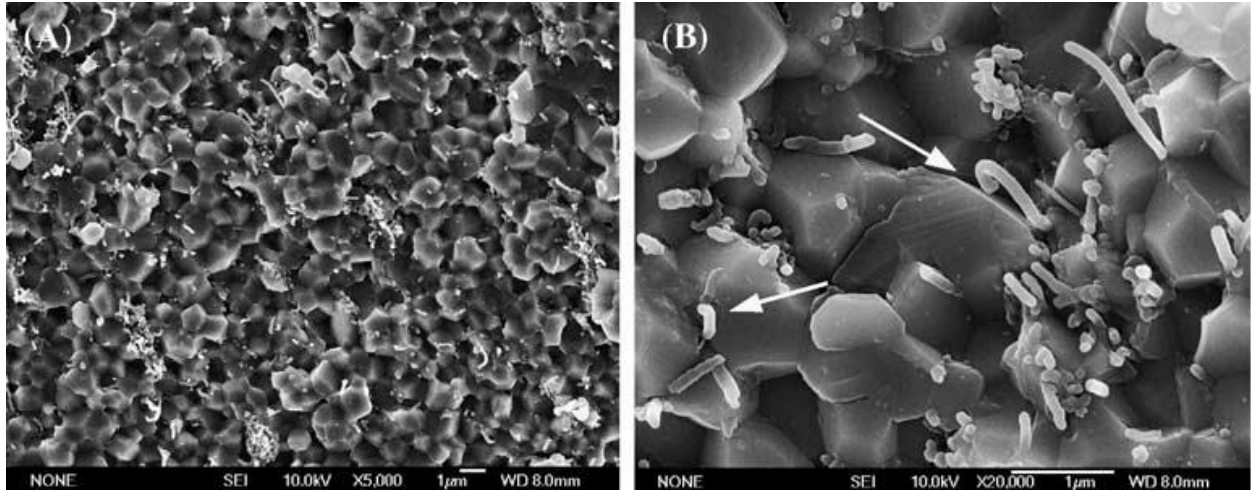


Figure 14: The SEM images of the fracture surface of the composite sintered at 1450°C [4]

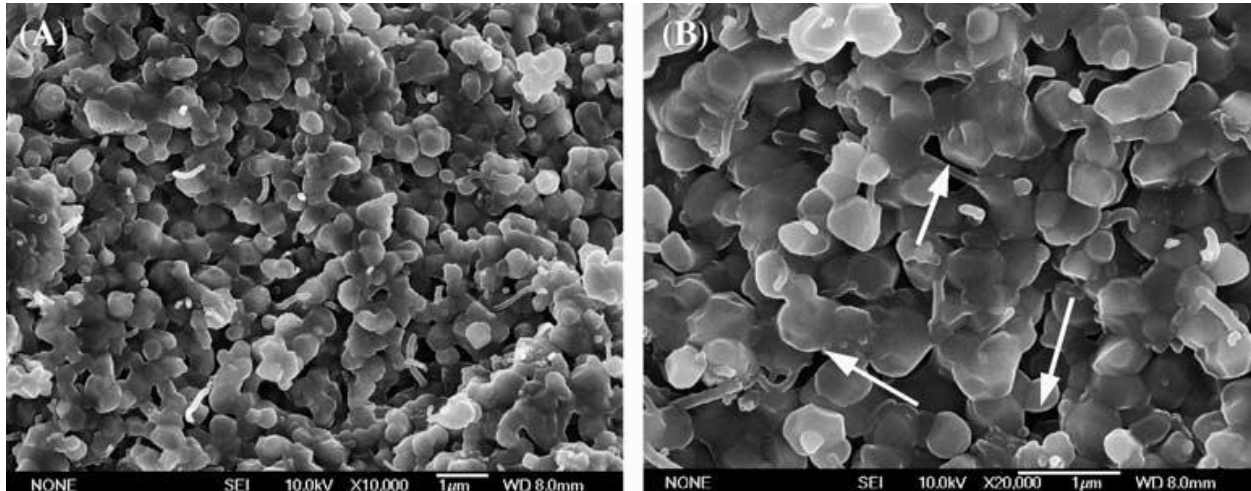


Figure 15: The SEM images of the fracture surface of the composite sintered at 1500°C [4]

The sample sintered at 1500°C had more pores compared to the sample sintered at 1450°C but it had density very close to the density of the sample sintered at 1450°C. The authors suspected that the measured density was higher than the true density of the sample sintered at 1500°C, since it is impossible to measure closed pores using Archimedes method [4].

Estili *et al.* [5] also worked on alumina reinforcement with CNT but they used Spark Plasma Sintering (SPS) instead of hot pressing or pressure less sintering. In their research, high purity CNTs were used, which had a high aspect ratio and a wide range of diameters (20 – 70 nm). The alumina that was used had an average particle size of 150 nm. CNTs were functionalized by

refluxing them in a mixture of nitric (HNO_3) and sulphuric (H_2SO_4) acid at 110°C for 10 – 20 minutes. Alumina suspension was prepared by adding alumina in deionized water and the pH was adjusted to 4.4 using 35 % HCl. The CNTs suspension was gently mixed with the alumina suspension with vigorous mixing using a stirrer bar. The mixing of the two powders was such that the final CNT content in Alumina was 3.5 vol. %. The resultant suspension was dried in an oven at 80°C .

The CNT- Al_2O_3 composite powder was sintered using SPS, at a temperature of 1500°C for 10 minutes under 50 MPa compressive stresses.

The results that were obtained showed that the relative density obtained was 99 % of the theoretical density. There was a 67 % increase in fracture toughness when SPS was used (from $3.12 \text{ MPa}\sqrt{\text{m}}$ of pure alumina to $5.20 \text{ MPa}\sqrt{\text{m}}$ of the reinforced alumina) ^[5]. This means that when SPS was used more CNTs survived high sintering temperature to improve fracture toughness of the ceramic as opposed to hot pressing which destroys them. CNTs were effective in crack deflection and bridging even at high temperature (1500°C) as shown in Fig. 16.

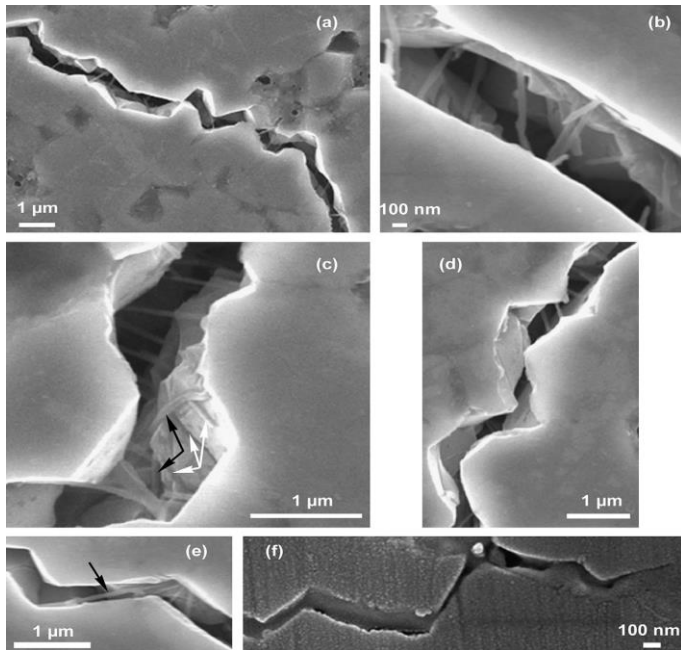


Figure 16: FESEM micrograms of the indentation crack of a SPS-consolidated 3.5 vol. % CNT in Al_2O_3 ceramic composite ^[5]

The CNTs that were situated perpendicular to the crack planes were effective in crack bridging and the ones situated parallel to the crack planes also contribute to crack bridging as shown in Figure 16 (e) but they contribute mostly to crack deflection as shown in Figure 16 (c) by black arrows. The CNT survive high sintering temperatures when SPS is used since minimum time is spent at those temperatures. It was also observed that even the inner wall of the multi walled CNTs contribute to crack bridging without complete pullout from the outer wall and therefore they also carry a load ^[40].

2.5 Boron nitride

Hexagonal Boron nitride (hBN) is also known as the “white graphite” due to the similarities it has to graphite. hBN has the same hexagonal crystal structure as graphite but it has superior properties comparatively ^[43]. hBN can be prepared in variety of ways depending on the intended applications. Commercially there are two grades being offered, namely the microcrystalline type with low purity but good sinterability and pure crystalline grade which has good thermal conductivity and mostly used as lubricant ^[44]. The hBN crystal structure is shown in Figure 17.

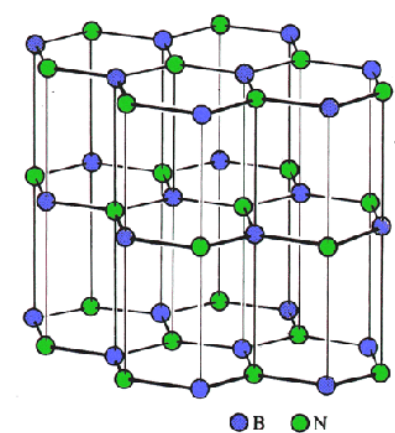


Figure 17: hexagonal crystal structure exhibited by hBN ^[45]

hBN offers good lubricating properties due to its low thermal expansion and low coefficient of friction ^[43]. It has good thermal resistance properties; it is stable up to 1000 °C in the air, 1400 °C in vacuum and 1800 °C in inert gases (e.g. Argon) ^[43].

The properties exhibited by hBN are listed in Table 9.

Table 9: The hBN properties ^[43]

Properties	Magnitudes
Density (g cm ⁻³)	2.3
Melting point (°C)	3000
Coefficient of friction	0.15 – 0.70
Young's modulus (MPa)	20 - 102
Thermal conductivity (cal/cm.sec.K) (at 20°C)	0.08
Thermal expansion coefficient (per °C)	1 x 10 ⁻⁶ (parallel to press direction) 4 x 10 ⁻⁶ (perpendicular to press direction)

The properties exhibited by hBN make it a suitable material for the protection of CNT in the alumina matrix, in-order to prevent CNTs instability at high sintering temperatures and to reduce CNTs frictionless sliding out of the matrix.

2.6 Coating CNTs with hexagonal Boron Nitride (hBN)

2.6.1 Urea route

The CNTs that were coated using this method were first functionalised. The process of functionalization is an attachment of organic groups on the surface of the tube (Fig. 18). These groups are usually attached by the use of an acid ^[46].

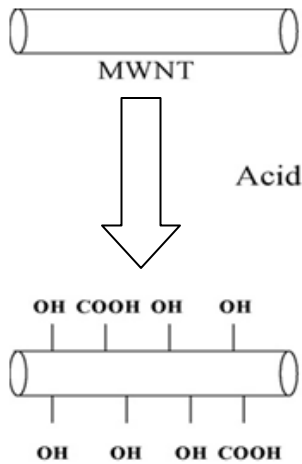


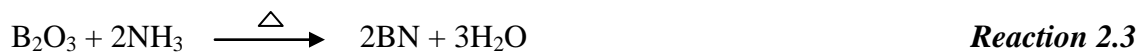
Figure 18: Schematic representation of functionalizing CNTs with nitric acid ^[46]

Gomathi *et al.* ^[45] published a method of coating carbon nanotubes with hBN using Urea route. In this route, boric acid (H_3BO_3) and urea ($CO(NH_2)_2$) mixture was made in a molar ratio of 6:1 ^[45]. This mixture was heated up to $70^\circ C$ to obtain a viscous mixture. The carbon nanotubes were then dipped into the viscous solution for 1 - 3 hours. The longer the time the MWCNTs are kept in the solution the thicker will be the h-BN coating on the CNTs walls. When the temperature of the solution was raised to $70^\circ C$, boric acid and urea will dissociate according to the Reactions:



The crucial reaction is the one between B_2O_3 and NH_3 where they form hBN which then gets deposited on the surface of CNT's walls.

After the soaking the CNTs they were heat treated in a tube furnace at 1000°C for 3 hours. Then the following reaction took place;



SEM and TEM were conducted on the coated CNTs to examine the coating morphology and also to measure the coating thickness.

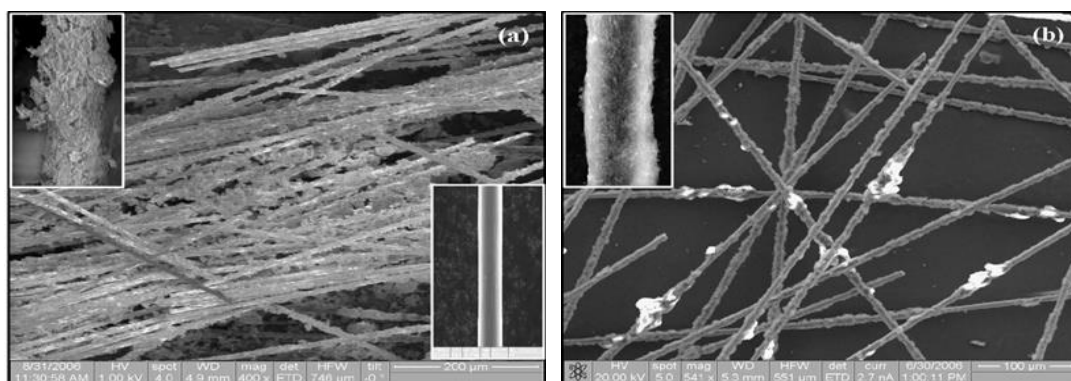


Figure 19: FESEM images of h-BN coated MWCNTs (a) heavily coated MWCNTs and (b) less coated MWCNTs ^[47]

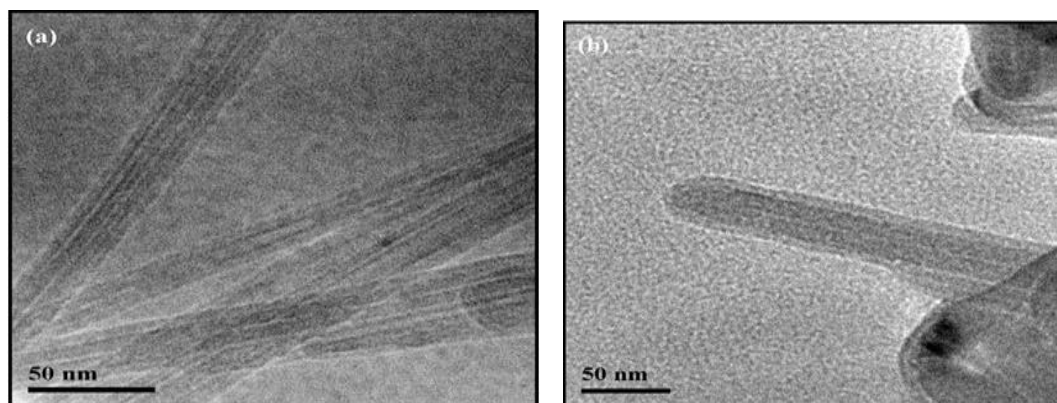


Figure 20: TEM images of hBN coated MWCNTs ^[47]

The hBN coating was achieved on the CNTs with the maximum coating thickness of ~10 nm (Fig. 20). The maximum coating thickness was achieved when the CNTs were soaked in the

Urea and boric acid mixture for 3 hours. The coating that was obtained was not uniform as shown by FESEM analysis in figure 19.

2.6.2 Nitridation route

Chen *et al.* [47] devised another method of coating CNTs with hBN. Nitridation method includes two steps: boric acid infiltration and nitridation [18]. Saturated boric acid was infiltrated through the preheated MWCNT's at 100°C. Then the boric acid dissociation reaction took place according to Reaction 2.1.



The MWCNT's were dried in air and then loaded into quartz boats and placed inside a tube furnace. The furnace was first purged with argon gas for 30 minutes. The temperature was then raised to a temperature between 1100 – 1200°C at a rate of 10 °C.min⁻¹; then 99.99% purity ammonia was introduced into the furnace at a rate of 20 ml.min⁻¹. The thickness obtained for hBN coating was an increasing function of ammonia purging time.

The h-BN coating would be formed on the CNT's walls according to Reaction 2.3.



During the acid infiltration at 100°C, boric acid would dissociate to H₂O and B₂O₃, water would evaporate and B₂O₃ would proceed to the nitridation step where it would react with NH₃ to form hBN which would then be deposited on the surface of CNT's.

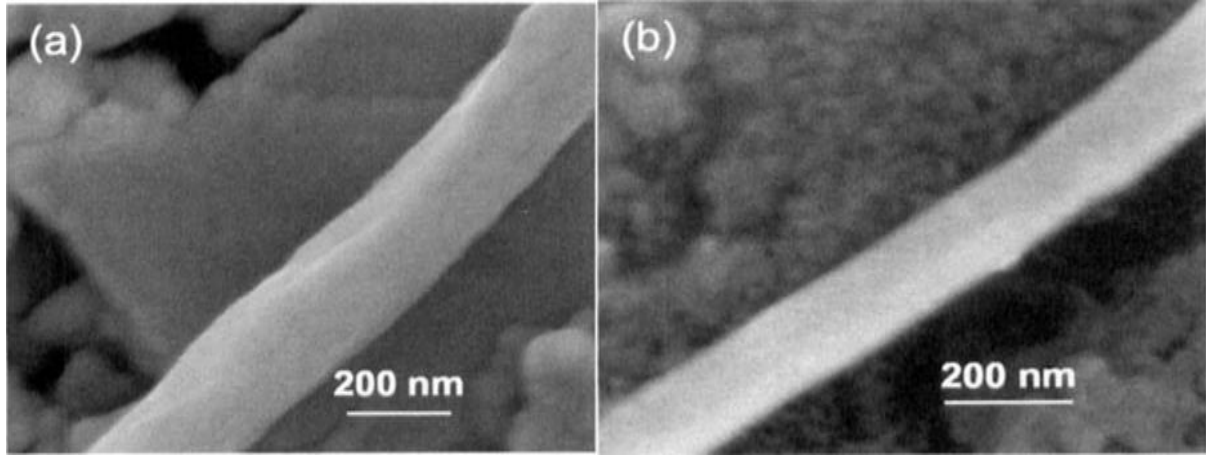


Figure 21: SEM images of heat treated MWCNTs after coating [47]

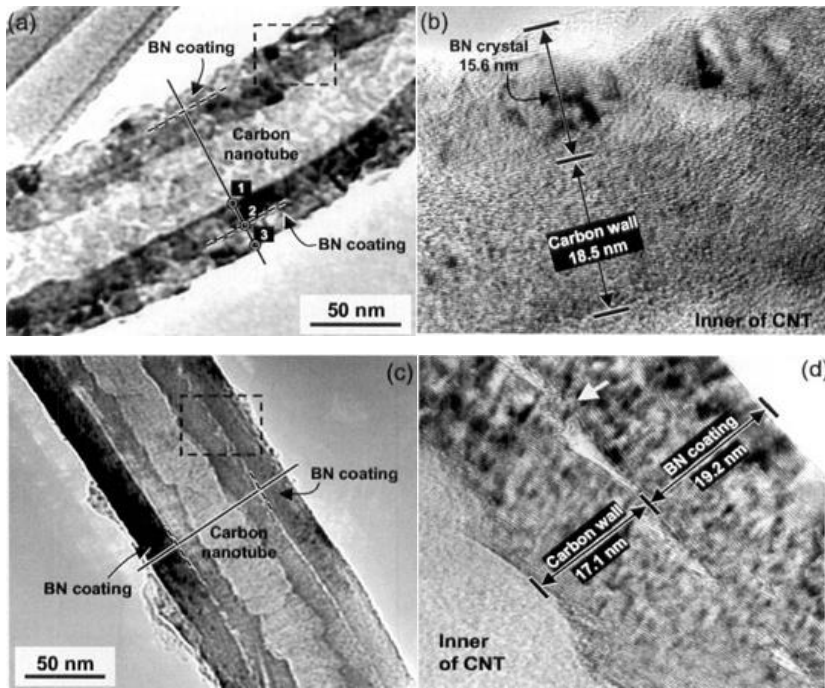


Figure 22: TEM images of BN coated MWCNT's ((a) and (b)), the solid lines indicate the line-scan EELS analysis (b) and (d) are HRTEM images of the framed region in (a) and (c) respectively [47]

The above literature survey has provided crucial and relevant information for this work. It has revealed most of the difficulties that has been experienced by other researchers in the same field of study. The previous work has revealed that reinforcing alumina with MWCNTs was not

successful because the CNTs had poor adhesion to the alumina matrix and also that CNTs are destroyed at high sintering temperature therefore they cannot serve as reinforcements. It was discovered that the dispersion of the CNTs is crucial for the densification of the Al₂O₃-CNT composite powder. It has revealed that reinforcing alumina with TiC can greatly increase the fracture toughness of alumina without compromising the other properties like hardness and density.

The approach to this study is slightly different to what has been done before in order to utilize the full potential of the CNTs as reinforcements. An attempt to improve CNTs adhesion to the alumina by coating them with hBN is going to be done. Therefore this method has a potential of eliminating the adhesion problem of the CNTs to alumina. The CNTs are to be dispersed using a dispersant in two different methods (more aggressive and less aggressive) to fully disperse the CNTs within the alumina matrix therefore utilizing their full potential. Al₂O₃-CNT composite powder was formed by milling the alumina and CNTs together to thoroughly mix the two components. The Al₂O₃-CNT composite was sintered using Spark Plasma sintering furnace which heats up to the sintering temperature at a high rate (250°C.min⁻¹). This high heating rate has the potential to sinter the alumina powder without destroying the CNTs. Therefore reinforcing alumina with well dispersed CNTs and sintering the composite powder at high enough heating rate will promote effective reinforcement. Therefore it should be possible for CNTs to improve both the alumina fracture toughness (through crack bridging) and electrical conductivity. The fracture toughness of alumina will be further increased by addition of TiC through crack deflection. Addition of CNTs and TiC to the alumina matrix would ensure improved mechanical and electrical properties which are the main inhibiting factors for increased use of alumina commercially.

Chapter Three

3.0 Experimental Procedure

This section describes how the starting powders CNTs, TiC and Al₂O₃ were processed and characterized. CNTs were characterized using transmission electron microscopy (TEM) to examine their surface and also to check for any amorphous carbon. TiC and Al₂O₃ were dispersed and analyzed using particle size analyzer to check for particle size distribution. This section further describes in details how the powders were dispersed and mixed together in suspensions, and also how the suspensions were dried. It then describes how the composite powders were sieved and the sintering conditions at which the composite powders were sintered.

3.1 Materials and Characterization

3.1.1 Materials used

The properties and suppliers of the materials that were used for this study are shown in Table 10.

Table 10: The list of materials used and their manufacturer's specifications

<u>Alumina</u> Average particle size: 200 nm Grade: TM-DAR Purity: 99.99 % Supplier: Taimicron	<u>Titanium Carbide</u> Average particle size: 200 nm Grade: AB 255320 Purity: 98 % + Nano Supplier: ABCR
<u>Carbon Nanotubes</u> Average length: 1.5 μm Average diameter: 9.5 nm Carbon purity: 95 % Supplier: Nanocyl	<u>Polyvinylpyrrolidone (PVP)</u> Molar Mass: 24 000 g mol ⁻¹ Particle size: 110 μm Supplier: Sigma Aldrich

<p><u>Hexane fraction</u></p> <p>Purity: 99.99%</p> <p>Aromatics: 0.01 %</p> <p>Sulphur content : 0.0005%</p>	<p><u>Lubrizol 2155</u></p> <p>Viscosity: 13 000 – 23 000 cP at 25°C</p> <p>Supplier: Carst and Walker</p>
<p><u>Boric Acid</u></p> <p>Grade: B0252</p> <p>Purity: 99 %</p> <p>Supplier: Sigma Aldrich</p>	<p><u>Ammonia Gas</u></p> <p>Purity: 99.99 %</p> <p>Supplier: Afrox</p>
<p><u>Ferrocene</u></p> <p>Purity: 99 %</p> <p>Supplier: Sigma Aldrich</p>	

3.1.2 Equipment used

The following equipments were used in order to successfully finish this work.

Ultrasonic probe

The ultrasonic probe used to disperse pure alumina and titanium carbide was HD 2200 Max. Power[®], it was purchased from Bendalin *Sonoplus* Pty Ltd (Fig.23). It was also used for dispersion of carbon nanotubes by breaking down CNT agglomerates.



Figure 23: The ultrasonic probe, HD 2200[®]

Particle size analyzer

Particle size analyzer used to measure particle size distribution of the powders in suspension was Mastersizer 2000[®] with hydro 2000 MU cell (Fig.24). This instrument was equipped with an ultrasonication system and a propeller to suspend the powder in solution before it measured the particle size distribution of the suspension.



Figure 24: The particle size analyzer, Mastersizer 2000[®]

Attritor mill

The attritor mill Reeves, Szegvari attritor system type B[®], supplied by Union Process (Fig. 25) was used to further disperse CNTs. The mixing vessel had a volume of 500 ml and was made of alumina. The alumina balls that were used were 2 mm in diameter.



Figure 25: Attritor ball mill Szegvari attritor system type B[®]

Planetary ball mill

The planetary mill *Fritsch Pulverisette 6*[®] (Fig. 26) was used for mixing the powders in suspensions. The mixing vessel had a volume of 250 ml and made of stabilized Zirconia. The alumina balls that were used had a diameter of 2 mm.

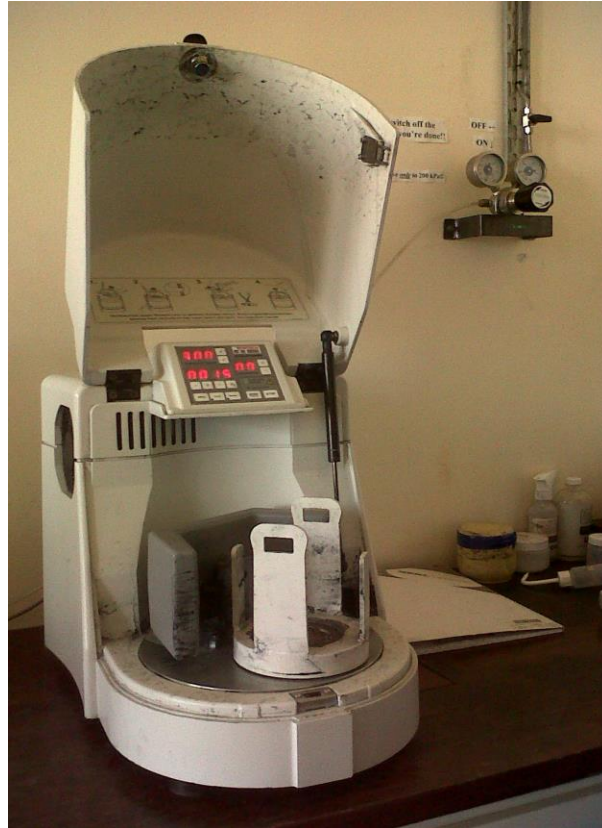


Figure 26: Planetary ball mill, Fritsch Pulverisette 6[®]

Spark Plasma Sintering (SPS) machine

The Spark Plasma Sintering machine HP D 5/2[®] from FCT Systeme GmbH (Fig. 27) was used for sintering of the samples. It uses graphite dies for pressing the powder sample. The same dies act as electrical heating elements. A heating rate of 250°C.min⁻¹ was used in this work.



Figure 27: The spark plasma sintering (SPS) machine, HP D 5/2[®]

Tube furnace

The tube furnace used in this work was Elite TSH17/75/150[®], supplied by Elite Thermal Systems Limited (Fig. 28) was used could reach maximum temperature of 1600°C. The tube that was used throughout this work was made of mullite.



Figure 28: The tube furnace, Elite TSH17/75/150[®]

Vickers hardness tester

The Vickers hardness tester, V-100-A2[®], supplied by LECO (Fig. 29) was used for measuring the hardness and fracture toughness of the sample. This instrument was equipped with a microscope and a measuring device to measure the lengths of the indentation diagonals and that of the cracks.



Figure 29: Vickers hardness tester, V-100-A2[®]

Electrical measurements

The DC 41-40 SMU, HC-2[®] from Air products (Fig. 30) instrument was used to measure the electrical properties of the samples. It applies a voltage and measures the current passing through the sample. This instrument then plots a graph showing the relationship between current and voltage.



Figure 30: The DC 41-40 SMU, HC-2[®]

Optical microscope

Optical microscope, Axiotech 25 HD[®], from Carl Zeiss in (Fig. 31) was used to examine the microstructure of the polished samples.



Figure 31: Optical microscope, Axiotech 25 HD[®]

Scanning electron microscope

A Philips scanning electron microscope, XL30 series[®] (Fig. 32) was used for a more detailed analysis of the sample microstructures.



Figure 32: A Philips scanning electron microscope, XL30 series[®]

Transmission electron microscope (TEM)

The TEM, model 3000[®], from Fischione Instruments Pty Ltd (Fig. 33) was used for CNTs characterization.



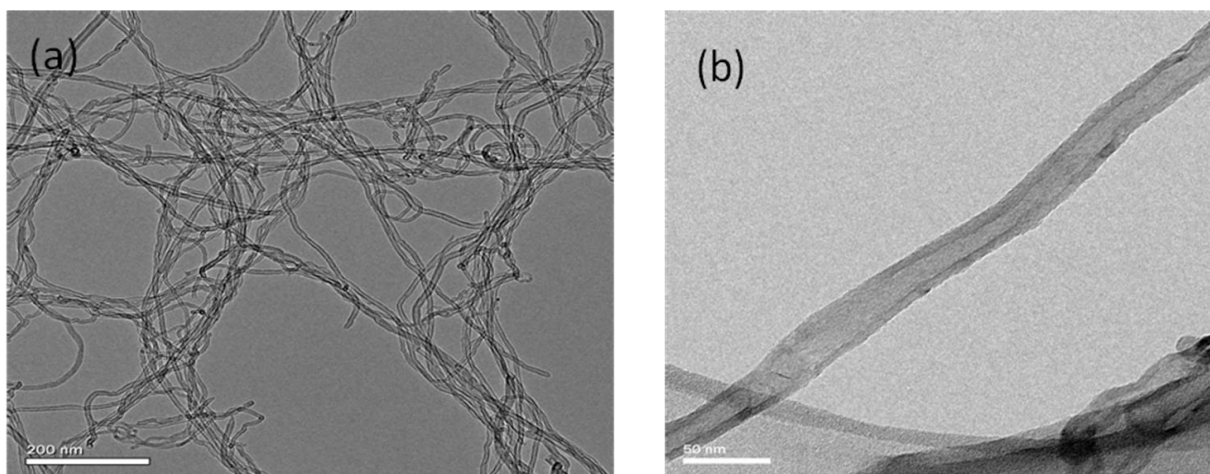
Figure 33: Transmission electron microscope, model 3000[®]

3.2 Preparation of multi walled carbon nanotubes (MWCNT)

Carbon nanotubes were produced in the nano-technology laboratory, University of Witwatersrand. The carbon nanotubes were produced by reaction of acetylene (C_2H_2) and

ferrocene [$\text{Fe}(\text{C}_5\text{H}_5)_2$] at a temperature of 800°C . Quartz wool was placed at the bottom of the vertical tube furnace and a mass of 2 g of ferrocene was placed on top of quartz wool (which is where the CNTs were collected). As the temperature was raised to 800°C ferrocene decomposed and Fe^{2+} particles were adsorbed onto the quartz wool. Then acetylene gas was pumped into the tube furnace at different flow rates which were between $50 \text{ ml}\cdot\text{min}^{-1}$ - $100 \text{ ml}\cdot\text{min}^{-1}$ for 25 minutes. The variation of time and flow rate of acetylene was done to promote production of MWCNTs and also to produce MWCNTs with smaller diameters. Acetylene served as the source of carbon atoms, which with the aid of Iron ion (Fe^{2+}) as a catalyst produced carbon nanotubes. The tube furnace was then left to cool down and carbon nanotubes were collected from the glass wool. The CNTs were purified using a mixture of HNO_3 (55% concentrated) and H_2SO_4 (98% concentrated) and then analyzed using TEM. The preparations of MWCNTs yielded nanotubes that had diameters between 40 – 200 nm (to be discussed later in Chapter 4). These MWCNTs could not be used for this study. The MWCNTs that were used for this work were purchased from Nanocyl Pty Ltd. They had an average length of $1.5 \mu\text{m}$ and an average diameter of 9.5 nm as measured by TEM. They were also specified to have carbon purity of 95 % measured using thermogravimetric analysis (TGA).

The “as received” MWCNT were analyzed using TEM at the University of Witwatersrand, Johannesburg. The TEM images showed that the “as received” MWCNTs had a smooth surface and there was no amorphous carbon (Fig. 34).



corresponds to the minimum viscosity on the graph shown in red is the amount of Lubrizol sufficient to fully disperse the TiC powder (Fig. 36)

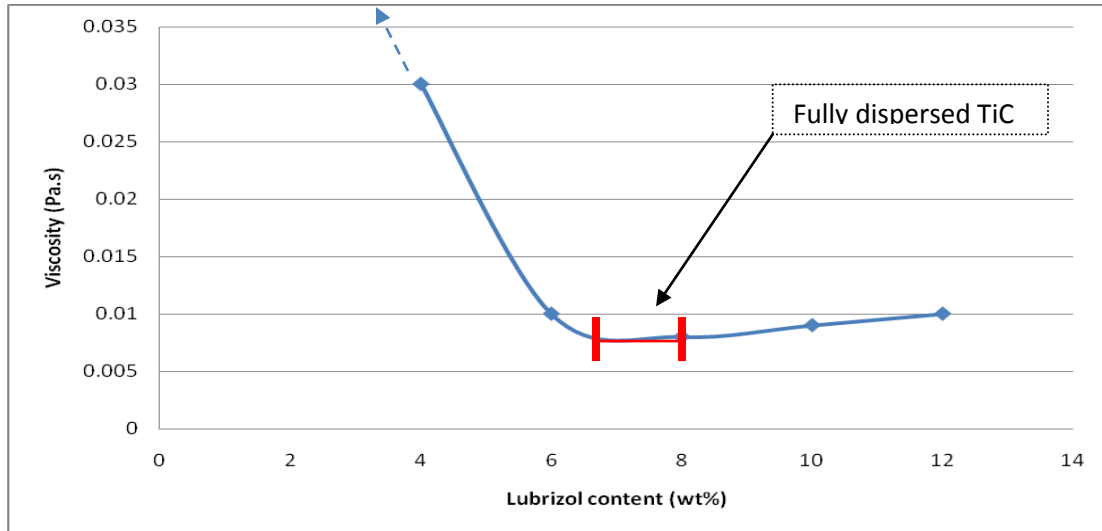
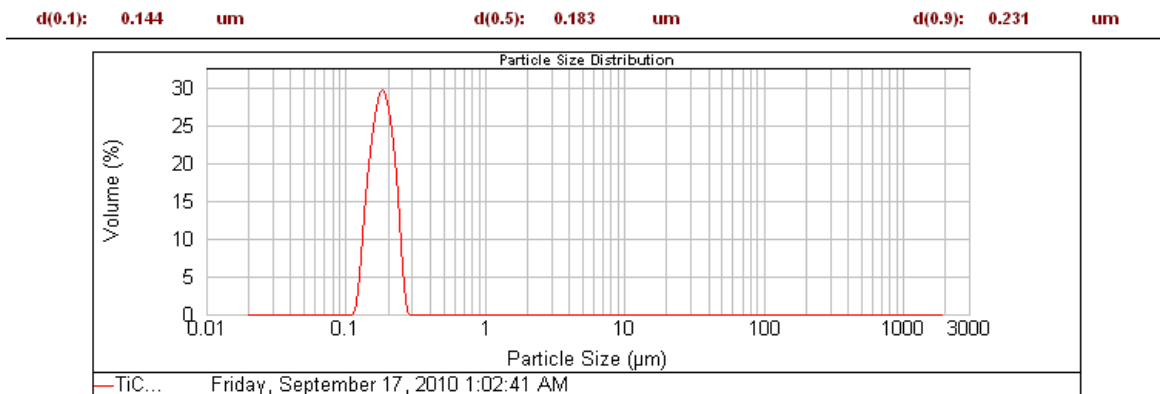


Figure 36: A graph showing the variation of viscosity in suspensions as a function of the Lubrizol content at a constant shear rate ($200s^{-1}$).

Figure 36 show that the minimum viscosity is in a range from $\sim 6.5 - 8$ wt% Lubrizol and that 2 wt. % of Lubrizol suspension had a very high viscosity (point not shown on the graph). Therefore a mass of 8.6 g of TiC was dispersed in 100 ml of hexane using ultrasonic probe for 2 hours with different Lubrizol weight percentages namely: 6.5, 7, 7.5 and 8. After ultrasonicing the suspensions, particle size analysis was done. The Lubrizol wt. % that yielded a unimodal particle size distribution (distribution with a single peak) and an average particle size that correspond to the powder specifications was 6.5 wt. % (Fig. 37).



The boron oxide (B₂O₃) covered CNTs were placed inside a tube furnace and it was purged with argon gas for 60 minutes. The temperature of the tube furnace was raised to 1165⁰C, and ammonia gas (99.99% pure) was pumped into the tube at a flow rate of 20 ml.min⁻¹ for 60 minutes. Ammonia gas reacted with boron oxide to form boron nitride onto the surface of CNTs according to Reaction 3.2.



3.6 Suspension formation and mixing of the suspensions

Dispersion and mixing of the powders was divided into three sections. This sections starts by describing the dispersion and mixing methods used to form Al₂O₃+CNTs suspension, it then proceeds by describing the formation of Al₂O₃+TiC suspension and lastly the Al₂O₃ + CNT + TiC suspension.

3.6.1 Al₂O₃ + CNTs suspension formation

The CNTs + Al₂O₃ suspension was done using two methods, varying the degree of intensity. Both the methods used alumina balls with a diameter of 2 mm.

3.6.1.1 High energy milling (more aggressive)

The high energy milling was done at Element Six Pty Ltd. A mass of 0.2 g of carbon nanotubes were dispersed in 100 ml of hexane, attritor milled at a speed of 1500 rpm for 1 hour, with the use of 0.02 g of PVP dispersant and 20 g of alumina balls (2 mm in diameter). After the CNTs were dispersed they were poured into with already dispersed 20 g of alumina suspension (in 150 ml hexane) in a beaker under constant stirring using a stirrer bar to obtain 3 vol. % (1 wt%) of CNTs in alumina. The resultant mixture was further stirred for 20 minutes. The mixture was then transferred back into the attritor mill and milled for 2 hours at a speed of 1500 rpm and with 100 g of alumina balls. The ball to powder ratio that was used was 5:1 and total hexane volume was 250 ml. The mixture was dried using a rotary evaporator and sieved through 80 μm sieve.

3.6.1.2 Low energy mill (less aggressive)

The low energy milling was done at the University of Witwatersrand, Johannesburg. A mass of 0.2 g of CNTs were dispersed in 100 ml of hexane using an ultrasonic probe for 30 minutes and they were milled for 2 hours in the attritor mill at a speed of 450 rpm, with the use of 0.02 g of PVP dispersant and 20 g of alumina balls (2 mm in diameter). After the CNTs were dispersed they were poured into an already dispersed alumina suspension containing 20g of alumina and 150 ml hexane. The mix was in a beaker under constant stirring using a stirrer bar to obtain 3 vol% (1 wt %) of CNTs in alumina. The resultant mixture was further stirred for 20 minutes. The mixture was then transferred into a planetary ball mill vessel and milled for 4 hours at a speed of 500 rpm and 100 g of alumina balls (2mm diameter). The ball to powder ratio used was 5:1 and the total hexane volume was 250 ml. The mixture was dried using a rotary evaporator and sieved through 80 μm sieve.

3.6.2 Al_2O_3 + TiC suspension formation

A mass of 8.6 g of TiC was dispersed in 100 ml hexane using ultrasonic probe as described in Section 3.4 and a mass of 20 g of alumina was also dispersed in 150 ml hexane using ultrasonic probe as described in Section 3.3. The suspensions were mixed in a beaker by slowly pouring the TiC suspension into the alumina suspension under constant stirring using a stirrer bar to obtain 30 wt. % (26 vol. %) of TiC in alumina. The mixture was further stirred for 20 minutes after the suspensions were mixed together. The mixture was then milled using a planetary ball mill for 5 hours at a speed of 500 rpm with 100 g of alumina balls (2 mm in diameter). The ball to powder ratio that was used was 5:1 and the total volume of hexane used was 250 ml. The mixture was dried using a rotary evaporator and sieved through 80 μm sieve. After the powder was dried, Lubrizol was burned-off in a tube furnace under argon atmosphere at 600°C for 1 hour.

3.6.3 Al_2O_3 + TiC + CNTs suspension formation

A mass of 0.2 g of CNTs was dispersed in 100 ml of hexane using ultrasonication and attritor milling as described in section 3.6.1.2 (low energy milling) and a mass of 8.6 g of TiC was dispersed in 100 ml of hexane using ultrasonic probe as described in section 3.4 and a mass of 20g of alumina was also dispersed in 150 ml hexane using ultrasonic probe as described in

section 3.3. The already dispersed CNT, Alumina and TiC suspensions were mixed in a beaker under constant stirring using a stirrer bar to obtain 2.1 vol. % (0.7wt%) of CNTs and 30 wt. % (26vol %) TiC in alumina. The suspension was then milled using a planetary ball mill for 4 hours at a speed of 500 rpm with 100 g of alumina balls (2 mm diameter). The ball to powder ratio used was 5:1 and the total volume of hexane used was 250 ml. The mixture was dried using a rotary evaporator and sieved through an 80 μm sieve. Lubrizol was burned-off from the powder before sintering in a tube furnace under argon atmosphere at 600°C for 60 minutes.

3.7 Compaction of Al_2O_3 + CNT sample

The [Al_2O_3 + CNT (3 vol. %)] powder was compacted using a compaction die in combination with a hydraulic press to examine whether the mixing method was sufficient and to examine the distribution of CNTs within the alumina powder. The powder was pressed with a pressure of 220 MPa for 15 minutes. The green compact had a bulk green density of 2.11 $\text{g}\cdot\text{cm}^{-3}$, which is 53% of the theoretical.

3.8 Sintering of the composites powders

A mass between 5 - 6 g of each powder was weighted and sintered using a graphite die. The graphite discs were coated with hBN to reduce any carbon diffusing into the samples. The sintering conditions for each composite powder are shown in Table 11.

Table 11: Sintering conditions used for sintering different composite powders using SPS

Composite powders	Sintering temperature (°C)	Sintering pressure (MPa)	Dwell time (minutes)	Heating rate (°C.min⁻¹)
Al_2O_3	1600	35	10	250
Al_2O_3 +CNTs	1600	35	10	250
Al_2O_3 +TiC	1600	35	10	250

Al ₂ O ₃ +TiC	1700	35	10	250
Al ₂ O ₃ +CNTs+TiC	1650	35	10	250

3.9 Thermal Etching of pure Al₂O₃ and [Al₂O₃+CNTs) samples

Polished alumina and [Al₂O₃+CNTs] samples were thermally etched to reveal the grain boundaries. Thermal etching is a process where heat energy is used to etch the grain boundaries of the sample hence revealing grains. This process was done using a tube furnace and an argon atmosphere. After the furnace was programmed to heat up at 10 °C.min⁻¹, furnace was purged with argon. The thermal etching was first done at 1200°C for alumina and at this temperature the alumina grains were not fully revealed. Therefore a higher temperature of 1300°C was used for both of the samples.

3.10 Density Measurements

After the samples were sintered they were sand blasted to remove hBN and any other particles on the surface. The density and open porosity of the sintered samples was determined using the Archimedes principle, taking the density of water to be 1 g.cm⁻³. The samples were first boiled in distilled water for 3 hours to displace any voids within the sample with water. After boiling the samples, three measurements of mass were done for each sample; these were suspended mass (M_S), wet mass (M_W) and dry mass (M_D). Density was measured using Equation 1.

$$\rho = \frac{M_D \times \rho_{\text{Water}}}{M_W - M_S} \quad \text{Equation 1}$$

And the open porosity can be calculated by

$$P_{\text{Open}} = \frac{M_W - M_D}{M_W - M_S} \quad \text{Equation 2}$$

3.11 Cutting, mounting and polishing the sintered samples

The samples were cut using a diamond blade into half so as to examine the cross sections. They were mounted using Polyfast[®] resin and a sample mounting machine. They were then polished using an automatic polishing machine according to the steps in Table 12.

Table 12: The grinding and polishing steps that were used to polish all the samples

Grinding			
Step	PG	FG 1	FG 2
Surface	MD-Piano 220	MD-Piano 1200	MD-Largo
Abrasive type			DP-Susp. P 9 µm
Lubricant type	Water	Water	Water
Speed [rpm]	200	150	150
Force [N]	10	10	10
Holder direction	»	»	»

Time [min.]	20	30	40
Polishing			
Step	PG	FG 1	FG 2
Surface	MD-Dac	MD-Nap	MD-Chem
Abrasive type	DP-Susp. P 3 μm	DP-Susp. P 1 μm	OP-S, P 0.04 μm
Lubricant type	DP-Blue	DP-Blue	-
Speed [rpm]	150	150	150
Force [N]	10	10	10
Holder direction	»	»	×
Time [min.]	30	15	5

3.12 Fracture surface of Al_2O_3 + CNTs

The Al_2O_3 + CNT sintered piece was fractured using a steel bar and the fracture surface was analysed using scanning electron microscope.

3.13 Analysis of materials

3.13.1 Optical Microscopy and Scanning electron microscopy

Optical microscope Axiotech 25 HD[®] from Carl Zeiss and Philips scanning electron microscope, XL30 SERIES[®] fitted with a field emission gun operating between 5 and 30 kV were used to examine the microstructure of the polished samples, the fracture surfaces of the samples and to examine the path taken by cracks when they are propagating through the sample. Optical microscopy was used as the starting analysis before scanning electron microscopy so as to obtain an idea whether the polishing process was successful.

3.13.2 Hardness and Fracture toughness measurements using indentation method

Hardness and fracture toughness were measured using an indentation method, where an indent was made on the surface of the polished sample under a 5 kg constant load for both hardness and fracture toughness measurements. The load was kept on the sample for 10 seconds. The diagonals and crack lengths that were induced by an indent (Fig. 39).

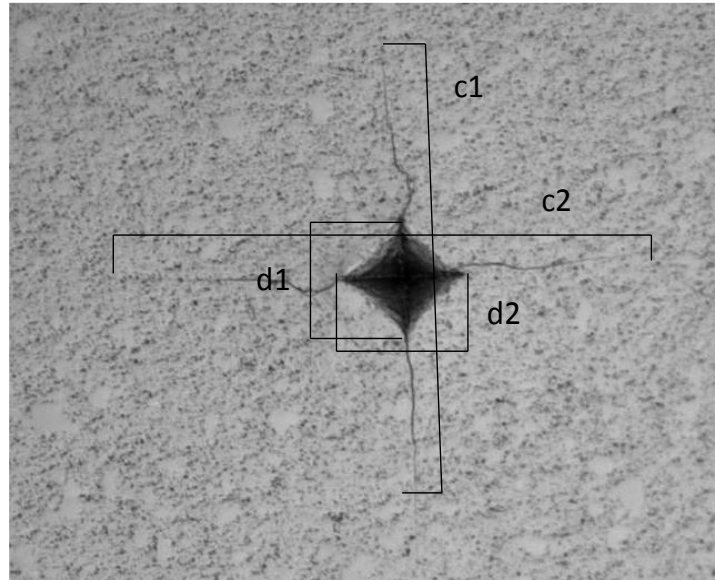


Figure 39: Indication of how the diagonals of the Vickers indentations and the crack lengths were measured

d = diagonals and c = crack length

Vertical and horizontal diagonals and crack lengths were measured and an average was taken for the calculations.

$$H_v = 1854.4 \frac{P}{d^2} \quad \text{Equation 3}$$

Equation 3 was used for calculating the Vickers hardness of the samples (HV), where P = the applied load in Newtons (N) and d is the average of the two diagonals in micrometers (μm).

$$K_{IC} = \xi \left(\frac{E}{H_v} \right)^{1/2} \left(\frac{P}{c^{3/2}} \right) \quad \text{Equation 4}$$

Equation 4 was used for the calculation of the fracture toughness of the samples (K_{IC}), where ξ the calibration constant (0.016), E is the Young's Modulus of Elasticity (GPa) and c the average crack length (μm).

3.13.3 Electrical conductivity measurement

The electrical conductivity was measured using DC 41-40 SMU which applied a voltage of different magnitudes to the samples depending on the conductivity of the sample and the resultant current was measured. The samples that were used to measure electrical conductivity were cut into the dimensions shown in Table 13.

Table 13: The dimensions of the samples and the calculated area

Sample	Length (mm)	Width (mm)	Breadth (mm)	Cross sectional Area (m^2)
Al_2O_3	1.80	0.43	0.40	1.7×10^{-7}
$\text{Al}_2\text{O}_3 + \text{CNTs}$	1.90	0.30	0.28	8.4×10^{-7}
$\text{Al}_2\text{O}_3 + \text{TiC}$	1.95	0.38	0.30	1.1×10^{-7}
$\text{Al}_2\text{O}_3 + \text{CNTs} + \text{TiC}$	1.80	0.40	0.38	1.5×10^{-7}

The shape of the cut samples is shown in Fig. 40. The DC 41-40 SMU instrument applies a voltage to the sample though two wires and measures the current passing through.



Figure 40: Images of the (Al_2O_3 , [$\text{Al}_2\text{O}_3 + \text{CNTs}$ (3 vol. %)] and [$\text{Al}_2\text{O}_3 + \text{TiC}$ (30 wt. %)] samples, the black samples being the conducting samples.

Chapter Four

4.0 Experimental findings

This section of the dissertation describes the results obtained from the experiments conducted. Firstly the results that were obtained from the production of the nanotubes and the coating of the sourced CNTs are described. Subsequently analysis and properties of pure Al_2O_3 , $\text{Al}_2\text{O}_3 + \text{CNTs}$, $\text{Al}_2\text{O}_3 + \text{TiC}$ and $\text{Al}_2\text{O}_3 + \text{CNT} + \text{TiC}$ are reported. The powders were mixed a systematic way so as to fully understand the system as described in chapter 3; therefore the results that were obtained are presented in a sequence corresponding to the way the powders were mixed. The results section starts with the comparison between pure alumina and mixture of alumina with CNTs, the pure alumina and mixture of alumina with TiC and lastly the comparison of all the results obtained from each sintered ceramic.

4.1 Preparation of the Carbon nanotubes

The CNTs production experiment was done at the University of Witwatersrand, showed that carbon nanotubes were formed (Fig. 41). The variation in acetylene flow rate had little effect on the amount of MWCNTs produced; therefore the results discussed here are for a flow rate of 60 ml/min and a time of 25 minutes. The MWCNTs that formed had diameter between the range of 40-150 nm (Fig. 41 and 42).

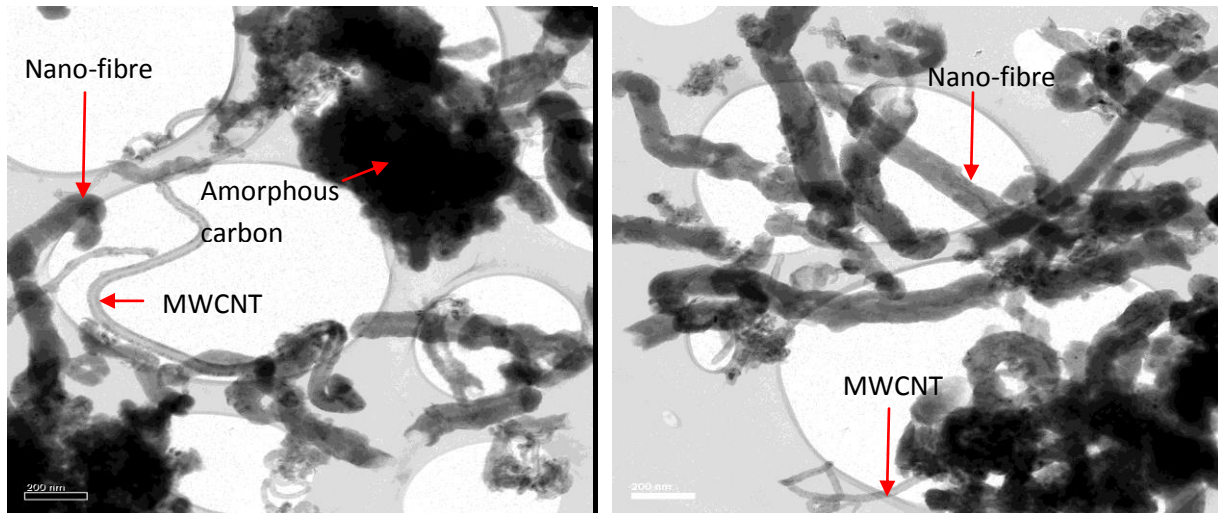


Figure 41: TEM images of multi walled carbon nanotubes in a mixture with amorphous and nano-fibres carbon as pointed by the red arrows.

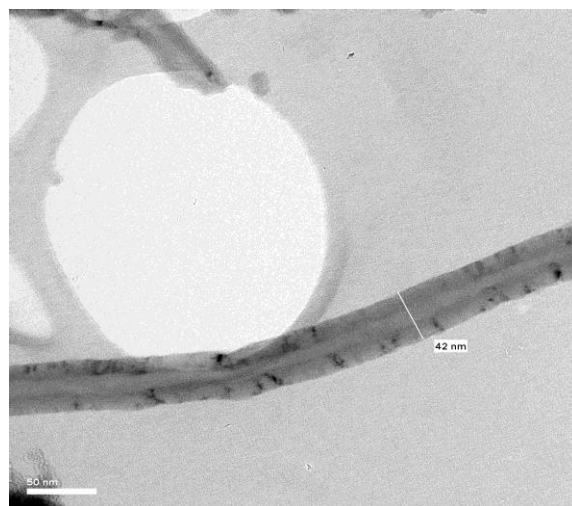


Figure 42: TEM image of carbon nanotube showing that it had a diameter of 42 nm

4.2 Coating and dispersion of Carbon nanotubes with hBN

The hBN coated CNTs were analyzed using TEM. The samples were first ultrasonicated for 20 minutes. The images in figure 43 show that the carbon nanotubes were possibly coated with hBN, but it could not be confirmed by EDX since the TEM used was not equipped with such an instrument.

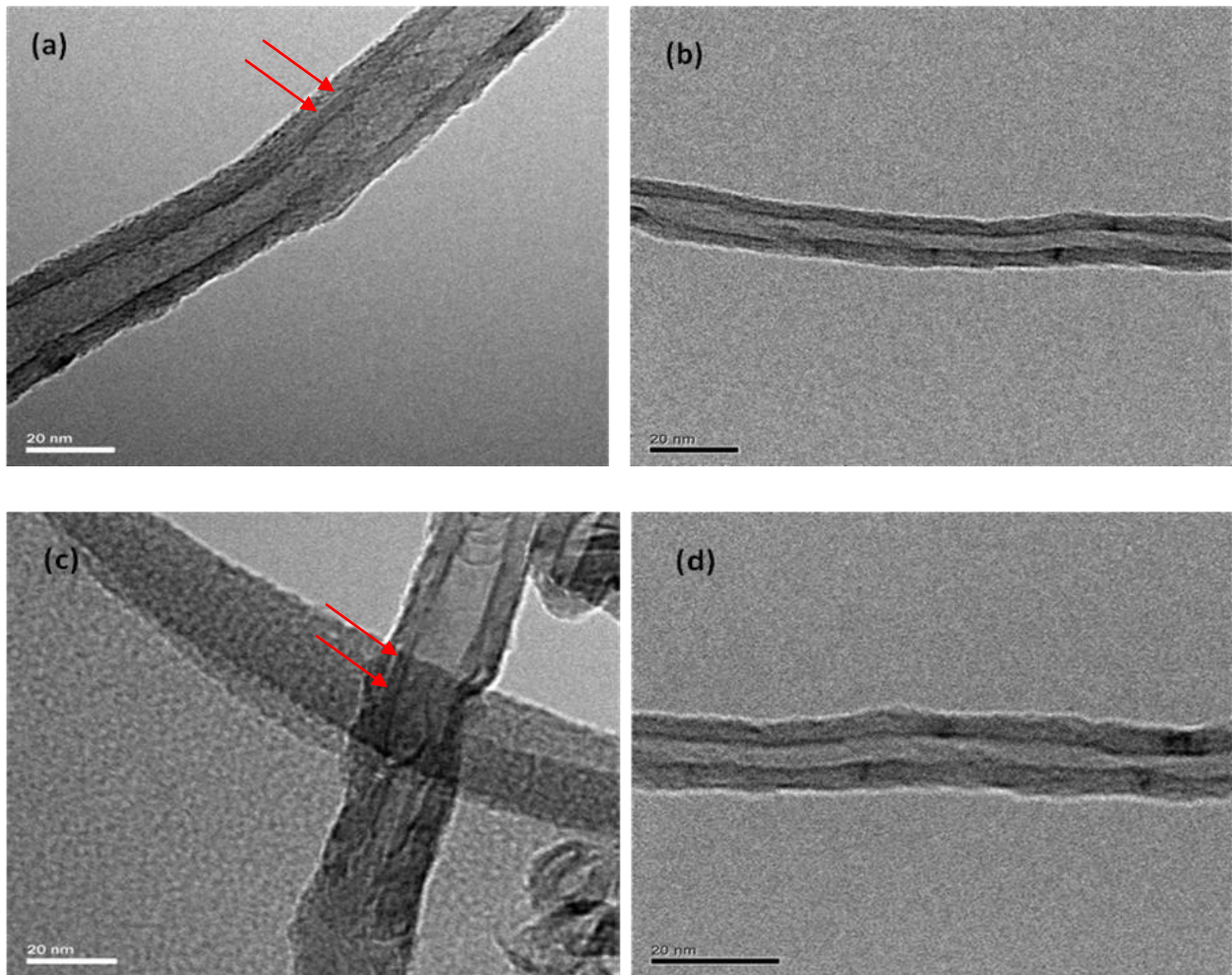


Figure 43: TEM images of hBN coated CNTs ((a), (c)) and uncoated CNTs ((b), (d)) the hBN coating is shown by the interface pointed by the arrows which is only present on the coated CNTs but not the uncoated CNTs.

The hBN coating was “flaking off” of the CNTs after ultrasonication for 20 minutes. The “flaking off” is evident by the uneven CNT walls. The images (Fig 44) show the “flaking-off” of the hBN coated CNT.

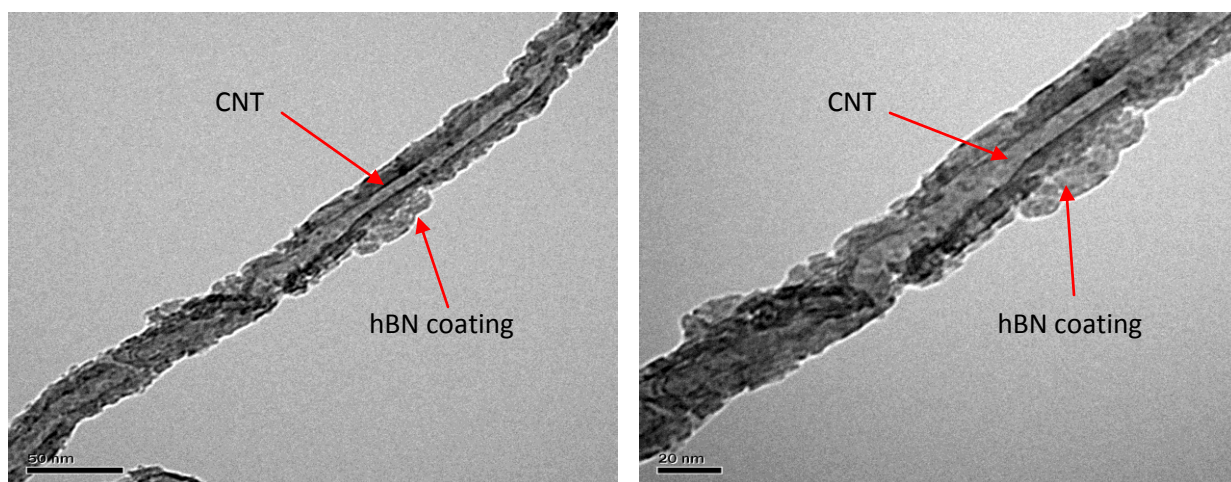


Figure 44: TEM images of CNTs coated with hBN, the uneven surface of the CNTs shows that the coating was flaking off due to the ultrasonication.

The major problem with the hBN coated CNTs was that boron oxide melts at $\approx 450^{\circ}\text{C}$ forming a carbon nanotube matte, so even if it was possible to coat single carbon nanotube during the reaction with ammonia it would be surrounded by excess hBN. The hBN coated CNT increased the difficulty of dispersion. The hBN coated CNTs were dispersed using ultrasonication for 20 minutes and the TEM results shows that the coating was “flaking off”. The “flaking off” of hBN coating reveals that the CNT- hBN interface was weak.

4.3 Compaction of Al_2O_3 + CNT sample

The [Al_2O_3 + CNT (3 vol. %)] green compact was analyzed using optical microscope to examine the CNTs distribution within Al_2O_3 . The CNTs were well distributed within the alumina (Fig.45).

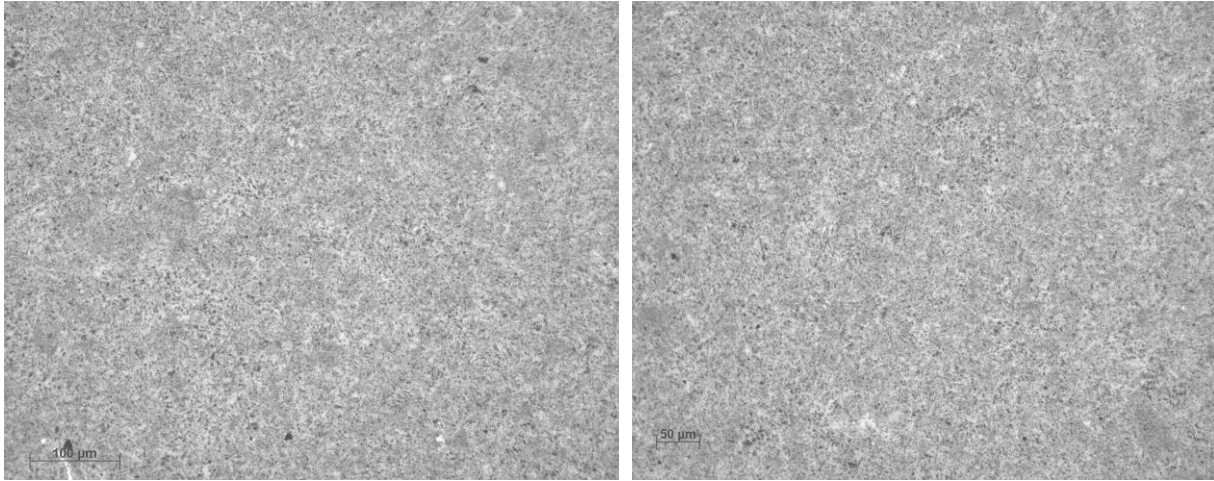


Figure 45: Optical microscope images of [Al_2O_3 + CNT (3 vol. %)] green compact

4.4 Sintering curves of the samples

The SPS sintering curves give information about the SPS machine status and information about the behavior of the material during sintering. For example from the SPS data after sintering, if there is a shift in the graph of temperature, density and time for the same sample that could mean there was a fault with the SPS machine itself. This section of the dissertation focuses on the behavior of the material during sintering more then the status of the SPS machine.

4.4.1 Al_2O_3 sample

The programmed sintering temperature for Al_2O_3 sample was 1600°C. The recorded temperature profile and piston travel was plotted against sintering time (Fig. 46 (a)) and piston speed was plotted against sintering time (Fig. 46 (b)).

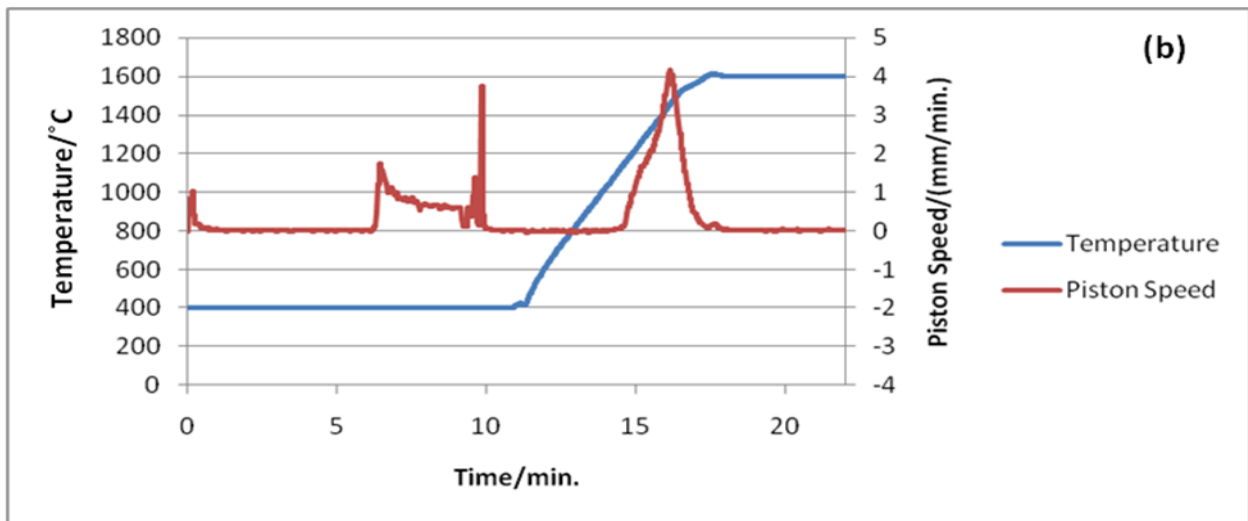
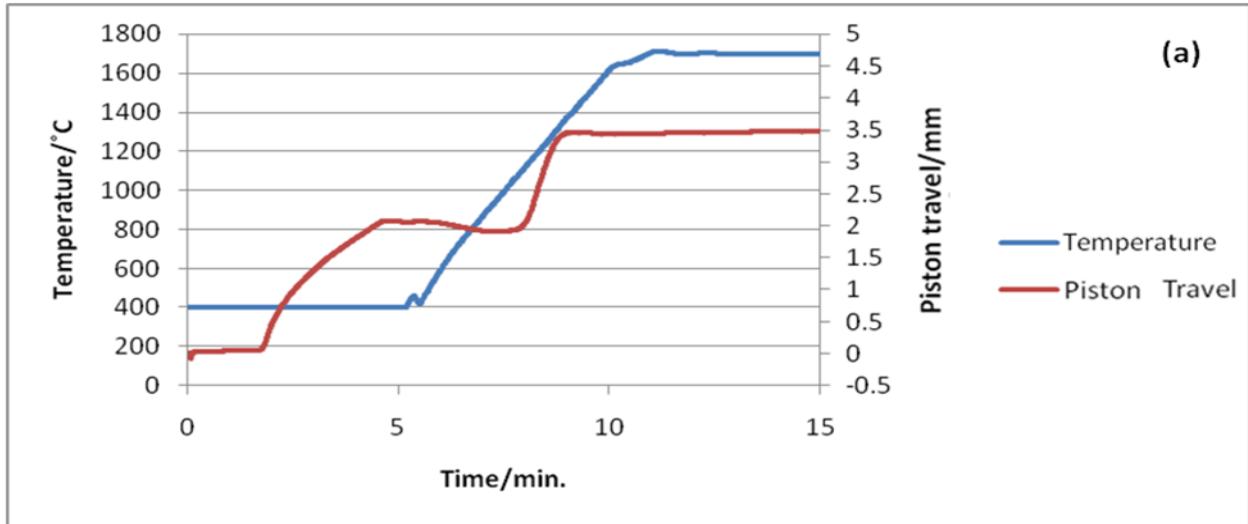


Figure 46: Relationship between temperature and piston travel (a) and temperature and piston speed (b) during sintering of Al_2O_3 sample

The sintering curves show that the sample was initially compacted at 400°C and the sintering of the sample occurred at 1600°C and dwelled for 10 minutes.

4.4.2 [Al₂O₃+CNTs] sample

The programmed sintering temperature for [Al₂O₃ + CNTs] sample was 1600°C. The temperature and piston travel against sintering time (Fig. 47 (a)) and piston speed against sintering time (Fig. 47 (b)).

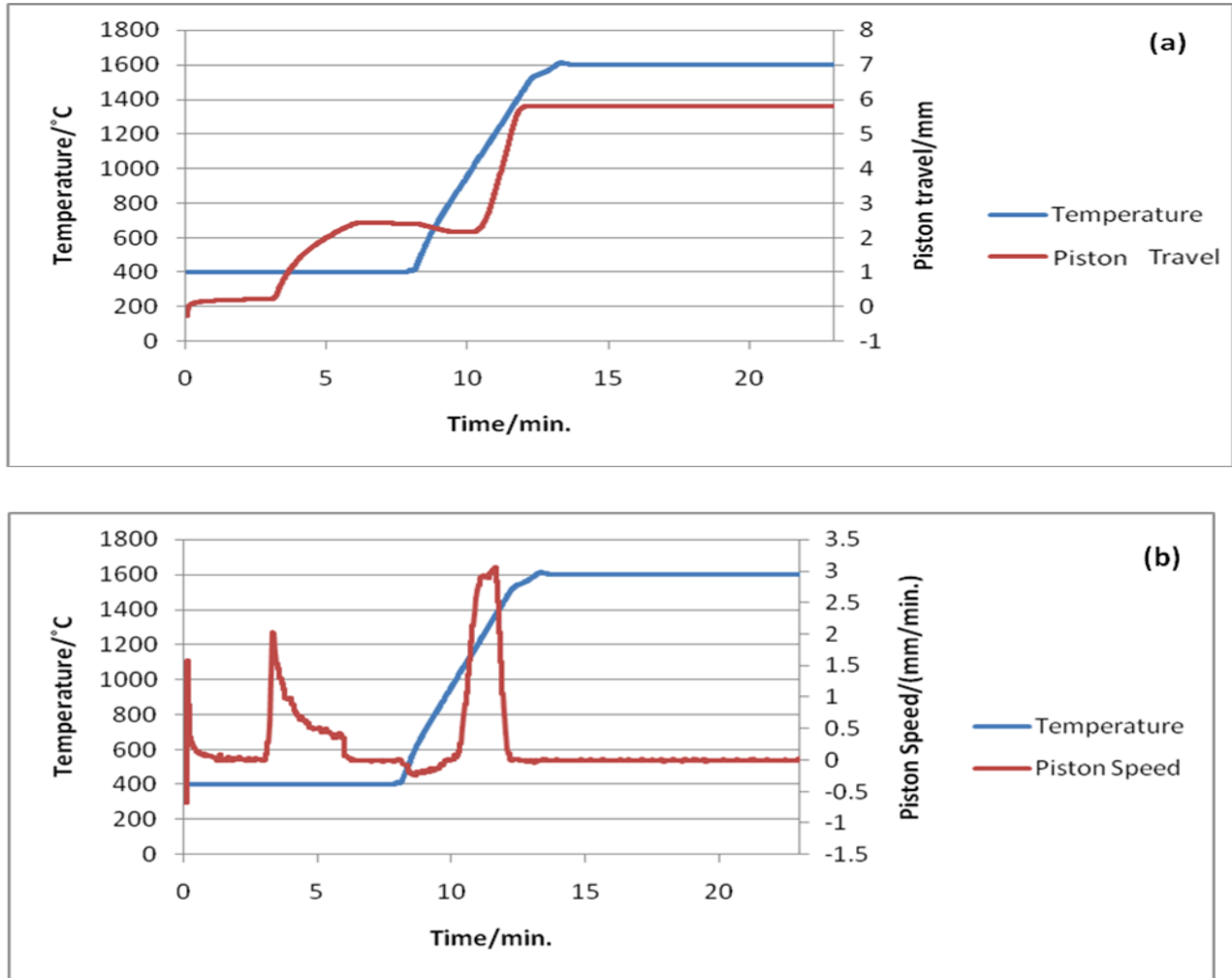


Figure 47: Relationship between temperature and piston travel (a) and temperature and piston speed (b) during sintering of [Al₂O₃ + CNTs (3 vol.%)] sample

The sintering curves show that the addition of the CNTs into alumina did not change the compaction process (Fig. 47(b)) which occurred at 400°C. The sintering of the sample occurred at 1600°C and dwelled for 10 minutes.

4.4.3 [Al₂O₃+TiC] sample

The programmed sintering temperature for [Al₂O₃ + TiC] sample was 1700°C. Temperature and piston travel against sintering time (Fig. 48 (a)) and piston speed against sintering time (Fig. 48 (b)).

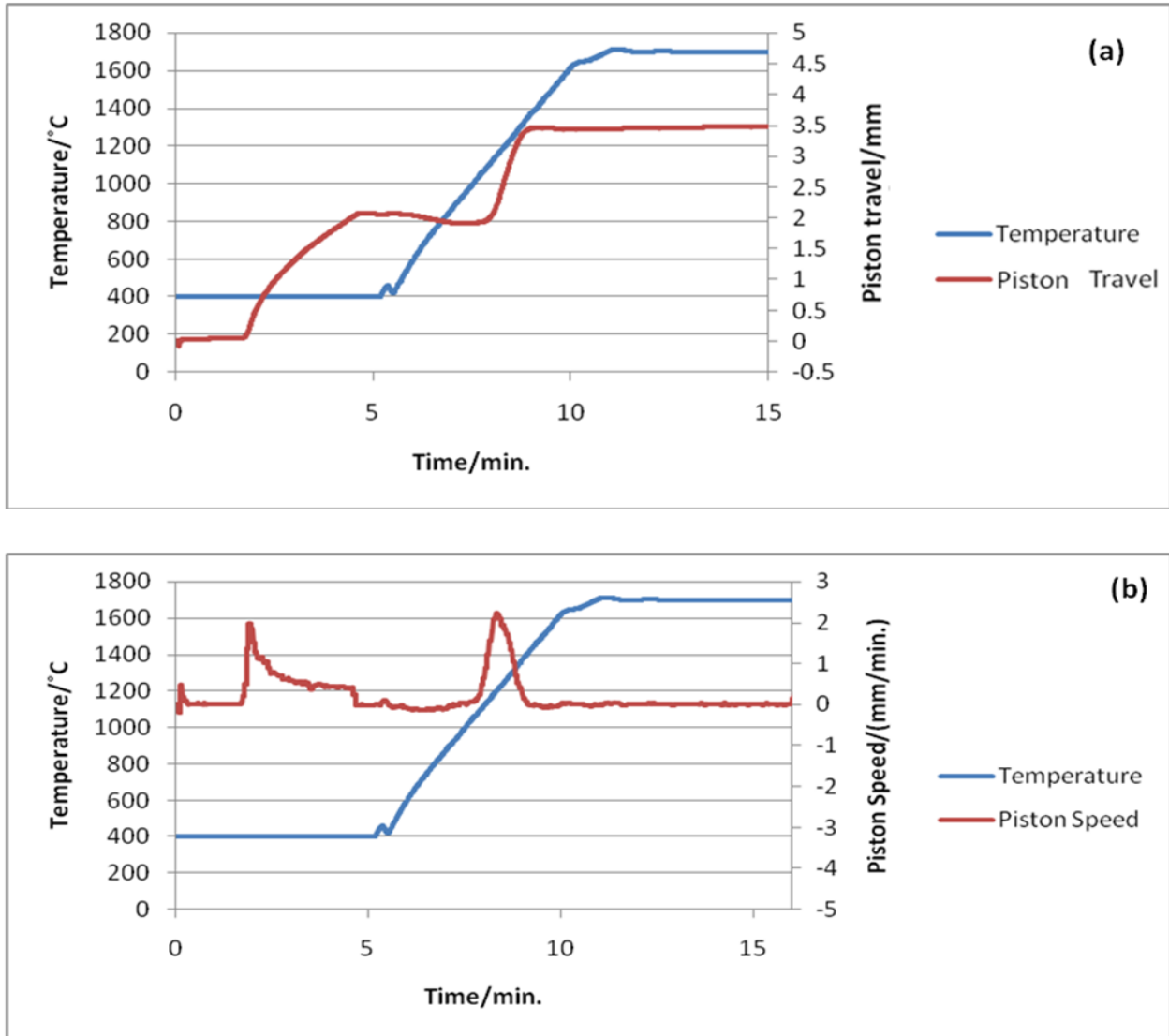


Figure 48: Relationship between temperature and piston travel (a) and temperature and piston speed (b) during sintering of [Al₂O₃ + TiC (30 wt%)] sample

The sintering curves show that the addition of TiC into alumina did not change the compaction process (Fig. 48(b)) which occurred at 400°C. The sintering of the sample occurred at 1700°C and dwelled for 10 minutes.

4.4.4 [Al₂O₃+CNTs +TiC] sample

The programmed sintering temperature for [Al₂O₃ + CNTs + TiC] sample was 1650°C. The temperature and piston travel was plotted against sintering time (Fig. 49 (a)) and piston speed was plotted against sintering time (Fig. 49 (b)).

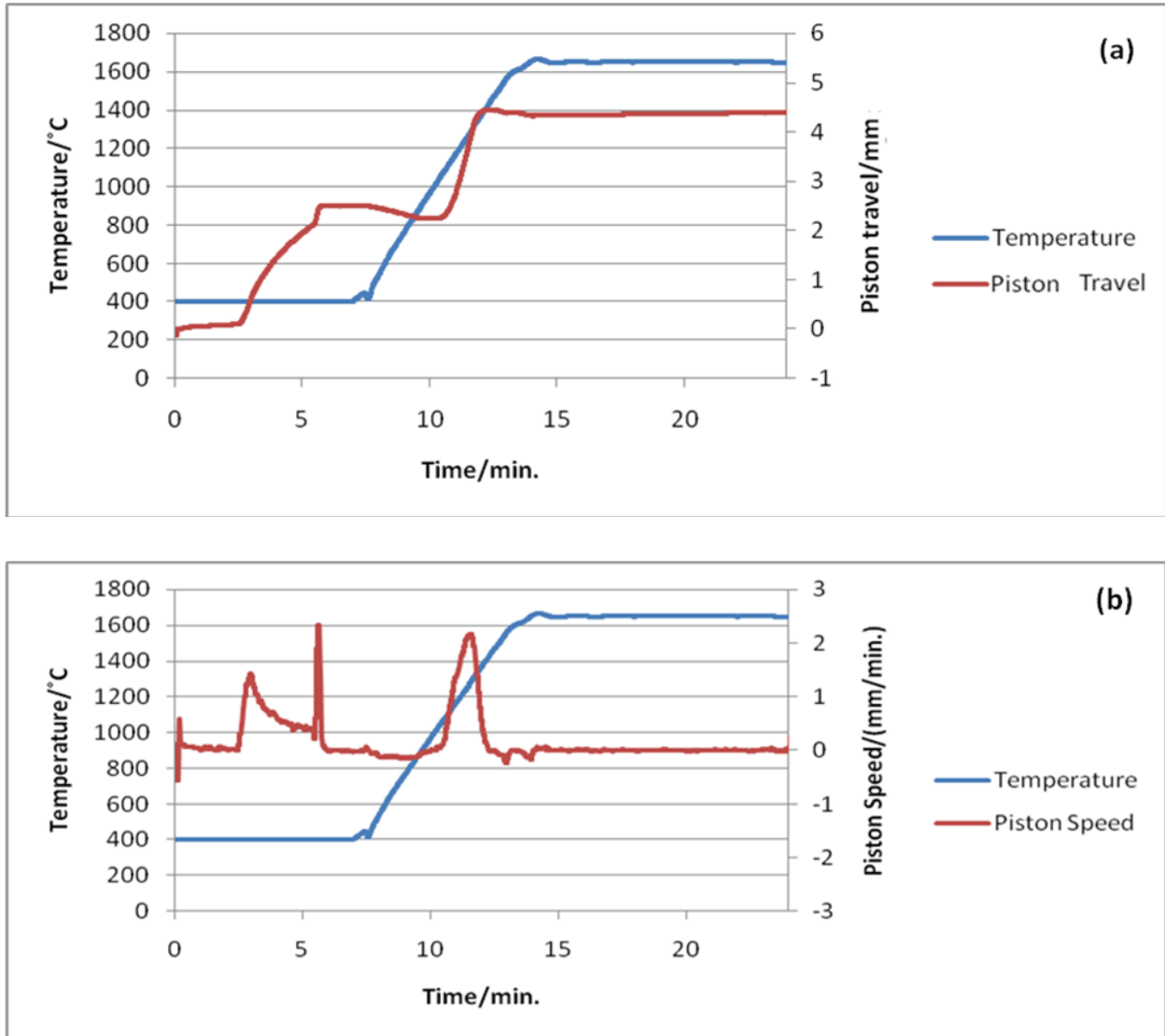


Figure 49: Relationship between temperature and piston travel (a) and temperature and piston speed (b) during sintering of [Al₂O₃ +CNTs +TiC] sample

The sintering curves show that the addition of both TiC and CNTs into alumina did not change the compaction process (Fig. 49(b)) which occurred at 400°C. The sintering of the sample occurred at 1650°C and dwelled for 10 minutes.

4.1 Density measurements of the sintered ceramics

The density of the samples was measured according to the method described in Chapter 3 and the results are given in table 14.

Table 14: The density results for all the samples, with their theoretical densities and the sintering temperatures

Material	Theoretical density (g.cm ⁻³)	Measured Density (g.cm ⁻³)	Density (%)	Sintering temperature (°C)
Pure Al ₂ O ₃	3.98	3.97 ± 0.04	99.8	1600
Al ₂ O ₃ +CNT (3 vol. %)	3.90	3.88 ± 0.06	99.4	1600
Al ₂ O ₃ +TiC (30 wt. %)	4.23	4.04 ± 0.08	95.5	1600
Al ₂ O ₃ +TiC (30 wt. %)	4.23	4.18 ± 0.03	99.0	1700
Al ₂ O ₃ +CNT (3 vol.%) +TiC (30 wt. %)	4.17	4.14 ± 0.06	99.2	1650

The theoretical densities of the composite powders were calculated according to Equation 5. The calculation for theoretical density of [Al₂O₃ + CNT (3 vol. %)] is shown and for the other composite powders, the calculations are shown in *Appendix A*.

$$\rho_f = \rho_1 (f) + (1-f) \rho_2$$

Equation 5

ρ_f = Final density of the mixture and f = volume fraction

ρ_1 and ρ_2 = Density of monolithic powder

Calculation of theoretical density of [Al₂O₃ + CNT (3 vol. %)] sample

$$\rho_1 (\text{Al}_2\text{O}_3) = 3.98 \text{ g.cm}^{-3} \quad \rho_2 (\text{CNTs}) = 1.3 \text{ g.cm}^{-3}$$

$$f (\text{CNTs}) = 0.03$$

$$\rho_T = 3.98 (0.97) + 1.3 (0.03) = 3.90 \text{ g.cm}^{-3}$$

4.2 Microstructural analysis of the sintered samples

After the samples were polished their microstructures were analyzed using optical and scanning electron microscopy. They were first analyzed using optical microscopy to determine whether the polishing was successful; they were re-polished if necessary.

4.2.1 Alumina sample

The images of pure alumina in figure 50 that was taken using an optical microscope shows that the sample was dense with no pores on the cross section (Fig. 50).

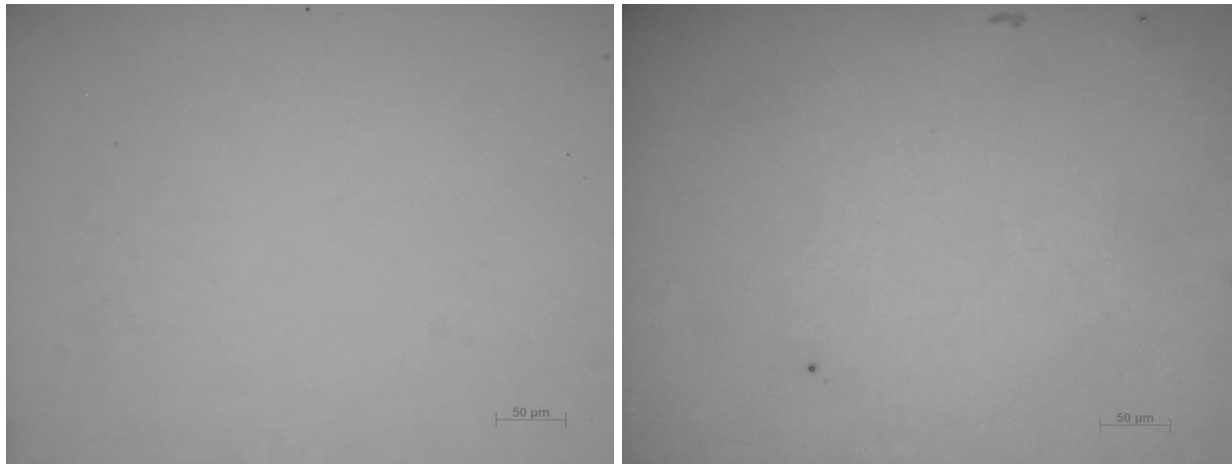


Figure 50: Optical microscope images of pure alumina showing that the sintering was successful since there are no pores showing on the polished cross section.

4.2.1.1 Thermal etching

Alumina samples were thermally etched according to the procedure described in chapter 3. Thermal etching was carried out at two different temperatures to determine which one gave better results. The results of samples thermally etched at 1200°C and 1300°C are shown in Fig. 51 and Fig. 52 respectively.

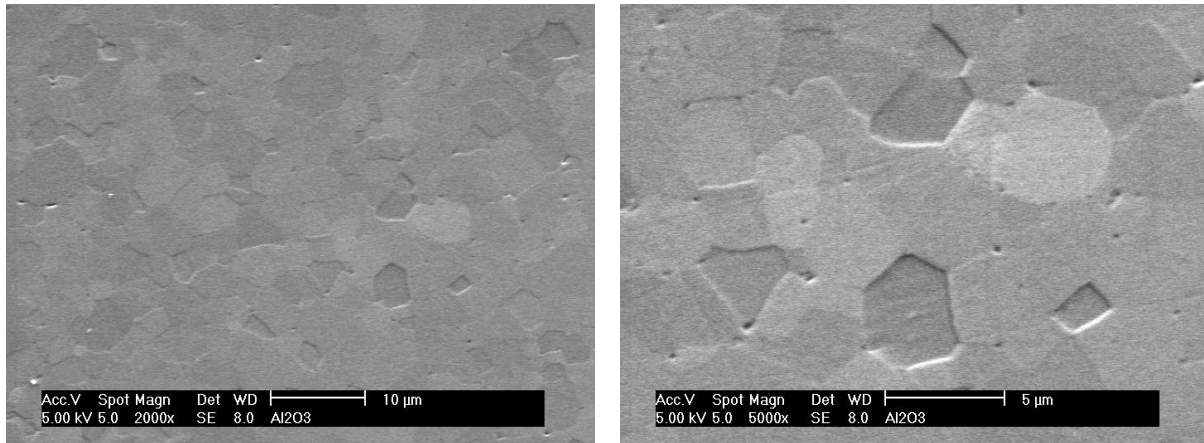


Figure 51: SEM images of alumina thermally etched at 1200°C for 60 min., showing alumina grain size between 2 – 4 µm

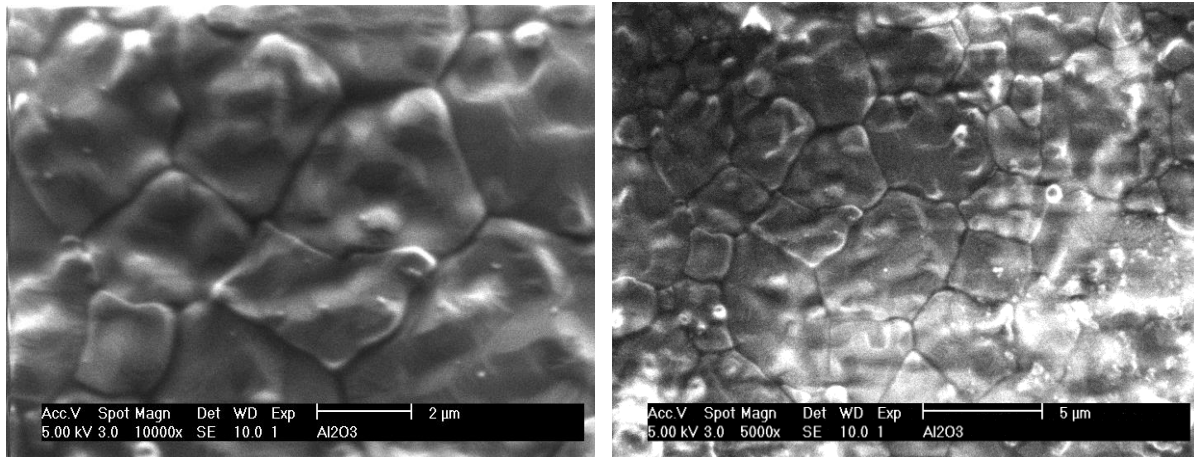


Figure 52: SEM images of alumina thermally etched at 1300°C for 60 min., showing alumina grain size between 2 – 4 µm

The results obtained from the thermal etching of the samples showed that the sample etched at 1300°C revealed the grains more clearly than the sample etched at 1200°C. Therefore thermal etching of [Al₂O₃ + CNTs (3 vol. %)] samples was done at 1300°C for 60 min.

4.2.2 [Al₂O₃ + CNTs (3 vol. %)] sample

A sintered sample of [Al₂O₃ + CNT (3 vol. %)] was analyzed using optical microscopy. The CNTs were evident as black spots pointed by the red arrows (Fig. 53 and Fig. 54). The CNT distribution dispersed using a high energy attritor mill at 1500 rpm (Fig. 53) was similar to the one operated at 500 rpm (Fig. 54) as described in chapter 3. The CNT were distributed within the alumina matrix even though it still had some agglomerates. The black bold arrows on the images show the sintering direction.

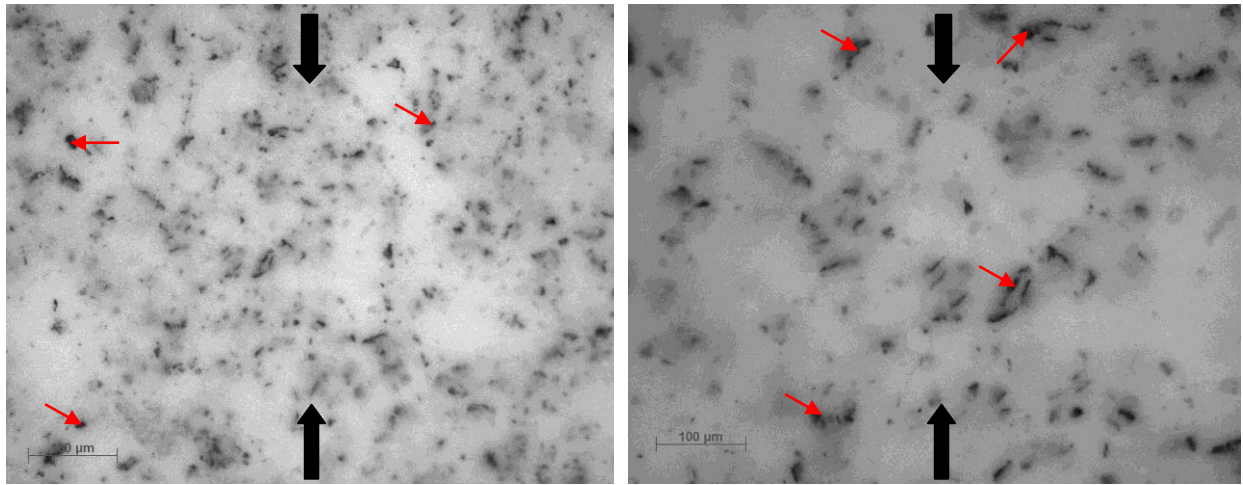


Figure 53: Optical microscope image of [Al₂O₃ + CNT (30 wt. %)] dispersed at 1500 rpm, sintered at 1600°C, 35 MPa

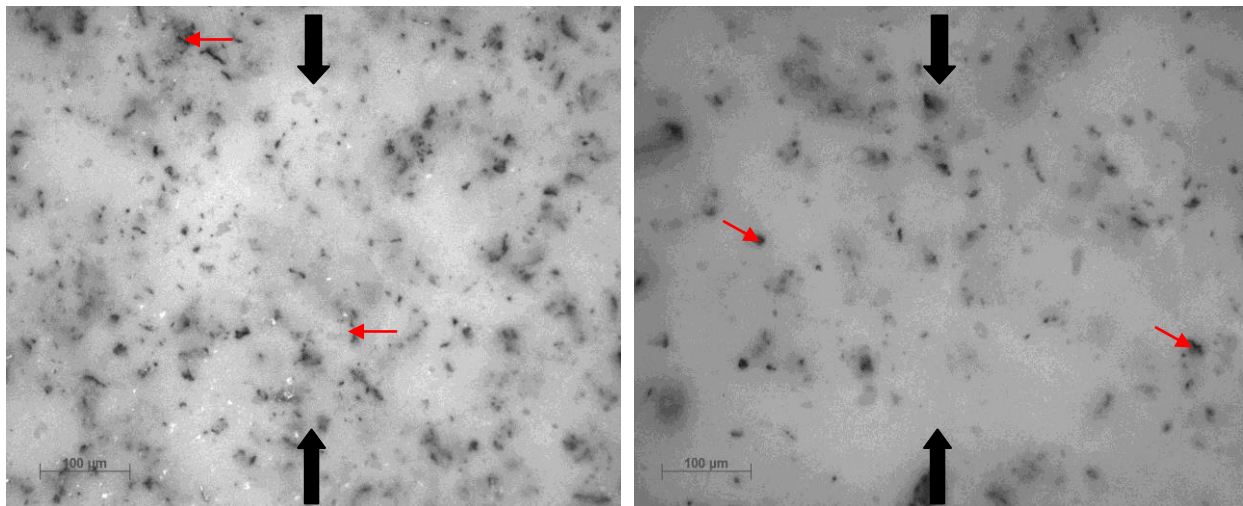


Figure 54: Optical microscope image of [Al₂O₃ + CNT (30 wt. %)] dispersed at 500 rpm, sintered at 1600°C, 35 MPa

The [Al₂O₃ + CNTs (3 vol. %)] samples were further analyzed using SEM. The SEM images show that the CNTs were distributed within the alumina matrix (Fig. 55 and Fig. 56). The black spots were analyzed using EDS and it was confirmed that they were carbon from CNTs (Fig.56).

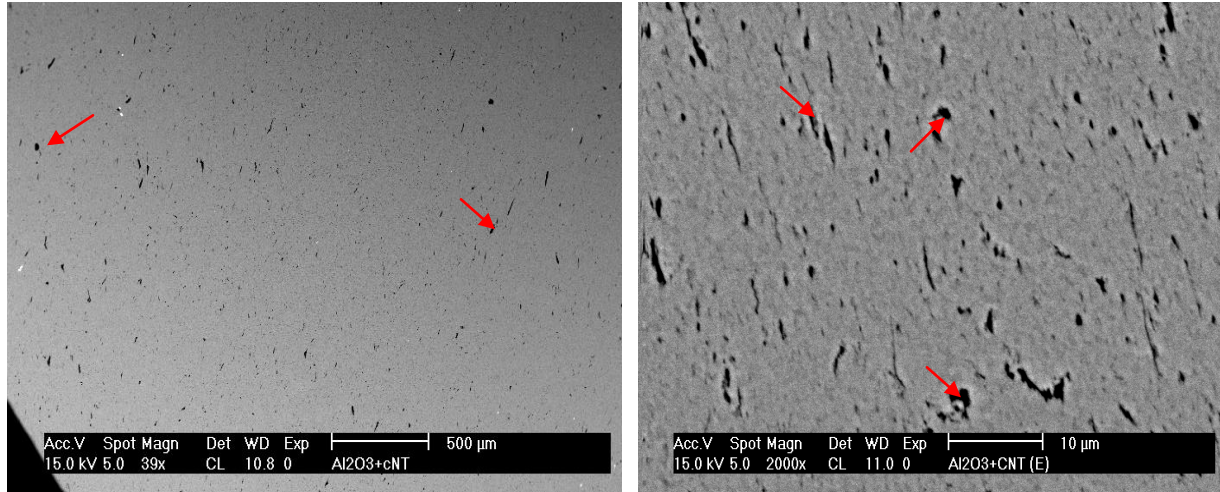


Figure 55: SEM images of [Al₂O₃ + CNTs (3 vol. %)] sample that was milled at 1500rpm, showing a distribution of carbon nanotubes (as black spots) within alumina.

[include other sem image of this at same magnification]

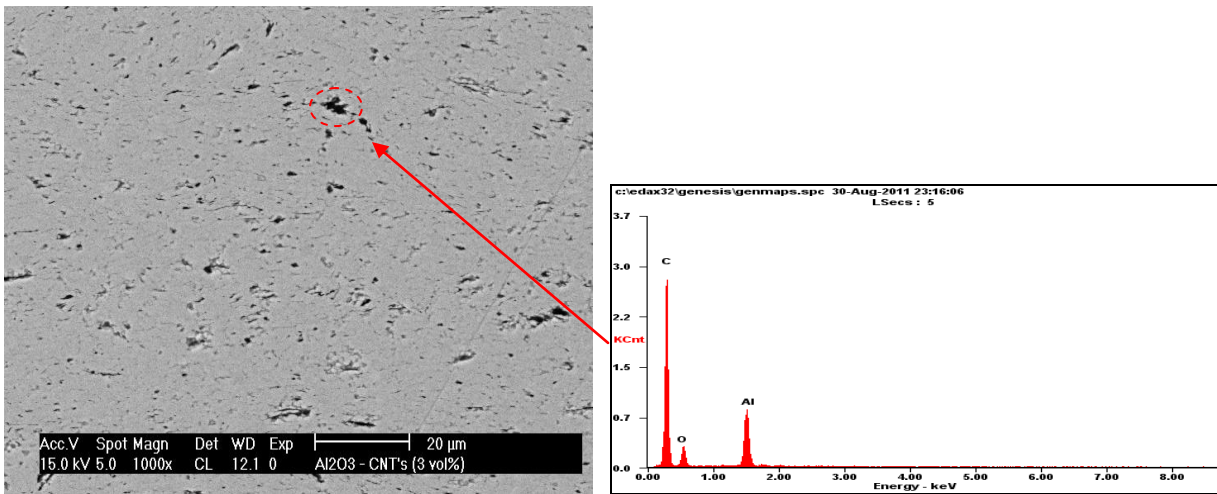


Figure 56: SEM images of [Al₂O₃ + CNTs (3 vol. %)] sample that was milled at 500rpm, showing a distribution of carbon nanotubes (as black spots) within alumina.

The SEM results obtained from the dispersion and distribution of CNT within alumina show that there was no difference observed between the aggressive milling method and the less aggressive milling method (Fig. 53 and Fig.54). Therefore the less aggressively dispersed samples were used for all other analysis.

4.2.2.1 Thermal etched sample

After thermally etching [Al_2O_3 + CNTs (3 vol. %)] sample, the grains revealed had a grain size were between 0.2 – 0.5 μm (Fig. 57).

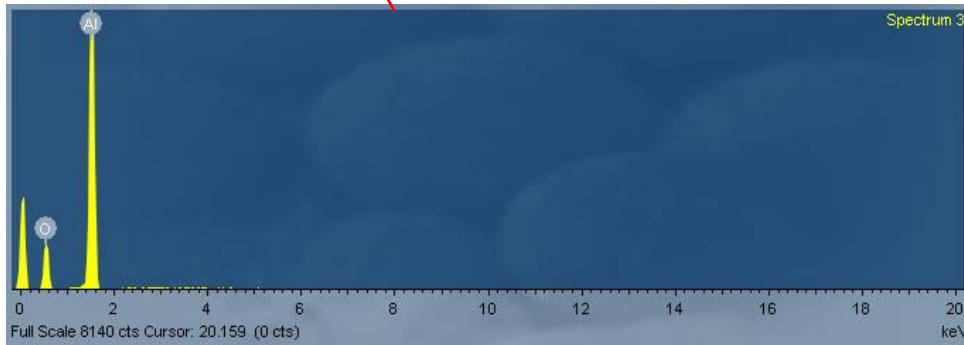
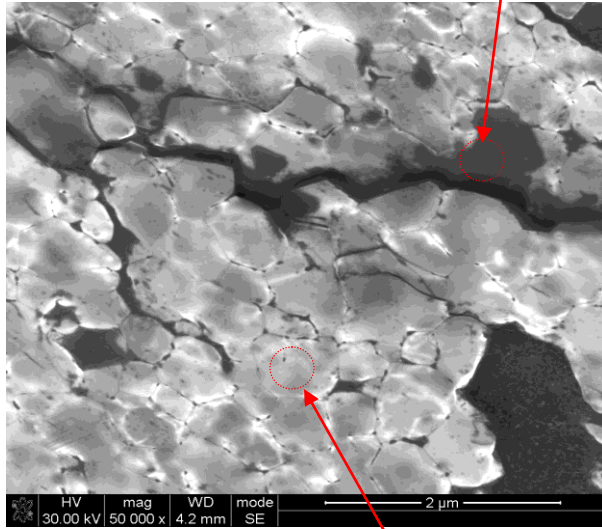
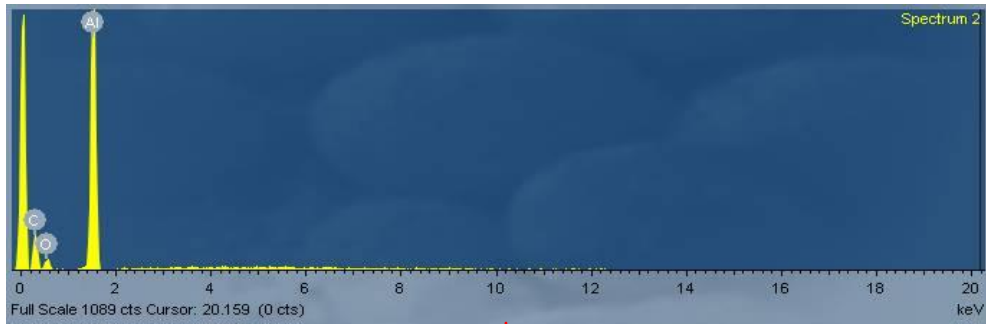


Figure 57: SEM images [Al₂O₃ + CNTs (3 vol. %)] sample, thermally etched at 1300°C under argon atmosphere, showing grain size between 0.3 – 0.5 μm. the EDS shows that carbon atoms are mostly found along the cracks and grain boundaries (as pointed by the arrows).

4.2.2.2 Fracture surface of the sample

The [Al₂O₃+CNTs (3 vol.%)] sample fractured surface was analyzed using SEM to show CNTs “sticking-out” of the alumina matrix. The fractured surface SEM results showed the CNTs pull-outs (Fig.58) revealing that CNTs survived the sintering conditions and therefore they can act as Al₂O₃ reinforcement.

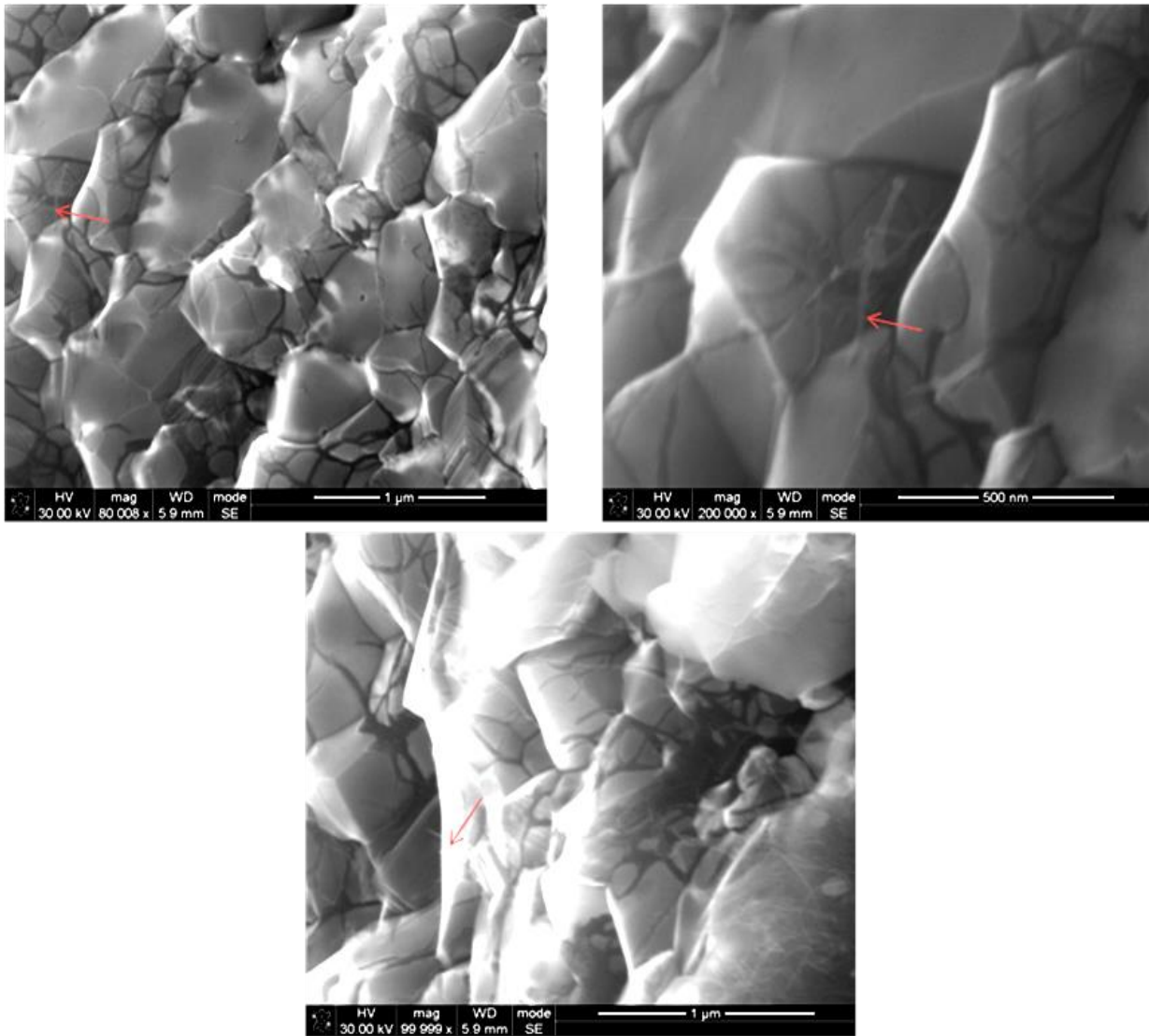


Figure 58: SEM images of [Al₂O₃ + CNTs (3 vol. %)] fractured surface showing CNTs sticking out of the alumina matrix as shown by the arrows.

4.2.3 [Al₂O₃ + TiC (30 wt. %)] sample

The Al₂O₃+TiC (30 wt. %) samples were sintered at 1600°C and 1700°C to determine which temperature was sufficient to densify the sample to highest density. The samples were both examined using optical microscopy. The results obtained show that TiC was well distributed (Fig. 59 and Fig. 60), but from the optical microscopy images it was not easy to determine which temperature was sufficient in densifying the sample.

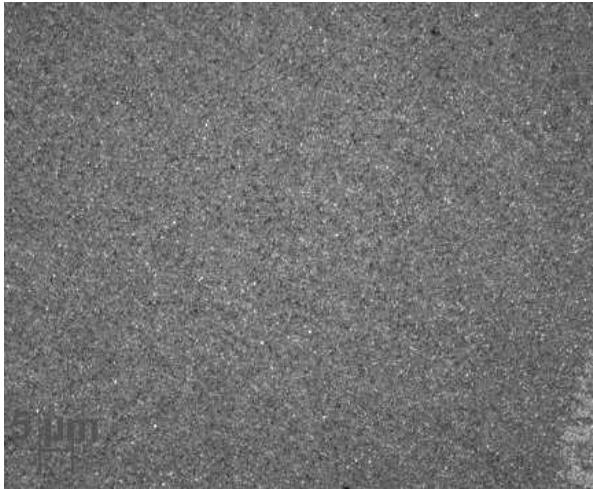


Figure 59: Optical microscope image of [Al₂O₃ + TiC (30 wt. %)] sintered at 1600°C, 35 MPa

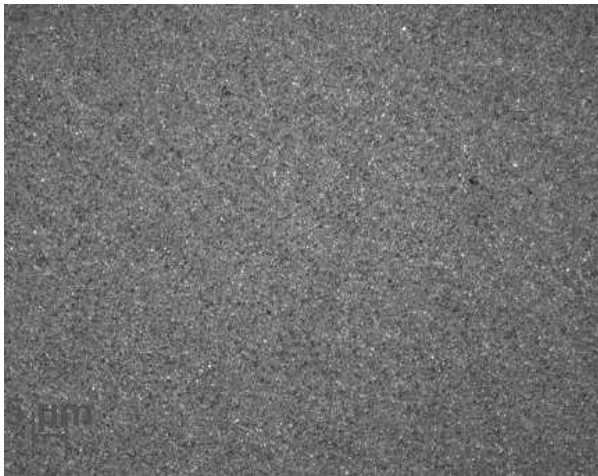


Figure 60: Optical microscope image of [Al₂O₃ + TiC (30 wt. %)] sintered at 1700°C, 35 MPa

In order to determine which temperature was sufficient to densify the sample, SEM analysis was done on the cross section of the sample (Fig. 61 and Fig. 62). The white particles are TiC and the grey matrix is alumina.

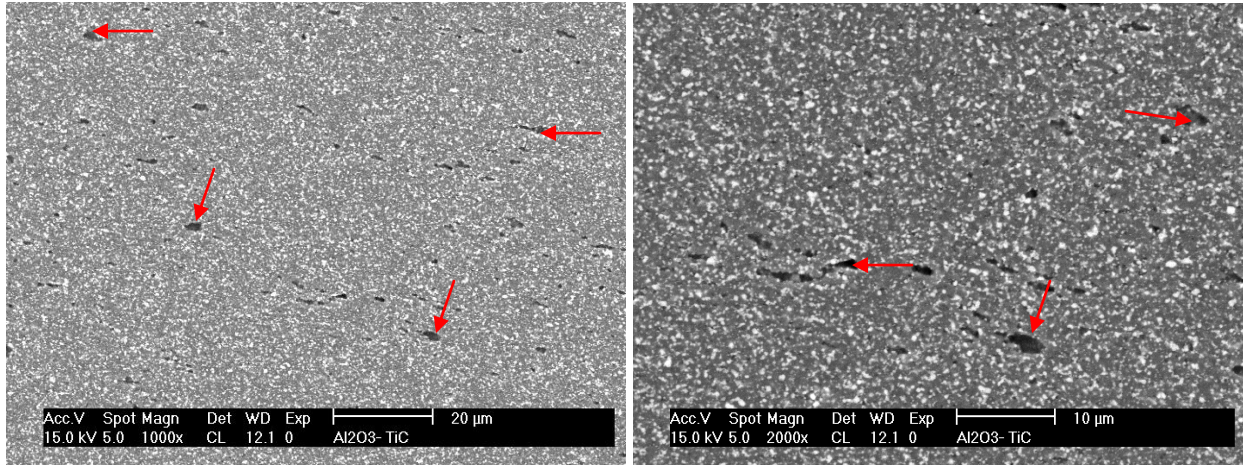


Figure 61: SEM images of [Al₂O₃ + TiC (30 wt. %)] sintered at 1600°C, 35 MPa

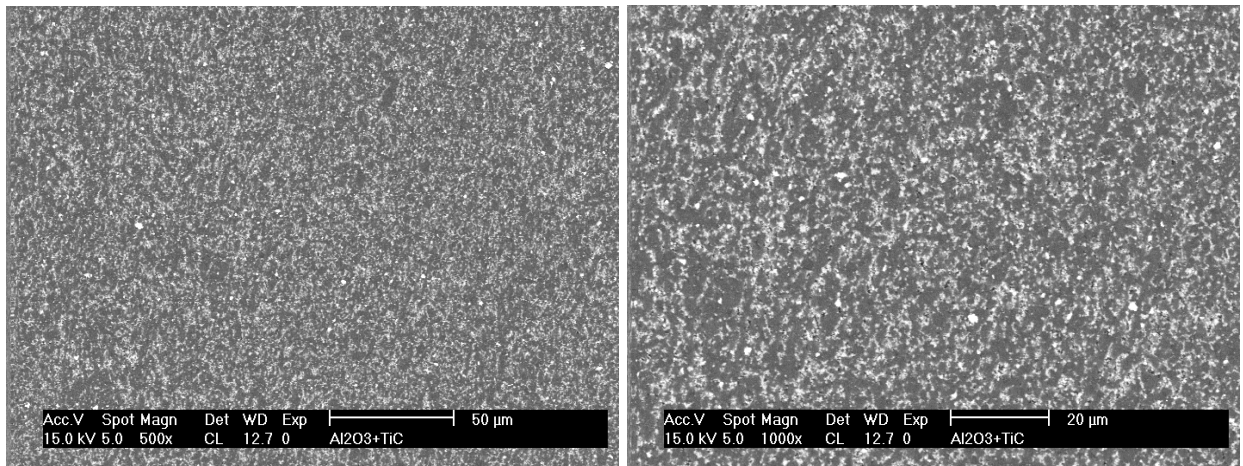


Figure 62: SEM images of [Al₂O₃ + TiC (30 wt. %)] sintered at 1700°C, 35 MPa

The SEM images of the samples sintered at 1600°C and 1700°C both show that the TiC was well distributed within alumina matrix. The sample sintered at 1600°C was porous as shown by the arrows (Fig.61), the sample sintered at 1700°C showed little porosity (Fig. 62). Therefore the sample sintered at 1700°C was further analyzed.

After it was determined that the sample sintered at 1700°C had well distributed TiC grains and was nearly completely densified, crack propagation was examined using SEM (Fig. 63).

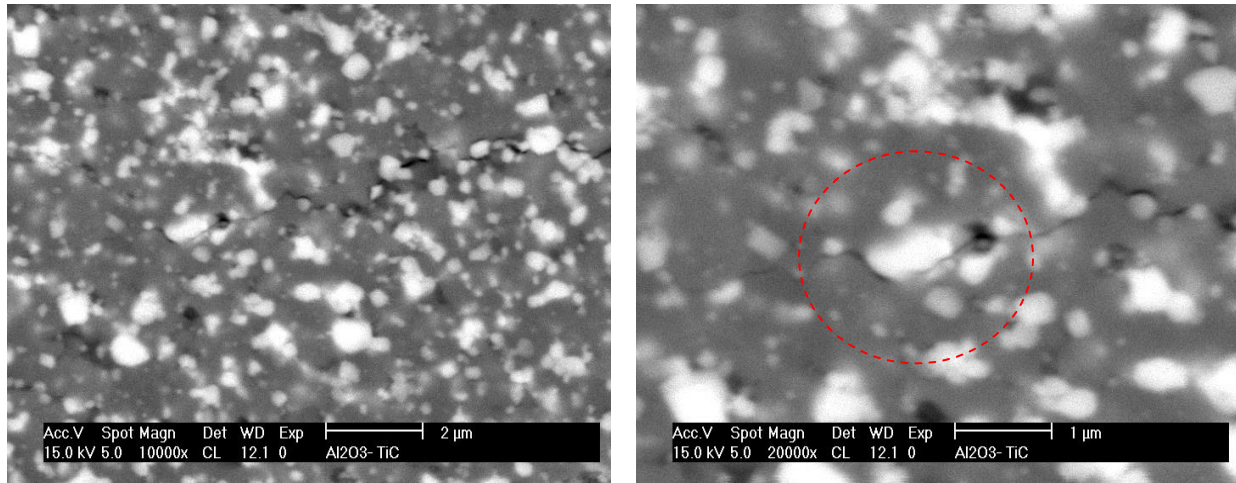


Figure 63: SEM images of [Al₂O₃ + TiC (30 wt. %)] sample, showing the path of a crack propagated through the surface of the polished sample. The TiC grains deflect the crack therefore changing the crack path.

The [Al₂O₃ + TiC (30 wt. %)] sample was fractured, and the fractured surface was analyzed with SEM, the results shows that the TiC grains were attached to Al₂O₃ matrix in a “ball and socket” mechanism (Fig. 64).

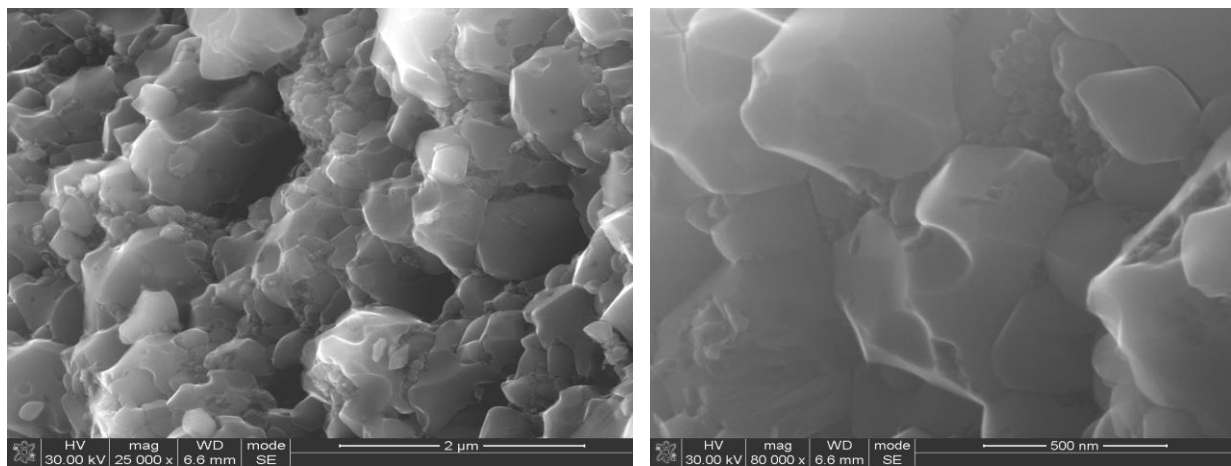


Figure 64: SEM images of [Al₂O₃ + TiC (30 wt. %)] sample fractured surface, the curved spaces could be where the TiC were attached to the alumina matrix.

4.2.4 Al₂O₃ + CNT + TiC

The sintered [Al₂O₃ + CNT (2.1 vol. %) + TiC (26 vol. %)] sample was analyzed using optical microscopy (Fig. 65) to determine the TiC and CNT distribution within the alumina matrix. The sample was further analyzed using SEM for a more detailed study of the sample cross section (Fig. 66).

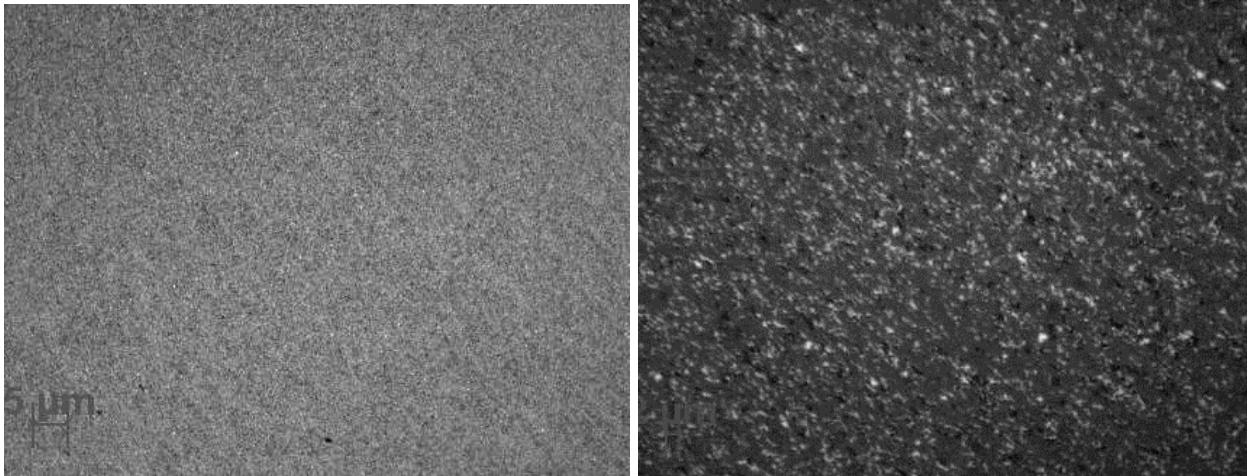


Figure 65: Optical microscope images of [Al₂O₃ + CNT (3vol. %) + TiC (30 wt. %)] sintered at 1650°C, 35 MPa

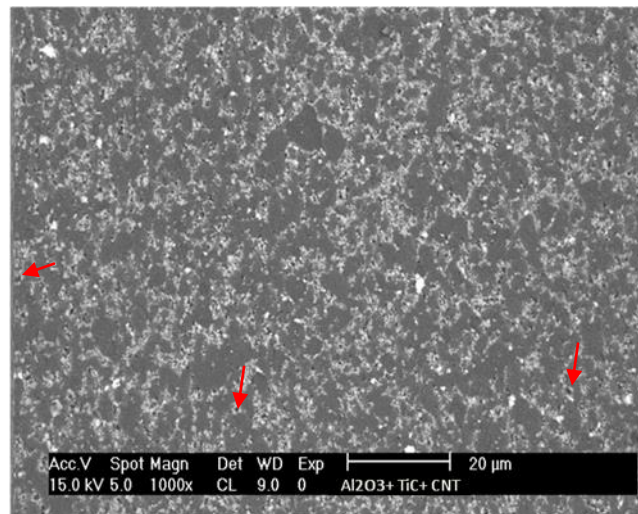


Figure 66: SEM images of [Al₂O₃ + CNT (3vol. %) + TiC (30 wt. %)] sintered at 1650°C, 35 MPa, showing that the TiC and CNTs (shown by the arrows) were well distributed within the alumina matrix.

4.3 Mechanical Properties

The mechanical properties that were measured were fracture toughness and hardness. These properties were measured using an indentation method and they are given in Table 15.

Table 15: Mechanical properties of alumina with different reinforcements

Material	Hardness (GPa)	Fracture toughness (Mpa√m)
Pure Al ₂ O ₃	18 ± 0.2	3.3 ± 0.2
Al ₂ O ₃ + CNTs (3 vol. %)	19 ± 0.3	4.2 ± 0.3
Al ₂ O ₃ + TiC (30 wt. %)	22 ± 0.4	4.8 ± 0.3
Al ₂ O ₃ + CNTs + TiC	23 ± 0.2	5.0 ± 0.4

4.4 Electrical Properties

The DC 41-40 SMU instrument applied a voltage through the sample and measured the current passing through. The measured current was then plotted against voltage. The gradient of the trend line is equal to the resistance of the sample.

4.4.1 Pure Alumina

Alumina sample cut into the dimensions shown in Table 13 in Chapter 3 was used for measuring electrical resistance using a voltage up to 10 Volts.

The pure Al₂O₃ sample showed a resistance higher than the measurement range of the equipment (resistance was higher than $5 \times 10^{10} \Omega$).

4.4.2 $Al_2O_3 + CNTs$

The relationship between voltage and current measured for $Al_2O_3 + CNTs$ sample (Fig. 67).

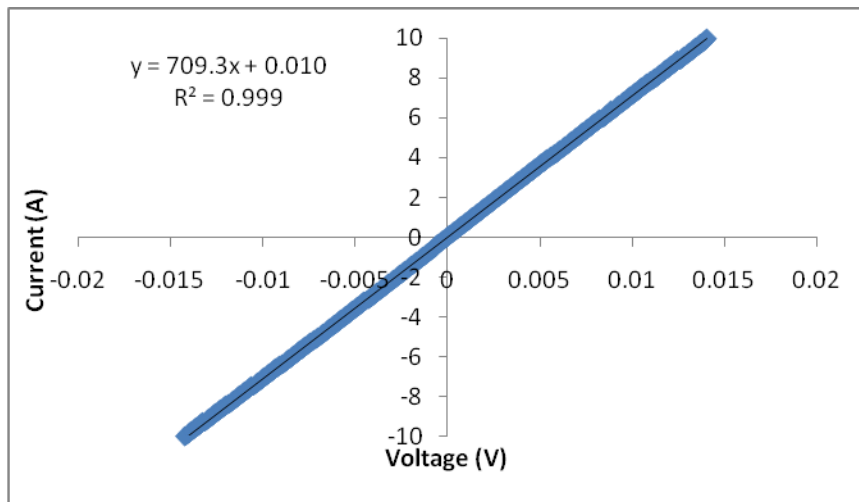


Figure 67: Relationship between voltage and current on the $Al_2O_3 + CNTs$ sample

4.4.3 $Al_2O_3 + TiC$

The relationship between voltage and current measured for $Al_2O_3 + TiC$ sample (Fig. 68).

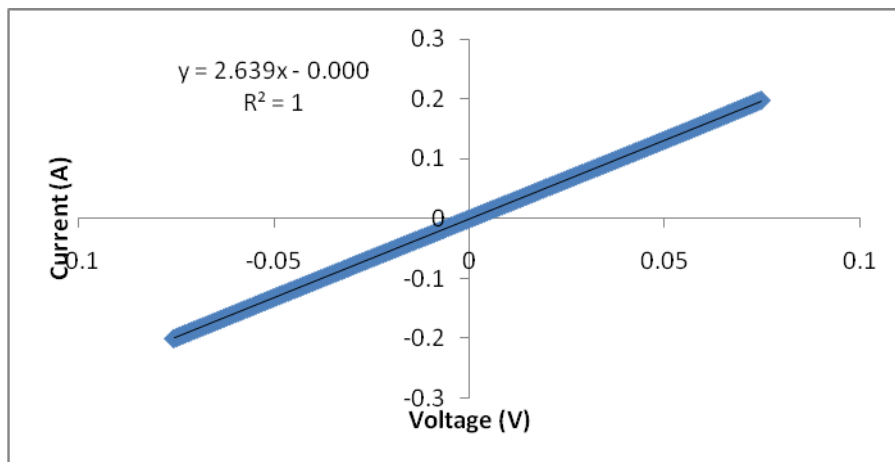


Figure 68: Relationship between voltage and current on the $Al_2O_3 + TiC$ sample

4.4.4 $Al_2O_3 + CNTs + TiC$

The relationship between voltage and current measured for $Al_2O_3 + CNTs + TiC$ samples (Fig. 69).

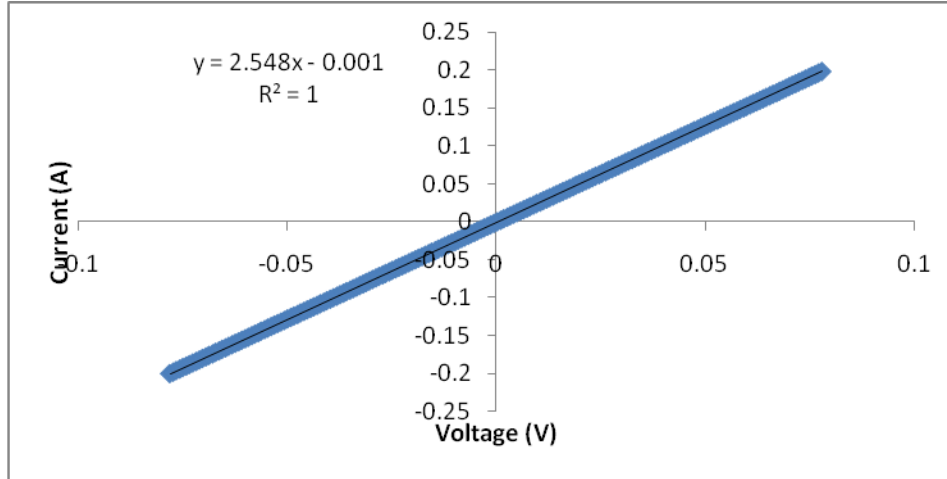


Figure 69: Relationship between voltage and current on the $Al_2O_3 + CNTs + TiC$ sample

The resistance of all the samples was determined from the slope of the voltage and current graphs. According to equation:

$$R = V/I \quad \text{Equation 5}$$

Once the resistance is derived from the graph, resistivity (ρ) of each sample can be calculated according to the equation;

$$\rho = (R.A)/l \quad \text{Equation 6}$$

Where,

R = resistance

A = Area of the sample

l = length of the sample

Electrical conductivity (δ) of each sample can be calculated from the resistivity values according to the equation;

$$\delta = 1/\rho \quad \text{Equation 7}$$

Calculation for Al₂O₃ + CNTs

$$R = \text{slope of the curve} = 709.3 \, \Omega$$

$$\rho = (R.A)/l = (709.3 \times 8.4 \times 10^{-8}) / 1.90 \times 10^{-3} = 3.15 \times 10^{-2} \, \Omega.m$$

$$\delta = 1/\rho = 31.75 \, S.m^{-1}$$

The electrical conductivity of all the samples are shown in Table 16, and the calculations are shown in Appendix B.

Table 16: Electrical properties of the different samples

Material	Resistance (Ω)	Resistivity ($\Omega.m$)	Conductivity ($S.m^{-1}$) at 25 °C
Al ₂ O ₃	--	--	--
Al ₂ O ₃ + CNT	709.3	3.15×10^{-2}	31.75
Al ₂ O ₃ + TiC	2.64	2.26×10^{-4}	4431
Al ₂ O ₃ + TiC + CNT	2.55	1.44×10^{-4}	6944

Chapter Five

5.0 Discussion

This chapter gives a detailed discussion of the results obtained in this study in comparison with the results obtained in the literature. The results are divided into the following sections: dispersion, densification, microstructural analysis, mechanical properties and electrical conductivity properties. The interpretation of the results of each section is then integrated with each other.

5.1 Preparation of carbon nanotubes

In this study the MWCNTs were prepared by reaction of acetylene with Iron (Fe^{2+} ion) catalyst at 800°C according to the procedure described in chapter 3. The TEM images of the MWCNT presented in Chapter 4 (Fig. 41) confirm that MWCNTs were formed within a mixture of nanofibres. The TEM analysis done on the MWCNTs revealed that they had a wide range of diameters; between 40 – 150 nm and also that amorphous carbon was present within the them (Fig 41). The nanofibres that were formed in abundance compared to the MWCNTs (Fig. 41). The formation of MWCNTs using this approach depends on the process parameters used, such as reaction temperature, carbon source flow-rate and time which the acetylene gas flows into the system (Iyuke *et al.* [25]). The literature results showed that the optimum conditions to produce MWCNTs were: 1 g of ferrocene, acetylene flow rate and time of 100 ml/min for 20 minutes respectively and reaction temperature of 800°C [25]. In this study the reaction temperature was 800°C , and the C_2H_2 flow rate was varied from 50 ml/min – 150 ml/min for 25 minutes. The flow rate was varied with the aim of reducing the diameter of the MWCNTs so that they would be suitable for this study. The flow-rate of C_2H_2 that yielded MWCNTs with a smaller diameter range was 60 ml/min. The reduction of the acetylene flow rate reduced the size of MWCNTs formed and increasing the flow rate to from 100 ml/min. to 150 ml/min. had no effect on the MWCNTs diameter, as shown in Table 17.

Table 17: The comparison of MWCNTs properties obtained in this study and in the literature

Author	Temperature	C ₂ H ₂ gas flow rate and time	Diameter range (nm)
Iyuke <i>et al.</i> ^[25]	800	100 ml/min for 20 min	100 - 200
In this study	800	150 ml/min for 25 min	80 - 200
	800	100 ml/min for 25 min	80 - 200
	800	60 ml/min for 25 min	40 - 150

The smallest diameter range of MWCNTs obtained in this study was 40 – 150 nm. The size of these MWCNTs and the presence of amorphous carbon made these MWCNTs unsuitable for this study. Therefore for this study the MWCNTs were purchased.

5.2 Coating of CNTs

In this study there were two methods that were considered for coating the MWCNTs with hBN: Nitridation method and Urea route as described in the literature. Due to time constraints only one method could be used for coating of the MWCNTs. Therefore these two methods were compared to find out which one would yield better results for this work. The results obtained by other authors (Gomathi *et al.* ^[45] and Chen *et al.* ^[47]) are given in table 18.

Table 18: Comparison of the results obtained after coating MWCNTs using Nitridation and Urea route

Author	hBN thickness produced (nm)
Chen <i>et al.</i> ^[47] (Nitridation route)	19
Gomathi <i>et al.</i> ^[45] (Urea route)	10

The nitridation method was chosen for this work because it was simple to conduct and it produced thicker coating. The crucial reaction in both the methods is *Reaction 3.2* ($B_2O_3 + 2NH_3 \xrightarrow{\Delta} 2BN + 3H_2O$). In the nitridation method ammonia (NH_3) can be introduced in excess to consume the entire boron oxide (B_2O_3) hence forming a thicker coating, whereas in the Urea method ammonia is formed in-situ. In this case the ammonia formed may not be sufficient to react with the entire boron oxide. The nitridation method has no byproducts as opposed to Urea method's reactions (*reaction 2.1 and 2.2*) and the nitridation method was less time consuming. Therefore this method was theoretically the better of the two.

The nitridation method was used on the MWCNTs and after TEM analysis some MWCNTs were coated with hBN. However the coating of the CNTs with hBN using nitridation was regarded as unsuccessful, since the CNTs could not all be coated individually. Those CNTs that were successfully coated had a layer on their surfaces which was approximately ~ 20 nm thick, which is not present on the uncoated CNTs (Fig. 43). However the layer could not be confirmed to be hBN by EDX since the TEM used was not equipped with such an instrument. The presence of the layer on the CNTs surface was further confirmed by the "flaking off" which was observed when the CNTs were ultrasonicated for 20 minutes (Fig. 44). This was not observed when the uncoated CNTs were treated similarly. These results were in accordance with the literature findings by Chen *et al.*, 2004 ^[47]. These authors reported that they formed homogenous hBN coating onto the surface of CNTs which was approximately 19 nm in thickness (Fig. 22). The

coating of the CNTs results obtained in this study were comparable with those obtained in the literature (Chen *et al.* ^[47]).

Table 19: Comparison of the results obtained after coating MWCNTs with the results from the literature

Author	HN ₃ dwell time (min.)	hBN later thickness (nm)
Chen <i>et al.</i> ^[47]	60	19
In this study	60	≈ 20

The CNTs were coated using the same conditions used in the literature (Chen *et al.* ^[47]), and the resulting hBN coating thickness was almost the same. In this study it was revealed that CNTs could not be coated individually using this method, therefore the hBN coating thickness reported above are not an average but the thickness of the hBN coated on the portion of the CNTs observed. The selectivity of the TEM also does not reveal the fact that it is difficult to coat all the CNTs individually.

The coating process will be briefly revisited while discussing the steps that made it difficult to coat CNTs individually. The coating process included depositing B₂O₃ onto the CNTs surface (*Reaction 2.1*). The B₂O₃ on the CNTs surface was heated to 1165°C before introducing NH₃ into the system. During the heating process B₂O₃ melted at 600°C forming a matte. When the reaction temperature was reached and NH₃ introduced into the system it reacted with the B₂O₃ matte which covered CNTs because of this it was difficult to coat each CNT individually but instead a bundle of CNTs was coated. The difficulty of coating each CNT individually was a challenge for this study since a bundle of CNTs coated with hBN will serve as stress raiser within an alumina ceramic.

In this study a further step of dispersing hBN coated CNTs was conducted which had not been reported in the literature before. The dispersion of the hBN coated CNTs was done by water bath ultrasonication of the sample and then analyzing it with TEM. The TEM analysis revealed that the hBN coat on the MWCNTs was “flaking off” the surface of the MWCNTs. The dispersion of hBN coated CNTs is a challenge yet to be overcome since the “flaking off” of the hBN coating revealed that hBN-CNT interface is a weak interface. The hBN-CNT interface is regarded as weak since it could not withstand water bath ultrasonication which is regarded as a least aggressive method of dispersion. The weak CNT- hBN interface was not ideal for this study since dispersion is crucial when these hBN coated CNTs are to be incorporated within a ceramic material, so as to eliminate agglomerates.

5.3 Relationship between microstructure and densification

The relationship between microstructure and densification of the samples is described systematically, starting with alumina and the effects of addition of CNTs into alumina, secondly with a comparison of alumina and the effects of adding TiC into it and lastly the addition of both CNT and TiC into alumina. The results obtained are compared with work done by other researchers.

5.3.1 Addition of CNTs into Alumina

In this study Al_2O_3 powder was dispersed in hexane and dried before sintering (as described in Chapter 3). The measured average particle size was 0.22 μm . This shows that the method used to disperse the alumina was effective since the particle size measured was close to the actual particle size (supplier specification). The dispersion results obtained in this study were in accordance with the literature Muchtar *et al.* ^[48]. Different methods of dispersion were investigated (Muchtar *et al.* ^[48]) and the results revealed that the colloidal method of dispersing powder was the most effective in eliminating agglomerates in the starting powders. The mono dispersed powders yield ceramic materials with higher densities, due to particle packing efficiency during compaction (Muchtar *et al.* ^[48]). The mono dispersed powder has almost no permanent agglomerates, those that were formed were destroyed during drying of the powder and most of them were destroyed during the sieving process (150 μm sieve was used in this

study). Almost each powder particle was placed individually in the green compact therefore theoretically increasing the potential of the green body to be sintered to higher density.

In this study Al_2O_3 powder was sintered at 1600°C , 35 MPa under vacuum using SPS. The measured density was $3.97\text{g}\cdot\text{cm}^{-3}$ (99.8% of the theoretical) for theoretical density of $\text{Al}_2\text{O}_3 = 3.98\text{g}\cdot\text{cm}^{-3}$ (Appendix A). The Al_2O_3 used in this study was submicron (average particle size: 200 nm) and had a purity of 99.99 %, with some trace element impurities (Ca, Mg, Si etc.). The presence of trace elements gives rise to the formation of a glassy phase of the sintered ceramic thus increasing the densification. Since these trace elements have low lattice solubility into alumina they segregate at the alumina grain boundaries during densification and they form intergranular amorphous film which effectively increases the density of the final sintered alumina piece. The sintering conditions used for sintering Al_2O_3 powder were sufficient to reduce the system energy (surface energy) which is the driving force for densification, thus producing a highly dense Al_2O_3 sample (99.8%). The optical micrograph of the sintered Al_2O_3 reveals that the sample was highly dense with few pores observed on the examined surface. The densification results in this study were compared with the results obtained by other authors (Zhan *et al.* ^[49] and Estili *et al.* ^[5]) who also sintered Al_2O_3 and obtained highly dense samples using the conditions included in table 20. The few pores that were observed using SEM (Fig. 51) seemed to be distributed homogeneously throughout the examined surface of the specimen.

Table 20: Comparison of the results obtained after sintering monolithic Al₂O₃ and the results from the literature

	Method of sintering	Sintering Conditions	Particle size (nm)	Density (%)
Zhan <i>et al.</i> [49]	SPS	1150°C, 50 MPa	350	100
Estili <i>et al.</i> [5]	SPS	1500°C, 50 MPa	150	99.5
This study	SPS	1600°C, 35 MPa	200	99.8

The results obtained in this study are close to the results obtained by other authors [ref]. They revealed that finer powders can be sintered at a lower temperature to densify compared to the coarser powder. The results by Estili *et al.* [5] shows that a submicron powder (150nm) can be sintered to 99.5% density at a temperature to 1500°C. Whereas a coarser powder (350 nm) can be sintered at a lower temperature (1150°C) and the samples can reach high density (Zhan *et al.* [49]).

The sintered Al₂O₃ sample was thermally etched for the purpose of measuring grain size. The Al₂O₃ sample that was thermally etched at 1300°C for 60 minutes gave better results than a sample thermally etched at 1200°C, as it revealed the Al₂O₃ grains more distinctly. The grain size was measured to be between 2 – 4 μm. The results from the thermal etching revealed that the Al₂O₃ sample didn't experience great amount of abnormal grain growth during sintering since the grains are equiaxed. The Al₂O₃ grain size was measured so that it could be compared with the grain size of the sample sintered with CNTs.

After fully densifying Al₂O₃ powder, the SPS conditions that were used were also used for the mixture of Al₂O₃ + CNTs. In this study [Al₂O₃ + CNTs] powder was sintered at 1600°C, 35 MPa under vacuum using SPS. The density was measured to be 3.88 g.cm⁻³ (99.6 % of the theoretical). The theoretical density of [Al₂O₃ + CNTs] was calculated to be 3.90 g.cm⁻³ (Appendix A). Therefore an addition of 1 wt% of CNTs into alumina slightly decreased the

alumina density from 99.8 % to 99.4 % of the theoretical. The results obtained in this study were compared to the results obtained by other authors (Sun *et al.* ^[4], Estili *et al.* ^[5]) in table 21.

Table 21: Comparison of the results obtained after sintering Al₂O₃ + CNTs and the results from the literature

Author	System	CNTs Dispersion method	Densification	Density (%)
Sun <i>et al.</i> ^[4]	Al ₂ O ₃ + CNTs (3 vol. %)	Ultrasonication + Dispersant (PEA)	HP;1500°C,30MPa, Argon Atm	100
Estilli <i>et al.</i> ^[5]	Al ₂ O ₃ + CNTs (3.5 vol. %)	Alteration of water pH to 4.4	SPS;1500°C,50MPa	90.0
This study	Al ₂ O ₃ + CNTs (3 vol. %)	Ultrasonication + planetary ball mill +dispersant (PVP)	SPS;1600°C,35MPa	99.6

The effect of CNTs on the Al₂O₃ density largely depends on the dispersion of CNTs and the mixing of the two components (Al₂O₃ and CNTs). The more dispersed the CNTs would have less negative effects on the Al₂O₃ density. Dispersion of CNTs is problematic since the more aggressively they are dispersed the higher the chances of their destruction, while a less aggressive approach risks producing agglomerated CNTs. The results obtained in this study were in accordance with the results obtained in the literature (Table 21), it was reported that full density was achieved for a mixture of Al₂O₃ + CNTs when the sample was hot pressed at 1500°C, 30 MPa in argon (Sun *et al.* ^[4]). Full density was achieved when the MWCNTs were dispersed using poly ethylene amine (PEA) as a dispersant and dispersed Al₂O₃ was dispersed using poly acrylic acid. The Al₂O₃ and CNTs suspensions were both vigorously stirred (Ultrasonication) and dried. The high density obtained was ascribed to the effectiveness of the PEA dispersant (Sun *et al.* ^[4]). Sun *et al.* ^[4] reported that full density was achieved but also reported that hot pressing a sample of Al₂O₃ + CNTs caused destruction of CNTs. This

compromised the mechanical properties (as described in the Literature review section). In this study SPS was used to reduce the risk of damage of the CNTs by dwelling at high temperature for a very short period of time, also by heating up to the sintering temperature at a high heating rate.

It was also reported that addition of 3.5 vol. % (≈ 1 wt. %) of CNTs in alumina reduced density of the material from 99.5% to 90.0% when SPS was used at 1500°C, 50 MPa (Estili *et al.* ^[5]). These authors dispersed the CNTs in distilled water with a pH of 4.4. The alteration of the water pH caused CNTs to be attracted to alumina particles through the induction of opposite charges (Estili *et al.* ^[5]). It was also reported that the higher CNTs volume fraction within Al₂O₃ resulted to significantly increased porosity (Kim *et al.* 2009 ^[40]).

The results obtained in this study and the related literature shows that the dispersion of CNTs is crucial in obtaining a dense sintered composite. The results obtained by Estili *et al.* ^[5] shows that the alteration of the pH was not a successful method of dispersing CNTs, since it drastically reduced the density of the sintered composite. Therefore in this study the CNTs were dispersed more aggressively with a dispersant to counter the Van der Waals forces acting between the CNTs. The other factor that determines the densification of Al₂O₃ + CNT is the sintering method and conditions. The conditions that were used in this study were sufficient to reduce the surface energy of the system and therefore yield a highly dense sample.

Since in this study the addition of CNTs reduced the density of monolithic alumina, it follows that the densification of the Al₂O₃-CNTs depended on the dispersion method used. The density results obtained by other researchers are different to ours because different CNTs dispersion methods were used. A more effective dispersion method used, would reduce the occurrence of agglomerates, leading to higher ceramic densities.

The results obtained from microstructural analysis of the cross section of Al₂O₃-CNTs specimen shows that the CNTs were agglomerated to a small extend as denoted by the arrows as shown in Figure 53, 54 and 55). These agglomerates decreased in number through aggressive dispersion but they were not entirely eradicated as revealed by SEM analysis (Fig. 55). This shows that the dispersion of CNTs is a challenge still to be overcome. Hilding *et al.* ^[50] reported that high

impact mixing of CNTs can generate a large amount of amorphous carbon, which means the CNTs would be largely destroyed. Therefore it seems that with CNTs there is a choice of either dispersing them less aggressively and obtaining a not well dispersed CNTs or dispersing them more aggressively thus obtaining well and uniform dispersion but risking destroying them. In this study these two methods were investigated, the results obtained indicated that similar dispersion was obtained in both cases; therefore the less aggressive dispersion method was selected in order to reduce the risk of causing damage to the CNTs.

Since the carbon of the CNTs is soluble in the alumina lattice, they would be expected to be present within the matrix and also segregated along the grain boundaries. The CNTs concentration would also be expected to increase at the interface as the alumina grains grow during sintering, which causes the total area of the interface to decrease therefore reducing the density of the material.

5.3.2 Addition of TiC into Alumina

The sintering conditions used to densify Al_2O_3 , namely 1600°C at 35 MPa, were also used to sinter $\text{Al}_2\text{O}_3 + \text{TiC}$ powder. The results showed that density of $\text{Al}_2\text{O}_3 + \text{TiC}$ sample had a density of $4.04\text{g}\cdot\text{cm}^{-3}$ (95.5% of the theoretical). Theoretical density of a mixture of $\text{Al}_2\text{O}_3 + \text{TiC}$ was $4.23\text{g}\cdot\text{cm}^{-3}$ (*Appendix A*). Due to the low density achieved when $\text{Al}_2\text{O}_3 + \text{TiC}$ was sintered at 1600°C at 35MPa, this material was then sintered at 1700°C and the density obtained was $4.18\text{g}\cdot\text{cm}^{-3}$ (99.0% of the theoretical). The low density of the sample sintered at 1600°C was in agreement with large pores observed when the specimen's cross section was analyzed by SEM (Fig. 61). The sample sintered at 1700°C had few pores (Fig. 62). The highest density obtained when TiC was added into Al_2O_3 was 99.0% which is lower than the density of the monolithic ceramic sintered at 1600°C , 35 MPa, therefore the addition of TiC into Al_2O_3 decreased the density of the monolithic ceramic.

Densification of powders to form ceramics is dependent on particle size and particle size distribution of the starting material, as well as the particle packing. The smaller the particle size the higher will be the speed of sintering. The powders (both TiC and Al_2O_3) used in this study were submicron, with particles size $\approx 200\text{nm}$. These powders were unimodally dispersed (Fig. 35 and Fig. 37). TiC was well distributed within the alumina as shown by SEM (Fig 62). The

composite powder of Al₂O₃-TiC had lower density than monolithic alumina sintered under the same conditions. This is caused by the presence of TiC particles in the green compact. In the presence of a secondary phase, the surface activity of the submicron powder is reduced therefore the sintering process is prolonged. In order to sinter a composite powder it is necessary to either increase dwell time or the sintering temperature ^[51]. In this study in order to densify Al₂O₃+ TiC composite powder the temperature was increased, with a resultant increase in density from 95.5% to 99.2%.

The results found in this study were compared with the results obtained by other authors i.e. You *et al.* ^[51] and Cutler *et al.* ^[3] as shown in Table 22

Table 22: Comparison of the results obtained after sintering Al₂O₃ + TiC and the results from the literature

Author	Particle size (Al ₂ O ₃ /TiC)	Densification method	Density (%)
You <i>et al.</i> ^[51]	(312/0.32)µm	HP; 1700°C,30 MPa, 1h	99.8
	(312/1.36)µm	HP; 1750°C,30 MPa, 1h	99.6
Cutler <i>et al.</i> ^[3]	Not reported	HIP;1600°C,200MPa	95.3
In this study	(200/200) nm	SPS;1600°C,35 MPa	95.5
	(200/200) nm	SPS;1700°C,35 MPa	99.0

You *et al.*, 2005 ^[51] reported that the addition of TiC into alumina slightly compromises the density of the sintered ceramic. You *et al.*, 2005 ^[51] reported that if the TiC particle size is smaller than that of alumina the sintering process is further facilitated and the resultant density increases as shown in table 22. The Al₂O₃+TiC ceramic which had a smaller TiC particle size size had a higher density (X.Q You *et al.*, 2005 ^[51]). The results obtained by Cutler *et al.* ^[3] shows that 1600°C sintering temperature was not sufficient to produce a highly dense ceramic. The results obtained in this study are in accordance with the results obtained by these authors.

5.3.3 Addition of CNTs and TiC into Al₂O₃

The addition of CNTs into alumina decreased the monolithic alumina density from 99.8% to 99.4% and the addition of TiC decreased the alumina density from 99.8% to 99.0%. The addition of both CNTs and TiC reduced the monolithic alumina from 99.8% to 99.2%. The effect on densification observed when the mixture of CNTs and TiC was added into Al₂O₃ was mostly due to the TiC particles. The reason TiC had a more pronounced effect on densification can be ascribed to the relative amounts added; 30wt% of TiC was added to the Al₂O₃, compared to only 1 wt. % of CNTs.

A comparison of ceramics measured densities are illustrated in Fig.70. The results show that monolithic Al₂O₃ had the highest density of them all.

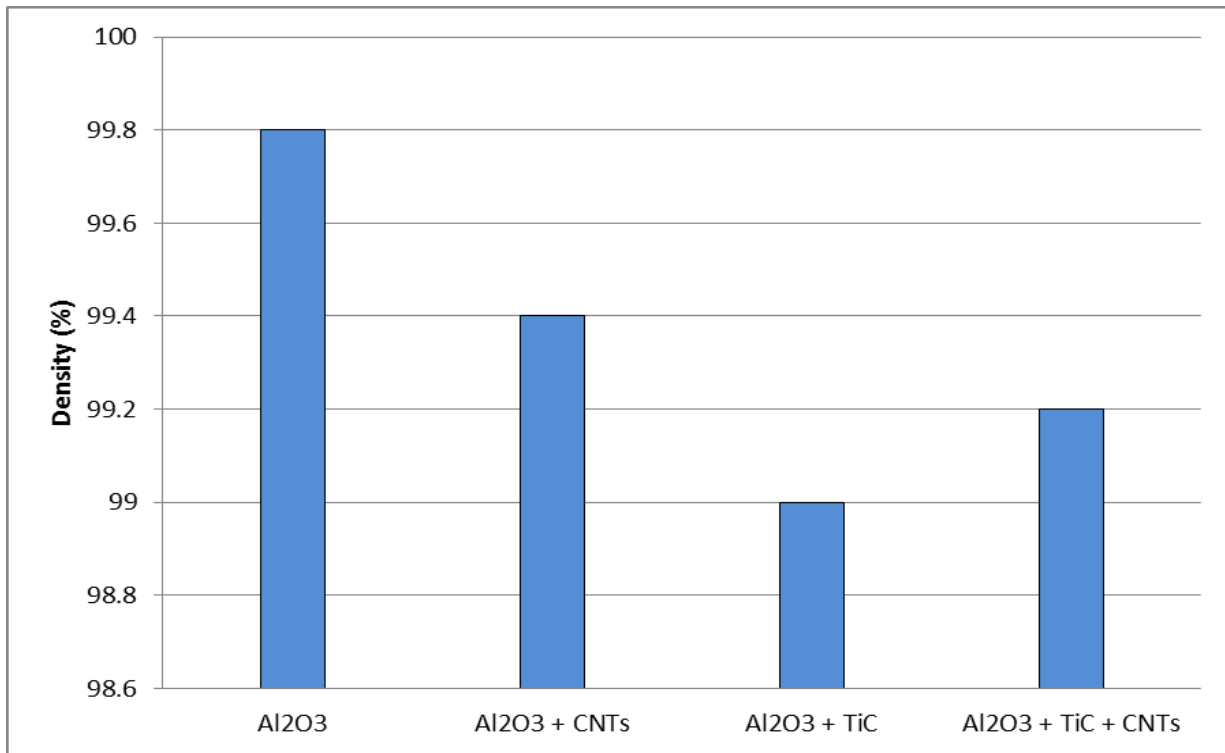


Figure 70: Variation of Al₂O₃ density when it is reinforced with CNTs and TiC and the mixture of TiC and CNTs

5.4 Relationship between microstructure and hardness

5.4.1 Addition of CNTs into Alumina

In this work Al₂O₃ powder was sintered using SPS; 1600°C, 35 MPa for 10 minutes. The Vickers hardness of Al₂O₃ sample was 18 ± 0.2 GPa for a 5 kg load. The results obtained in this study were compared with the results obtained by other authors (Zhan *et al.* ^[49] and You *et al.* ^[51]) as given in Table. 23.

Table 23: Comparison of the mechanical properties obtained after sintering Al₂O₃ + CNTs and the results from the literature

Author	Densification method	Hardness (GPa)
You <i>et al.</i> ^[51]	HP; 1650°C,30 MPa, 1h	17
Zhan <i>et al.</i> ^[49]	SPS;1150°C/50 MPa	20
This study	SPS;1600°C,35MPa,	18

The hardness obtained in this study seems to be lower than that of the samples sintered at a lower temperature using SPS (Zhan *et al.* ^[49]). The lower temperature used by these authors might have caused higher hardness through reduced grain growth. The sample sintered at a lower temperature is less likely to have experienced grain growth to an extent comparable to the samples sintered in this work. The hardness is expected to have increased with decreasing grain size. Therefore the Al₂O₃ + CNTs sample sintered at 1150°C had smaller grains than the sample analyzed in this study. The results obtained by You *et al.* were close to the results obtained in this study. This is because the sintering temperature used for both these studies were close to each other. In this study a higher hardness was obtained compared to You *et al.* ^[51]. This might be caused by the fact that the samples sintered in this study experienced milder sintering conditions since SPS was used as opposed to hot pressing which exposes samples to higher temperatures for much longer time intervals.

The addition of CNTs (3 vol. %) increased the hardness of monolithic Al₂O₃. The hardness increased from 18 GPa to 20 GPa (11% increase).

SEM showed that the CNTs were well distributed within the alumina matrix (Fig. 57). Fracture surface of Al₂O₃-CNT sample shows that the CNTs survived the sintering process (Fig. 59) as they can be seen to be “sticking” out of the fracture surface. Sun *et al.* ^[4] reported that the CNTs were destroyed during the sintering process and therefore were not effective in improving the mechanical properties of monolithic alumina. The destruction of the CNTs was noticed when the samples were hot pressed, pressure less sintered and hot isostatic pressed. In this study SPS was employed for the sintering of all the samples. This machine was programmed to increase to the sintering temperature at a heating rate of 200°C.min⁻¹. This heating rate and dwell time of 10 minute at the sintering temperature minimized the CNTs destruction.

The thermally etched Al₂O₃-CNT sample shows that the CNTs were also situated along the cracks and possibly Al₂O₃ grain boundaries as detected by the EDS (Fig. 57). The CNTs along the grain boundaries are capable of inhibiting the alumina grain growth, which will effectively improve the hardness of this ceramic. The grain size of monolithic alumina was between 2 - 4 μm (Fig. 52) and the sample Al₂O₃-CNTs showed a grain size between 0.2 – 0.5 μm (Fig. 57). The reduced alumina grain size accounts for the 11% increase in hardness (from 18 GPa to 20 GPa) when CNTs are added to the sample.

5.4.2 Addition of TiC into Alumina

In this study a composite powder of Al₂O₃ + TiC was sintered using SPS (1700°C, 35 MPa) and the Vickers hardness measured by indentation was 22 ± 0.4 GPa. Addition of TiC improved the hardness of monolithic alumina by 22% from 18 to 22 GPa. The results obtained in this study were compared with the results obtained in the literature (You *et al.* and Cutler *et al.*) as shown in Table 24.

Table 24: Comparison of hardness property obtained after sintering Al₂O₃ + TiC and the results from the literature

Author	Densification method	Hardness
You <i>et al.</i> ^[51]	HP; 1700°C, 30 MPa, 1h	21.7
Cutler <i>et al.</i> ^[3]	HP; 1700°C, 35 MPa, 10 min.	20.1
This study	SPS; 1700°C, 35 MPa	22.0

The observed 22% increase in the hardness of monolithic alumina by the addition of TiC can be attributed to the pinning effect that these nano particles have when they are within alumina grain boundaries. The TiC pinning effects is beneficial for inhibiting alumina grain growth. The reduced alumina grains will contribute in increasing the hardness. The addition of TiC into alumina had superior effects on the hardness compared to the addition of CNTs. This can be because of the different amounts and shape of each powder introduced into the system, TiC particles are cubic in shape which is similar to those of Al₂O₃ as opposed tubes of CNTs. Also since 3 vol.% of CNTs was used while 26 vol. % of TiC was used.

5.5 Relationship between microstructure and fracture toughness

5.1.1 Addition of CNTs into Alumina

In this work Al₂O₃ powder was sintered using SPS; 1600°C, 35 MPa for 10 minutes. The measured indentation fracture toughness was 3.3 MPa√m using a load of 5 kg. The measured fracture toughness was between the correct ranges as reported in the literature ^[5].

In the light of the sintering conditions used for monolithic Al₂O₃ as given above, Al₂O₃ + CNTs sample was sintered using SPS; 1600°C, 35 MPa for 10 minutes. The fracture toughness achieved was 4.2 MPa√m. The results obtained in this study were compared with the results obtained by Zhan *et al.* ^[49] and Sun *et al.* ^[4] as seen in Table 25.

Table 25: Comparison of the fracture toughness and density obtained after sintering Al₂O₃ + CNTs and the results from the literature

Author	Densification method	Density (%)	Fracture toughness (MPa√m)
Sun <i>et al.</i> ^[4]	HP;1500, 30 MPa	100	2.2
Estilli <i>et al.</i> ^[5]	SPS;1500°C, 50 MPa	90	5.2
This study	SPS;1600°C,35MPa,	99.4	4.2

The fracture toughness values obtained in this study seemed to be lower than those reported in the literature by Estilli *et al.* ^[5], as shown in Fig. 71 below.

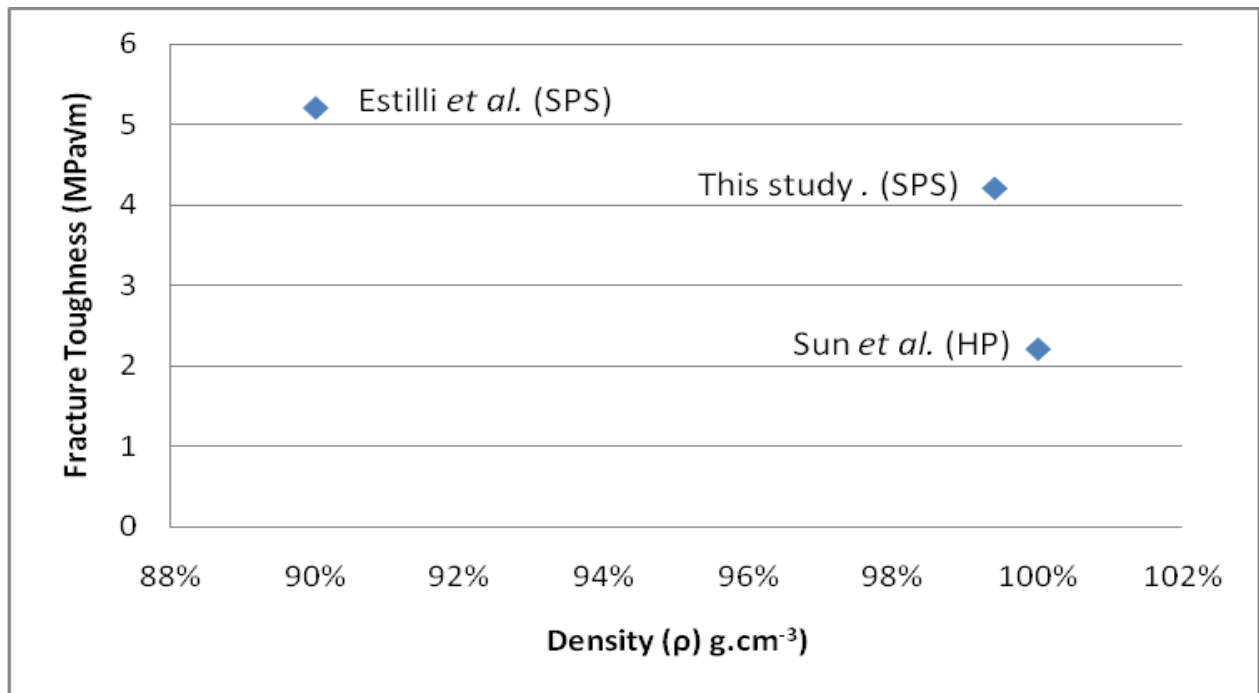


Figure 71: The comparison of fracture toughness and density obtained in the study with other authors

The reason for this difference in fracture toughness can be ascribed to the differences in densities obtained in this work as compared to work reported in the literature. Estilli *et al.* obtained a density which was 90% as opposed to 99.4% obtained in this work. Porosity affects the fracture toughness of a material. The higher the porosity of the ceramic the more inaccurate is it. Therefore the fracture toughness results obtained by Estilli *et al.* ^[5] are inaccurate, since they are influenced by the high porosity of the sample. The low fracture toughness obtained by Sun *et al.* ^[4] can be attributed to the destruction of CNTs during sintering. The results obtained by Sun *et al.* ^[4] confirm that CNTs are responsible for increasing Al₂O₃ fracture toughness if they survive sintering conditions.

The CNTs situated in the alumina matrix are capable of bridging any propagated cracks and restrain any further crack opening and growth. The CNTs deflecting the crack can only be detected by high resolution SEM (unavailable for this study) as reported by Estilli *et al.* ^[5]. The increase in fracture toughness upon addition of CNTs means that these additives were involved in crack deflection and bridging which are known toughening mechanisms. Figure 58 shows clearly CNT pull out. Such an event will cause crack bridging with its concomitant toughening effect. The work required for the pulling out of the CNTs increases the work of fracture and therefore helps reinforce the ceramic. The compressive stresses applied by the Al₂O₃ matrix onto the CNTs during cooling down after sintering enhances the frictional forces associated with the CNT pull outs which will effectively increase the reinforcing efficiency of these additives ^[5]. Since the composite ceramic was highly dense (99.0% dense) the interfacial contacts were tight.

5.1.2 Addition of TiC into Alumina

In this study a composite powder of Al₂O₃ + TiC was sintered using SPS at 1700°C and 35 MPa. The fracture toughness measured by indentation was 4.8 MPa√m. Addition of TiC increased Al₂O₃ fracture toughness by 42 % from 3.3 MPa√m to 4.8 MPa√m.

The results obtained in this study were compared with the results obtained in the literature (You *et al.* ^[51] and Cutler *et al.* ^[3]) as shown in Table 26.

Table 26: Comparison of fracture toughness obtained after sintering Al₂O₃ + TiC and the results from the literature

Author	Densification method	Density (%)	Fracture toughness (MPa√m)
You <i>et al.</i> ^[51]	HP; 1700°C,30 MPa, 1h	96.8	6.48
Cutler <i>et al.</i> ^[3]	HP; 1700°C,35 MPa, 10 min.	95.3	5.25
In this study	SPS;1600°C,35MPa,	99.4	4.80

The fracture toughness obtained in this study is lower than the fracture toughness achieved by You *et al.* ^[51] and Cutler *et al.* ^[3]. This could be due to the different sintering technique used and the densities obtained. These authors used hot pressing which may have given rise to grain growth, thus causing decrease in fracture toughness. The low density of the ceramic material causes a concomitant increase in fracture toughness.

The results obtained in this study were comparable to the results obtained by other researchers since the samples show the presence of intergranular carbide particles in their microstructures. The crack deflection around the white TiC grains through grey alumina matrix is illustrated in figure 63. Addition of TiC secondary phase in alumina is recognized for its role in crack deflection and divergence as a form of toughening mechanism to increase fracture toughness. The difference in thermal expansion coefficient between alumina and TiC induces internal residual stresses which cause propagating cracks to be deflected. TiC grains appear white in the micrograph (Fig. 63) and they were well dispersed within the alumina matrix with a size between 0.2 – 0.5 μm. Figure 63 shows a crack propagating on the surface of the composite ceramic. The crack path was investigated using SEM. It can be seen from this micrograph that the TiC grains are responsible for crack deflection. The TiC grains are also responsible for pinning the alumina

grain boundaries, thus inhibiting grain growth. This effect will help increase the strength of this ceramic.

5.1.3 Addition of CNTs and TiC into Al₂O₃

The addition of both TiC and CNTs (3 vol. %) increased the monolithic alumina hardness and fracture toughness (Fig. 71 and 72). Monolithic alumina hardness was 18 GPa and the addition of TiC and CNTs increased it to 23 GPa (22.5% increase). The fracture toughness was increased by 44% from 3.3 MPa√m to 5.0 MPa√m. The addition of both TiC and CNTs only slightly increase the hardness of monolithic alumina compared to the Al₂O₃-TiC or Al₂O₃-CNT composites. This is due to the fact that both these additives operate in the same way in the ceramic during sintering, to pin grain boundaries and inhibit grain growth. The 44 % increase in fracture toughness is due to both crack deflection mostly from TiC particle and crack bridging from CNTs.

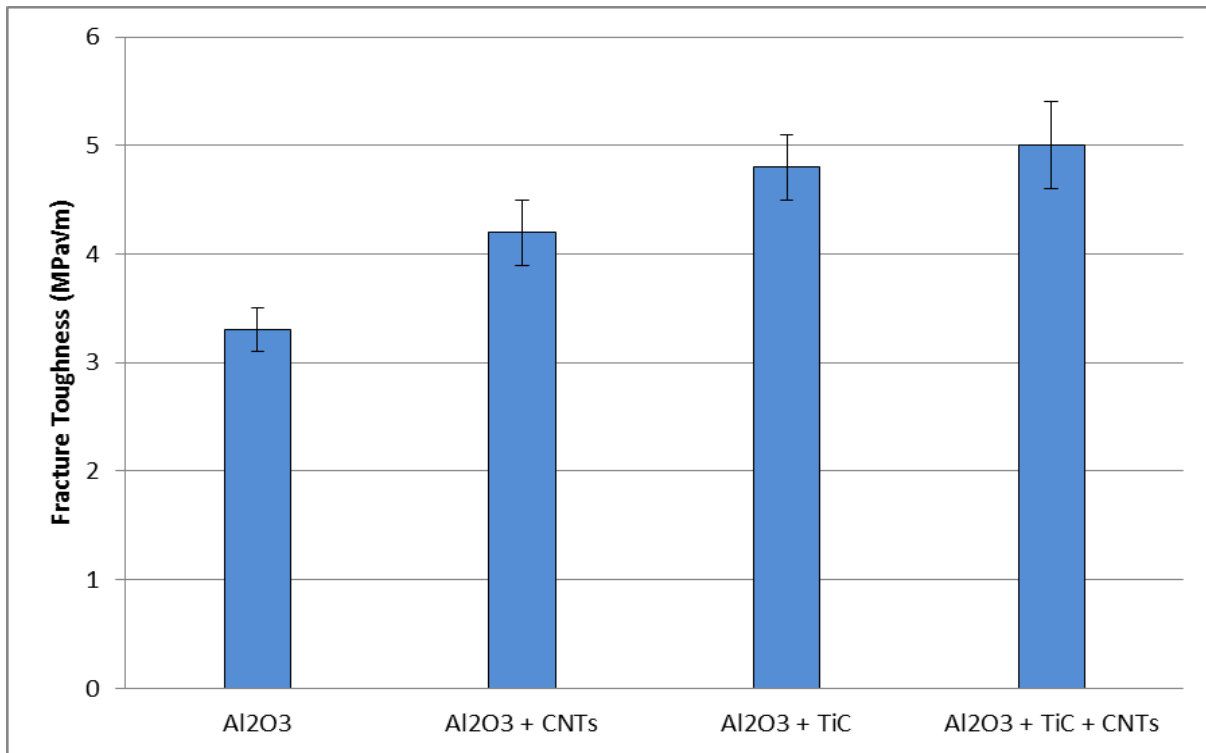


Figure 72: Variation of Al₂O₃ fracture toughness after reinforce with CNTs and TiC and the mixture of TiC and CNTs

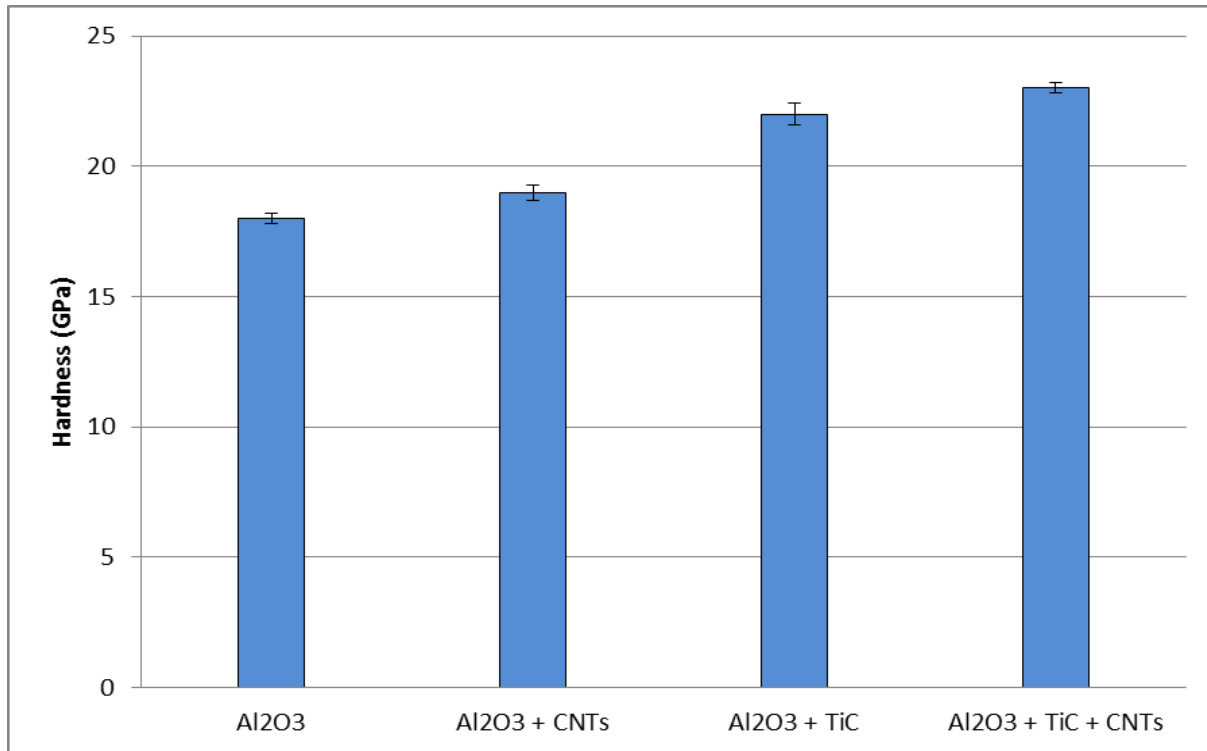


Figure 73: Variation of Al₂O₃ hardness when it is reinforced with CNTs, TiC and the mixture of TiC and CNTs

5.6 *Electrical properties measurements*

It is well known that Al₂O₃ is an electrical insulator. Alumina electrical insulating properties limit its wide use commercially. For instance because of its low electrical conductivity, it is not possible to use Electron Discharge Machine (EDM) alumina; instead a diamond wheel cutting is employed. This approach is more expensive than EDM. The processing cost of alumina is a major component of its final cost. CNTs are well known for their high electrical conductivity of 100 Ω.m (Coleman *et al.* ^[14]) which is dependent on the formation of the nanotube (Zigzag, arm chair and chiral).

In this study addition of 1 wt. % of CNTs into the alumina matrix increased alumina electrical conductivity from 0 S.m⁻¹ to 31.75 S.m⁻¹. The location and distribution of CNTs within the ceramic matrix determines their efficiency in increasing its electrical conductivity. During the mixing and sintering process of Al₂O₃-CNTs composite powder, the CNTs are either located along the grain boundaries or within the grains. The increase in electrical conductivity when CNTs were introduced into alumina was attributed to the presence of these additives along the

alumina grain boundaries (Fig 57). When the CNTs are well dispersed in the matrix, they form a network along the grain boundaries where they efficiently conduct electrons. The results obtained from this study are in agreement with the results obtained by other researchers.

Lee *et al.* ^[53] reported that the electrical conductivity of Al₂O₃-CNTs is related to the alumina grain size and the distribution of CNTs within the matrix. The same authors also reported that increasing the amount of CNTs into the alumina matrix and fixing its grain size will also increase the electrical conductivity of the ceramic. Inam *et al.* ^[52] reported that the Al₂O₃-CNTs electrical conductivity can be increased by reducing the ceramic grain size and keeping the CNT content fixed. In both these studies it is shown that the electrical conductivity of the Al₂O₃-CNTs is related to the density of CNTs along the grain boundaries which are said to be the CNT network electron conductive paths. Therefore the CNTs located along the grain boundaries are responsible for increasing the Al₂O₃-CNTs composite electrical conductivity. Lee *et al.* ^[53] also reported that there is a threshold amount of CNTs that can be incorporated into Al₂O₃ to effectively increase the electrical conductivity; this was found to be 3 vol. %. A large increase in electrical conductivity was found when 1 wt. % (3 vol. %) of CNTs was added. When an amount exceeding 1 wt. % was added the electrical conductivity only slightly increased as shown in literature review Chapter 2 (Fig.11).

The other important factor that is directly related to the electrical conductivity of Al₂O₃-CNTs is the dispersion of CNTs within the matrix. The more agglomerated the CNTs the less will be the electrical conductivity increase. The CNTs are responsible for the electrons transfer within alumina to increase its electrical conductivity, therefore they have to form a CNT network that will transfer the electrons efficiently. Therefore the CNTs have to be well dispersed so that they occupy most of the grain boundaries but yet still be in contact with each other along the grain boundaries for an effective electron transfer. The increase of electrical conductivity shows that 1 wt. % of CNTs was sufficient to provide enough CNTs network along the alumina grain boundaries.

The electrical conductivity results reported in this study and those reported by other authors were measured from a highly dense Al₂O₃-CNTs composite sample. Therefore the electrical

conductivity results presented (Table 16) were not affected by porosity of the sample. The results found in this study are related to the results reported by Inam *et al.* ^[52] and Lee *et al.* ^[53].

In this study the Al₂O₃-CNTs composite powders were sintered using SPS; 1600°C and 35 MPa. A high density was achieved. Therefore the effect of porosity on electrical conductivity is insignificant. The difference in the electrical conductivities between this study and the results reported by other authors was due to the difference in particle size of Al₂O₃ used, which give rise to different grain size after sintering. Such a difference in microstructure will affect the density and length of conduction paths available for the passage of electricity. Other factor that made the results to be different was that the CNTs would differ in their properties as well as differences in processing approach used by the different authors.

TiC is a metallic conductor with an electrical conductivity between 125 – 333.33 Ω.m Lee *et al.* ^[53]. When it is incorporated into alumina which is an insulator it has a potential of increasing alumina electrical conductivity. Incorporation of 30 wt. % of TiC into alumina increased alumina electrical conductivity up to 4431 S.m⁻¹, which was measured from a sample that was highly dense therefore the porosity effects on electrical conductivity was considered insignificant. Lee *et al.* ^[53] reported that the electrical conductivity increased with the TiC volume fraction and that there is a rapid increase in the electrical conductivity when the TiC content was between a range of 20 – 23 wt. %. This implies that within this range there was the formation of continuous TiC networks within the ceramic, which increased the electrical conductivity of Al₂O₃-TiC ceramic.

In this study the TiC content that was used was 30 wt. % and it increased the electrical conductivity up to 4431 S.m⁻¹. The 30 wt. % of TiC content provided enough continuous TiC phase within alumina, which were responsible for conduction of electrons hence increase electrical conductivity. The distribution of TiC has an effect in the electrical conductivity of Al₂O₃-TiC sample. The TiC powder was well distributed within alumina matrix (Fig. 62 and 63) which contributed to a large increase in the electrical conductivity of Al₂O₃-TiC composite ceramic.

Addition of both TiC and CNTs increased the electrical conductivity of monolithic alumina up to 6944 S.m^{-1} . The mixture of TiC and CNTs increased the conductivity of monolithic alumina better than CNTs or TiC individually. The reason for this large increase in conductivity is due to the fact that TiC and CNTs increase electrical conductivity by different mechanisms. TiC increased it by forming a continuous secondary phase within alumina and CNTs increase the conductivity by being along the grain boundaries of the alumina. When CNT and TiC are both present within the alumina matrix both mechanisms are combined to increase electrical conductivity. Since there were more boundaries therefore there were more CNTs in the conductive paths which lead to a larger increase in the electrical conductivity.

Chapter Six

6.0 Conclusions and Future Work

The reaction of acetylene with Fe^{2+} produced the MWCNTs which were then collected onto quartz wool. The MWCNTs that were formed were by this method had a diameter of 40 -150 nm as analyzed by TEM. The production of MWCNTs using this method is in agreement with what has been done previously (Iyuke *et al.* [25]) since they also obtained similar results. In this study the variation of acetylene flow rate was done in-order to favor the production of MWCNTs with smaller diameters. However the results from TEM showed no difference in the amount of MWCNTs and only small difference in their size. Therefore this MWCNT production method can only be used if the MWCNTs with diameter ranging from 40-150 nm are required.

The MWCNTs that were prepared at the University of Witwatersrand were not used for this study because they had big diameters and they were formed within nanofibres; therefore the MWCNTs were purchased from Nanocyl Pty Ltd, which had defined specifications. These MWCNTs were then coated with hBN. The results obtained from TEM revealed that the hBN coating was ≈ 20 nm. The results obtained from this study are in agreement with the result previously obtained (Chen *et al.* [47]). The MWCNTs that were formed were surrounded by excess hBN and also that coating every CNT separately was impossible. Boron oxide melts at $\approx 450^\circ\text{C}$ which then formed a matte around MWCNTs therefore making it impossible to coat every CNT separately. Those MWCNTs that were separately coated with hBN were analysed by TEM, and it was discovered that after 20 minutes of ultrasonication the hBN coating was “flaking-off” the surface of the MWCNTs. The flaking off of hBN coating implies that the hBN-CNT interface is weak.

The variation of ammonia gas flow rate and the temperature at which it is reacted with boron oxide are two parameters that can affect the thickness of the hBN coating. In the future the variation of these parameters can be tested in order to improve hBN-CNT interface strength. If the coating parameters that improve the hBN-CNT interface can be found then CNTs can be coated with hBN. This would eliminate their destruction during sintering, using cheaper sintering

methods like hot pressing and pressureless sintering etc. The CNTs destruction during sintering is currently minimized by using SPS which is an expensive sintering method.

Ultrasonic probe ultrasonication for 30 minutes was an efficient way of dispersing Al_2O_3 submicron powder (particle size 200nm) in hexane as confirmed by particle size analyzer. The Al_2O_3 powder was sintered at 1600°C , 35 MPa and a densification of 99.8% was obtained as measured using Archimedes principle, showing that the sintering conditions were sufficient to densify the powder. The incorporation of CNTs into the monolithic Al_2O_3 slightly reduced densification from 99.6% to 99.4%. The effects of CNTs to the densification is dependent onto the method used to disperse them, as more dispersed CNTs will have a less negative effect onto the densification process. The CNTs in this study were dispersed by both ultrasonication and milling using a PVP dispersant; this method was regarded as aggressive enough to counteract the Van der Waals forces present within the nanotubes. The CNTs in this study were still agglomerated to a certain degree, meaning the problem of CNTs agglomeration is yet to be solved. The challenge with CNTs is that dispersing them less aggressively will leave agglomerates but dispersing them more aggressively will destruct them and they will have less positive effects within the ceramic. Despite the CNTs slightly reducing the monolithic Al_2O_3 they improved the Al_2O_3 mechanical properties like fracture toughness and hardness, which was the main objective of the study. Incorporation of CNTs increased the monolithic Al_2O_3 hardness from 18 GPa to 20 GPa (11% increase) and fracture toughness from $3.3 \text{ MPa}\sqrt{\text{m}}$ to $4.2 \text{ MPa}\sqrt{\text{m}}$ (27% increase). The 11% increase in hardness was explained by the reduction of the Al_2O_3 grain size upon addition of CNTs and 27% increase in fracture toughness was explained by the crack bridging and crack deflection mechanisms which were observed upon addition of CNTs. CNTs are well known for their high electrical conductivity properties, therefore incorporating them into a non-conducting like Al_2O_3 ceramic had the potential of increasing the electrical properties. Incorporation of 1 wt% of CNTs into non conducting Al_2O_3 increased the electrical conductivity to $30 \text{ S}\cdot\text{m}^{-1}$. The increase in electrical conductivity was explained by the CNTs which were observed along the Al_2O_3 grain boundaries, since the grain boundaries are electron conducting paths, the CNTs located along the Al_2O_3 grain boundaries were useful in increasing the electrical conductivity and pinning the grain boundaries during sintering hence increasing Al_2O_3 hardness.

In this study only one CNT content (3 vol. %) was investigated due to the time constraints of the project. In future work the CNT content can be increased to investigate whether electrical properties will also be increased proportionally. Other methods of dispersing CNTs can also be investigated to see whether they improve the CNT agglomeration, which is still a challenge to be overcome.

Ultrasonication for 2 hours was successful in dispersing TiC nano powder (particle size = 200 nm) as it was confirmed by particle size analysis. The mixture of Al₂O₃ and TiC was made using a planetary ball mill which produced a well mixed composite powder. This powder was sintered at 1600°C and 1700°C to investigate which temperature would be sufficient for sintering it. The sample sintered at a lower temperature of the two was 95% dense of the theoretical while the density of the one sintered at 1700°C was 99% dense of the theoretical. Therefore 1700°C was considered a better temperature at which to sinter the composite powder. The incorporation of TiC (30 wt. %) into monolithic Al₂O₃ reduced the densification from 99.6% to 99.0%. The reduction of density was attributed to the presence of the second phase (TiC) within the Al₂O₃ matrix. The fact that TiC and Al₂O₃ have different thermal expansion coefficients implies that during cooling after sintering they will contract at different rates, with TiC contracting less than Al₂O₃. Therefore Al₂O₃ matrix will be constrained from achieving the density it could have if the TiC phase was absent. Despite the reduced density, the addition of TiC improved both the mechanical and electrical properties. The hardness was increased from 18 GPa to 22 GPa (22% increase) and the fracture toughness from 3.3 MPa√m to 4.8 MPa√m (42% increase). The 22% increase in hardness was explained by the reduced Al₂O₃ grain size because of grain boundary pinning effects as well as by the fact that TiC is much harder than Al₂O₃. The 42% increase in fracture toughness was explained by crack deflection around the TiC grains and the fact that different thermal expansion between TiC and Al₂O₃ induces internal stresses which interferes with the propagation of micro cracks in the material, thus increasing fracture toughness. Addition of TiC phase into a non conducting Al₂O₃ increased the electrical conductivity up to 4431 S.m⁻¹. This increase attributed to the presence of the conducting continuous TiC phase within Al₂O₃; the TiC phase was responsible for conducting electrons. The conduction of electrons from TiC grain to another TiC was possible since 30 wt% of TiC produced enough contiguity of this electrically conducting phase. The addition of both TiC and CNTs into Al₂O₃ reduced the

densification from 99.6% to 99.2%. With addition of both TiC and CNTs also improved hardness from 18 GPa to 23 GPa (22.5% increase) and the fracture toughness from 3.3 MPa√m to 5 MPa√m (44% increase). It was observed that when both TiC and CNTs phases were present, the mechanical properties of Al₂O₃ increased i.e. hardness only increased within the same error. This was due to the fact that CNTs and TiC increased the hardness by the same mechanism of inhibiting Al₂O₃ grain growth. Addition of TiC and CNTs phases increased the electrical conductivity up to 6944 S.m⁻¹. The large increase in electrical conductivity when both the TiC and CNTs phases were present was attributed to the fact that these two phases do not conduct electrons in the same way. CNTs conduct electrons along the grain boundaries which are conducting paths and TiC grain conduct electrons by passing them to the next adjacent TiC grains within the ceramic.

7.0 References

- [1] R. Riedel and W. Chen, "Ceramics Science and Technology", Vol. 2, WILEY-VCH, 2008, pp 3-7.
- [2] S. Somiya, F. Aldinger, N. Claussen, R.M Spriggs, K. Uchino, K. Koumoto and M. Kaneno. "Advanced Ceramic handbook", Vol. 1, 2003, Materials Science, pp198-210.
- [3] R.A Cutler and A.C Hurford "Pressureless-sintered Al₂O₃-TiC composites", Vol. 105 and 106, 1988, Materials Science and Engineering, pp 183-192.
- [4] J. Sun, I. Gao and X. Jin, "Reinforcement of alumina matrix with multi-walled carbon nanotubes", Vol. 31, 2005, Ceramic International, pp 893-896.
- [5] M. Estili, A. Kawasaki, H. Sakamoto, Y. Mekuchi, M. Kuno and T. Tsukada, "The homogeneous dispersion of surfactantless, slightly disordered, crystalline, Multiwalled carbon nanotubes in Alumina ceramics for structural reinforcement", Vol. 56, 2008, Acta Materialia, pg 4072.
- [6] W. Acchar and J Fonseca "Sintering behavior of alumina reinforced with (Ti, W) carbides", Vol. 371, 2004, Materials Science and Engineering, pp. 382-384.
- [7] A. Krell, "Ceramics based on alumina: Increasing the hardness for Tool applications", Handbook of Ceramic Hard Materials, Vol.12, R. Riedel, Wiley VCH, 2000, pp. 648-682.
- [8] S. Naeem, N. Zahra, U. Zafar and S. Munawar. "Adsorption studies of lead on α -alumina", Vol. 44, 2009, Journal of the Chemical Society, pg. 406.
- [9] H. Reveron, O. Zaafrani, G. Fantozzi, "Microstructure development, hardness, toughness and creep behaviour of pressure less sintered alumina/SiC micro-nanocomposites obtained by slip-casting", Vol.30, 2010, Journal of the European Ceramic Society, pp. 1351-1357.
- [10] www accuratus.com (date accessed 17/03/2010)
- [11] William D. Callister, Jr., "Materials Science and Engineering an Introduction", 7th Ed. Pub. (2007), pp. 448 and 700.
- [12] S.W Kim, W.S Chung, K Sohn, C Son and S Lee. "Improvement of flexure strength and fracture toughness in alumina matrix composites reinforced with carbon nanotubes", Vol. 517, 2009, Material Science and Engineering A, pp. 293 - 299.

- [13] M.V Vesali, A.A Khodadadi, Y. Mortazavi, O.A Sahraei, F. Pourfayaz and S.M Sedghi. "Functionalization of Carbon Nanotubes Using Nitric Acid Oxidation and DBD Plasma", Vol. 49, 2009, International Journal of Engineering Research and Applications, pg. 177.
- [14] J. N. Coleman, U. Khan, W. J Blau and Y. K Gun'ko "Small but strong: A review of the mechanical properties of carbon nanotubes-polymer composites", Vol. 44, 2006, Journal of Carbon, pp.1624-1652.
- [15] P. J. F. Harris, "Carbon Nanotube Science" Cambridge University Press, New York, 2009, pg. 1548.
- [16] Mohammad Naraghi. "Carbon Nanotubes Growth and Applications", Open Access Publisher, Intech., 2011, pg. 56-59.
- [17] www.core.kmi.open.ac.uk (date accessed 26/04/2010)
- [18] N. Grobert, "Materials Today", Vol. 10 2007, pp. 28–35.
- [19] J. Hone, M. Whitney, C. Piskoti, and A. Zettl, "Thermal conductivity of single-walled Carbon Nanotubes," Rev. B 59, , 1999, Phys., pg. 2514.
- [20] J. E. Fischer, H. Dai, A. Thess, R. Lee, N.M. Hanjani, D.L. Dehaas and R. E. Smalley, "Metallic Resistivity in Crystalline ropes of Single Wall Carbon Nanotubes", Rev. 55, 1997, Phys., pp. 4921- 4924.
- [21] T. W. Ebbesen, H. J. Lezec, J. Hiura, J. W. Bennett, H.F. Ghaemi and T. Thio, "Electrical conductivity of individual carbon nanotubes", Vol. 382, 1996, Nature, pp. 54-56.
- [22] Y. Ando and X. Zhao."Synthesis of Carbon Nanotubes by Arc-Discharge Method" Vol. 16, 2006, New Diamond and Frontier Carbon Technology, pg. 468.
- [23] www.mrsec.wisc.edu (date accessed 12/05/2010)
- [24] M. José-Yacamán, M. Miki-Yoshida, L. Rendón, J. G. Santiesteban,. "Catalytic Growth of Carbon Microtubules with Fullerene Structure", Vol. 62, 1993, Application Physics, pg. 657.

- [25] S.E Iyuke, T.A Mamvura, K. Liu, V. Sibanda, M. Meyyappan and V.K Varadan. "Process synthesis and optimization for the production of carbon nanotubes", Vol. 20, (2009, Nanotechnology, pg. 5.
- [26] www.baytubes.com (accessed on 25/02 2010).
- [27] S. P. Mitri and S. V. Sotirchos. "Production of Carbon nanotubes using Chemical Vapour Deposition study of the operation parameters", Vol. 10, 2005, Advanced Material Science, pp. 314-319.
- [28] H. T. Pu, F. J. Jiang, Z. Yang, B. Yan, and X. Liao, Vol. 102, 2006, *J. Appl. Polym. Sci.* pg. 1653
- [29] M. Jianhua, W. Meining, D. Yihong, C. Suqin, L. Guoxing, and H. Jianbo "Synthesis of nanocrystalline Titanium carbide with a new convenient route at low temperature and its thermal stability", Vol. 153, 2008, Material Science and Engineering B, pp. 96-97.
- [30] D.W Lee, S.V Alexandrovskii, B.K Kim "Novel synthesis of substoichiometric ultrafine Titanium carbide", Vol. 58, 2004, Materials letters, pp. 1471-1472.
- [31] E.K Stroms "The Refractory Carbides" Vol.2, 1967, Refractory Materials Series, Academic Press, New York, pg. 68.
- [32] L.E Toth "Transition Metal Refractory Carbides and Nitrides" Academic Press, New York, pp56-87.
- [33] H.O Pierson "Handbook of Refractory Carbides and Nitrides", 1996, Noyes Publications, Westwood, pp. 54-98.
- [34] R. Hsiao, D. Miller, S. Nhuyen, A. Kellock "Titanium carbide etching in high density plasma", Vol. 148, 1999, Applied surface science, pp. 1-2.
- [35] www.memsnet.org (date accessed 15/09/2011)
- [36] W. Acchar and A.M Segadaes "Properties of sintered alumina reinforced with niobium carbide", Vol. 27, 2009, Refractory Metals and Hard Materials, pp. 427-430.

- [37] P. Ettmayer, H. Kolaska, W. Lengauer, K Dreyer, Vol.13, 1995, Int. J. Refractory Materials, pg. 343.
- [38] H. Preiss, L.M Berger, D. Schultze, J. Eur. Ceramic Society. Vol. 19, 1999, pg. 195.
- [39] D.S Patil and B.C Mutsuddy “Processing and properties of zirconia-toughness alumina ceramics”, Vol. 17, 1994, Bulletin of Material Science, pp. 1435-1435.
- [40] S.W Kim, W.S Chung, K. Sohn, C. Son and S. Lee. “Improvement of flexure strength and fracture toughness in alumina matrix composites reinforced with carbon nanotubes”, Vol. 517, 2009, Material Science and Engineering, pp. 293 – 299.
- [41] N.P Padture, W.A Curtin, Vol.58, 2008, Scripta Mater. pg. 989.
- [42] D. Jiang, A.K Mukhejee, Vol. 58, 2008, Scripta Mater, pg. 991.
- [43] M Hubacek, M Uek, T Sato and V Brozek “High temperature behavior of hexagonal boron nitride”, Vol. 282/283, 1996, Thermochemica Acta, pg. 360.
- [44] www.advancedmaingroupchemistry.com (date accessed 15/05/2010)
- [45] A. Gomathi, M.R. Harika and C.N.R Rao, “Urea route to coat inorganic nanowires, carbon fibers and nanotubes by boron nitride”, Vol. 476, 2008, Material Science and Engineering A, pp. 29-33.
- [46] I.D Rosca, F. Watari, M. Uo and T. Akasaka. “Oxidation of multiwalled carbon nanotubes by nitric acid”, Vol.43, 2005, Journal of Carbon, pg. 3124.
- [47] L. Chen, H. Ye and Y Gogotsi. “Synthesis of Boron Nitride Coating on Carbon Nanotubes”, Vol. 87 (1), 2004, Journal of the American Ceramic Society, pp. 147-157.
- [48] A. Mughtar and L.C Lim “Indentation fracture toughness of high purity submicron alumina”, Vol. 46, 1998, Pergamon, Acta Mater., pp. 1683-1690.
- [49] Guo-Dong Zhan and Amiya K. Mukherjee “Carbon Nanotube Reinforced Alumina-based Ceramics with Novel Mechanical, Electrical, and Thermal Properties”, Vol.2, 2004, Applied Ceramic Technology, pp. 161-171.

- [50] J. Hilding, E. Grulke, Z. Zhang and F. Lockwood “Dispersion of Carbon Nanotubes in Liquids”, Vol. 24, 2003, Journal of dispersion science and technology, pp. 38-40.
- [51] X.Q You, T.Z Si, N. Liu, P.P Ren, Y.D Xu and J.P Feng “Effect of grain size on thermal shock resistance of Al₂O₃-TiC ceramics”, Vol. 31, 2005, Ceramic international, pp. 33-38.
- [52] F. Inam, H.X Yan, D. Doni, M.J Reece, T. Peijs, “Stability of carbon nanotubes in ceramic nano-composites prepared by spark plasma sintering”, Press 2008, Nanotechnology, pg. 68.
- [53] D.W Lee, S.V Alexandrovskii and B.K Kim “Novel Sythesis of substoichiometric ultrafine titanium carbide”, Vol. 58, 2004, Material Letters, pp. 1471-1474.

8.0 Appendix

APPENDIX A: THEORETICAL DENSITY OF THE COMPOSITE POWDERS CALCULATIONS

$$\rho_T = \rho_1 (f) + (1-f) \rho_2 \quad \text{Equation 5}$$

ρ = density and f = volume fraction

Calculation of theoretical density of [Al₂O₃ + CNT (1 wt%)] sample

$$\rho_1 (\text{Al}_2\text{O}_3) = 3.98 \text{ g cm}^{-3} \quad \rho_2 (\text{CNTs}) = 1.3 \text{ g cm}^{-3}$$

$$f (\text{CNTs}) = 0.03$$

$$\rho_T = 3.98 (0.97) + 1.3 (0.03) = 3.90 \text{ g cm}^{-3}$$

Calculation of theoretical density of [Al₂O₃ + TiC (30 wt. %)] sample

$$\rho_1 (\text{Al}_2\text{O}_3) = 3.98 \text{ g cm}^{-3} \quad \rho_2 (\text{TiC}) = 4.93 \text{ g cm}^{-3}$$

$$f (\text{TiC}) = 0.258$$

$$\rho_T = 4.93 (0.258) + 3.98 (0.742) = 4.23 \text{ g cm}^{-3}$$

Calculation of theoretical density of [Al₂O₃ + CNT (0.96 wt. %) + TiC (30 wt. %)] sample

$$\rho_1 (\text{Al}_2\text{O}_3) = 3.98 \text{ g cm}^{-3} \quad \rho_2 (\text{CNTs}) = 1.3 \text{ g cm}^{-3} \quad \rho_3 (\text{TiC}) = 4.93 \text{ g cm}^{-3}$$

$$f (\text{Al}_2\text{O}_3) = 0.73 \quad f (\text{CNTs}) = 0.022 \quad f (\text{TiC}) = 0.25$$

$$\rho_T = 3.98 (0.73) + 1.3 (0.022) + 4.93 (0.25) = 4.17 \text{ g cm}^{-3}$$

Appendix B: ELECTRICAL CONDUCTIVITY CALCULATIONS OF THEORETICAL DENSITY OF THE COMPOSITE POWDERS CALCULATIONS

Calculation for Al₂O₃ + TiC

$$R = \text{slope of the curve} = 2.639 \, \Omega$$

$$\rho = (R \times A) / l = (2.639 \times 1.50\text{E-}07) / 1.8\text{E-}03 = 2.26\text{E-}04 \, \Omega.\text{m}$$

$$\delta = 1 / \rho = 4431 \, \text{S.m}^{-1}$$

Calculation for Al₂O₃ + CNTs + TiC

$$R = \text{slope of the curve} = 2.548 \, \Omega$$

$$\rho = (R \times A) / l = (2.548 \times 1.10\text{E-}07) / 1.9\text{E-}03 = 1.44\text{E-}04 \, \Omega.\text{m}$$

$$\delta = 1 / \rho = 6944 \, \text{S.m}^{-1}$$

APPENDIX C: RAW DATA OF ELECTRICAL PROPERTIES MEASUREMENTS